VOLUME 36, NUMBER 2, APRIL 2013

HADRONIC JOURNAL Volume 36, Number 2, April 2013

HADRONIC JOURNAL

Founded in 1978 by Prof. R. M. Santilli at Harvard University. Some of the past Editors include Professors S. L. Adler, A. 0. Barut, L. C. Biedenharn, N. N. Bogoliubov, M. Froissart, J.Lohmus, S. Okubo, Nobel Laureate Ilya Prigogine, M. L. Tomber, J. P.Vigier, J. Wess, Nobel Laureate Chen Ning Yang.

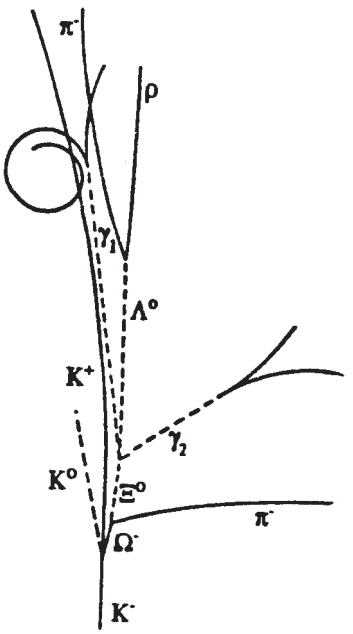

EDITORIAL BOARD
A.O.Animalu
D. P. Bhattacharyya
G.-C. Cavalleri
V. De Sabbata
T. L. Gill
L. P. Horwitz
H. Hurst
S. L. Kalla
S. I. Kruglov
S. S. Moskaliuk
M. Nishioka
R. F. O'Connell
Z. Oziewicz
E. Recami
M. Saleem
D. V. Shirkov
S. Silvestrov
D.S. Sourlas
H. M. Srivastava
A. I. Studenikin
R.I. Tsonchev
QI-Ren Zhang
C.A.Wolf
YI-Zhong Zhuo

FOUNDER:
RUGGERO M. SANTILLI

EDITOR IN CHIEF
CHRISTIAN CORDA

HADRONIC PRESS, INC.

HADRONIC JOURNAL

VOLUME 36, NUMBER 2, APRIL 2013

GENO-BRAGG'S LAW AND GENO-EINSTEIN'S GENERAL RELATIVITY THEORY FOR QUASICRYSTAL STRUCTURES, 149
Alexander O.E. Animalu
Department of Physics and Astronomy
University of Nigeria, Nsukka
and
Enugu State, Nigeria & International Centre for Basic Research
20 Limpopo Street, FHA, Maitama, Abuja, Nigeria

DYNAMIC ISO-TOPIC LIFTING WITH APPLICATION TO FIBONACCI'S SEQUENCE AND MANDELBROT'S SET, 167
Nathan O. Schmidt
Department of Mathematics, Boise State University
1910 University Drive
Boise, ID 83725 USA

ACTIVE SITES, COMPLEXITY STRUCTURES AND HYPERSTRUCTURES IN CATALYSTS, 177
M. Piumetti
Department of Applied Science and Technology
Politecnico di Torino, 10129 Torino, Italy
N. Lygeros
LGPC (UMR 5285), Université de Lyon
69616, Villeurbanne, France

DARK ENERGY, INERTIA AND MACH'S PRINCIPLE, 197
C. Sivaram
Indian Institute of Astrophysics
Bangalore – 560 034, India
Kenath Arun
Christ Junior College
Bangalore – 560 029, India

MAGNETIC EFFECT OF NON-COMMUTATIVITY, 205
B.G. Sidharth
G.P. Birla Observatory & Astronomical Research Centre
B.M. Birla Science Centre
Adarsh Nagar, Hyderbad – 500 063 India
C.V. Aditya
University of Stuttgart, Germany

MADELBROT ISO-SETS: ISO-UNIT IMPACT ASSESSMENT, 211
Reza Katebi
Department of Physics, California State University
Fullerton, 800 North State College Boulevard
Fullerton, CA 92831 USA
Nathan Schmidt
Department of Mathematics, Boise State University
1910 University Drive
Boise, ID 83725 USA

ISO-GALOIS FIELDS, 225
Arun S. Muktibodh
Department of Mathematics
Mohota College of Science
Nagpur-440009 India

ON THE MASS-ENERGY RELATIONSHIP $E=mc^2$, 237
John Shim

FERMIODYNAMICS THROUGH GENERALIZED ELECTRODYNAMICS, 243
Sushama V. Vaidya
Physics Department S.B. College of Science
Aurangabad – 431001, India
M.T. Teli
Physics Department
Dr. Babasaheb Ambedkar
Aurangabad – 431004, India (Retd.)

GENO-BRAGG'S LAW AND GENO-EINSTEIN'S GENERAL RELATIVITY THEORY FOR QUASICRYSTAL STRUCTURES

Alexander O.E. Animalu
Department of Physics and Astronomy
University of Nigeria, Nsukka

Enugu State, Nigeria & International Centre for Basic Research
20 Limpopo Street, FHA, Maitama, Abuja, Nigeria
nascience@aol.com

Received October 16, 2013

Abstract

The synthesis of quasicrystals and the observation of their diffraction pattern with unexpected 10-fold point-symmetry by D.Shechtman and co-workers as well as our recent observation of the diffraction pattern of white light by a glass of water (~conical pyramid) are reviewed in the context of geno-Bragg's law for cube-hexagon (holographic) structures and used to characterize a cyclic time in O(4,2)xSU(3)xU(1) lattice gauge theory. The cyclic time is then correlated with Santilli's four arrows of time, namely, isotimes, genotimes and genohypertimes,. and as a result, an elaboration of Einstein's general relativity theory into geno-Einstein's general relativity is derived. Various implications of the theory are discussed.

PACS Nos. 03.65.Nk, 11.30.Cp, 03.65.-w

Copyright © 2013 by Hadronic Press, Inc., Palm Harbor, FL 34684, USA

1. INTRODUCTION

The synthesis of quasicrystals and the observation by D.Shechtman and co-workers[1] of their diffraction pattern with unexpected 10-fold point-symmetry[2] and our recent observation[3] of the diffraction pattern of white light by a glass of water (~conical pyramid) (see, Figs. 1 and 2) have opened up a new vista within the purview of solid state (condensed matter) physics and geno-Bragg's law[4] for cube-hexagon (holographic) structures in O(4,2)xSU(3)xU(1) lattice gauge theory. The new vista from solid state physics arises, on one hand, from geno-Bragg's law due to the constraint of *translational periodicity* on rotational point-symmetry in three-dimensional(3D) space which demands the replacement of the forbidden 5-fold point symmetry (such that 5+5 = 10) by a deformation of two allowed (4-fold and 6=fold) point symmetries (such that 4+6=10) is required to account for the observed diffraction pattern, as indicated in Fig. 1

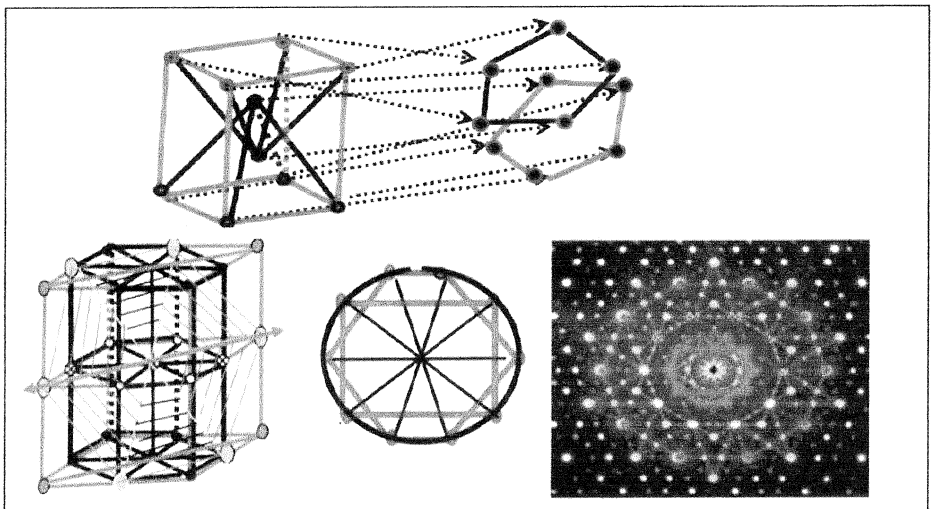

Fig. 1(Top) Double Pentagon (5+5=10) and (bottom) Cube-hexagon (4+6=10) geno-Bragg's law characterization of the observed 10-fold symmetric diffraction pattern of quasicrystal $Ca_{13}Cd_{76}$ structure[1,2] discussed in ref.[4].

On the other hand, bearing in mind Newton's fascination with the splitting of white light by solid glass prism, our observation[3] of the diffraction of white light by a pyramid of water into a 4x4 matrix of 16 points as indicated in Fig.2, is a further experimental confirmation of the $O(4,2)\times SU(3)\times U(1)$ lattice gauge theory.

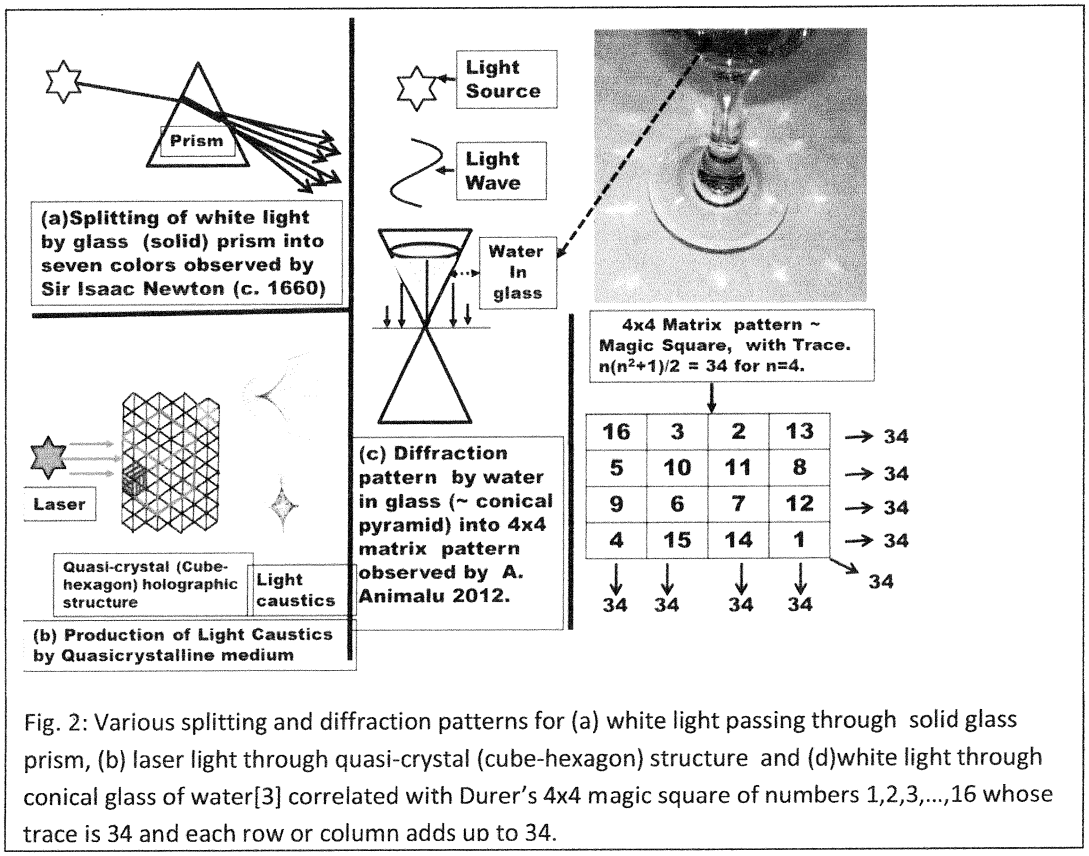
Prism
(a)Splitting of white light by glass (solid) prism into seven colors observed by Sir Isaac Newton (c. 1660)
Light Source
Light Wave
Water In glass
(c) Diffraction pattern by water in glass (~ conical pyramid) into 4x4 matrix pattern observed by A. Animalu 2012.
4x4 Matrix pattern ~ Magic Square, with Trace. n(n²+1)/2 = 34 for n=4.
16 3 2 13 → 34
5 10 11 8 → 34
9 6 7 12 → 34
4 15 14 1 → 34
34 34 34 34 34
Laser
Quasi-crystal (Cube-hexagon) holographic structure
Light caustics
(b) Production of Light Caustics by Quasicrystalline medium

Fig. 2: Various splitting and diffraction patterns for (a) white light passing through solid glass prism, (b) laser light through quasi-crystal (cube-hexagon) structure and (d)white light through conical glass of water[3] correlated with Durer's 4x4 magic square of numbers 1,2,3,...,16 whose trace is 34 and each row or column adds up to 34.

The outline of the rest of this paper is as follows. In Sec. 2. we shall review geno-Bragg's law and use it to characterize and correlate cyclic time with Santilli's four arrows of time[5,6] in the context of the $O(4,2)\times SU(3)\times U(1)$ (cube-hexagon) lattice gauge theory. In Sec. 3, the result will be used to elaborate Einstein's general relativity theory into geno-Einstein's theory. Finally, in Sec. 4, further implications will be discussed and conclusions drawn.

2. *REVIEW OF GENO-BRAGG'S LAW*

Our derivation of geno-Bragg's law[4] within the purview of Maxwell-Dirac electromagnetic field equations was based on a correspondence principle (see, Fig. 3)

points⇔ particles, lines ⇔ fields, planes ⇔ currents,

between points, lines and planes of projective 3D space tetrahedron of reference and particles, fields and currents of Maxwell-type gauge field theories, so that

$$(\mathbf{k} \Leftrightarrow \mathbf{p},\ \mathbf{g} \Leftrightarrow \mathbf{J} \equiv e\mathbf{v} \text{ or } e\gamma) \Rightarrow \begin{Bmatrix} \mathbf{g}^2 \pm (\mathbf{g}.\mathbf{k} + \mathbf{k}.\mathbf{g}) \\ (\mathbf{k}^2 \pm (\mathbf{k}.\mathbf{g} + \mathbf{g}.\mathbf{k}) \end{Bmatrix} \Leftrightarrow \begin{Bmatrix} \mathbf{J}.\mathbf{J} \pm (\mathbf{J}.\mathbf{p} + \mathbf{p}.\mathbf{J}) \\ \mathbf{p}.\mathbf{p} \pm (\mathbf{p}.\mathbf{J} + \mathbf{J}.\mathbf{p}) \end{Bmatrix} \quad (2.1)$$

where $\mathbf{p}, \mathbf{J}$ are the momentum and current three-vectors, $e\mathbf{v}$ or $e\gamma$ is the electric current associated with particle velocity($\mathbf{v}$) or Dirac γ–matrix. and, e is the electric charge, in units such that $\hbar = c = 1$

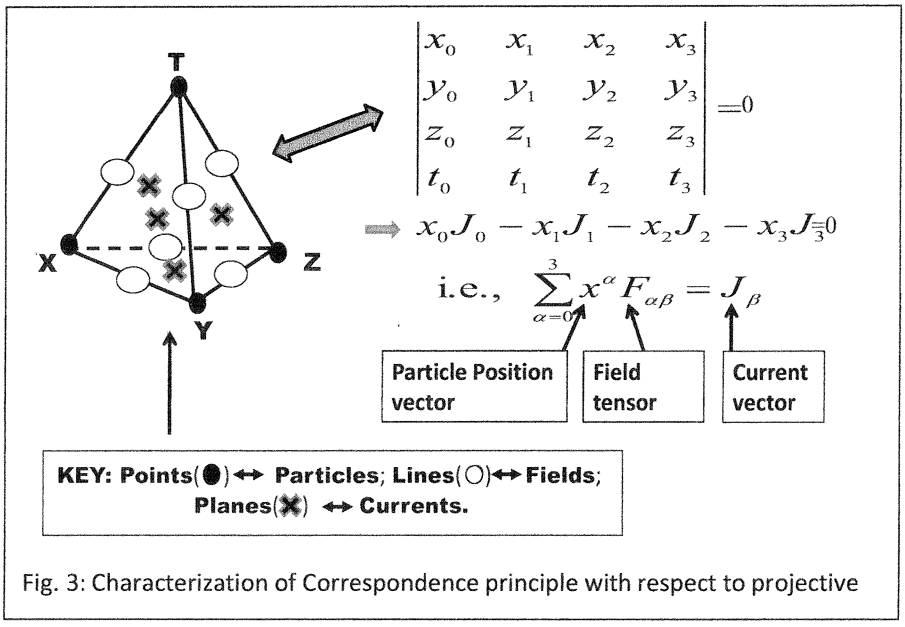
T
X
Z
Y
$\begin{vmatrix} x_0 & x_1 & x_2 & x_3 \\ y_0 & y_1 & y_2 & y_3 \\ z_0 & z_1 & z_2 & z_3 \\ t_0 & t_1 & t_2 & t_3 \end{vmatrix} = 0$
$\Rightarrow x_0 J_0 - x_1 J_1 - x_2 J_2 - x_3 J_3 = 0$
i.e., $\sum_{\alpha=0}^{3} x^\alpha F_{\alpha\beta} = J_\beta$
Particle Position vector
Field tensor
Current vector
KEY: Points(●)↔ Particles; Lines(○)↔Fields; Planes(✖) ↔ Currents.

Fig. 3: Characterization of Correspondence principle with respect to projective

Geometrically, the number (S) of the points, lines and planes (like Miller indices in solid state physics) of various geometric objects, e.g.S= 4+6+4 for the tetrahedron in Fig. 3 correspond to possible distribution of atomic spheres in a lattice, and in high-energy physics S corresponds to the dimensions that occur in the product 8x8=64 = (1+8+27)+(8+10+10*) = 36 (symmetric) + 28 (antisymmetric) parts, and equivalently, 64= 26+38 = 32+32=24+40, etc of the 8x8 representations of SU(3)[7] (see, Table 1) as elaborated in ref. 4.

Table 1: Representations[7] of the unitary symmetry group SU(3)

Complete Designation	Abbr Dsgn	⊗D³(1,0)	⊗D⁶(2,0)	⊗ D⁸(1,1)	⊗ D¹⁰(3,0)
D¹(1,0)	1	3	6	8	10
D³(1,0)	3	6+3* = 9	10+8 = 18	15+6*+3 = 24	15*+15 = 30
D³(0,1)	3*	8+1 = 9	15+3 = 18	15*+6+3* = 24	24+6 = 30
D⁶(2,0)	6	10+8 = 18	15*+15+6*= 36	24+15*+6+3* = 48	24+21+15* = 60
D⁶(0,2)	6*	15*+3* = 18*	27+8+1 = 36	24*+15+6*+3 =48	42+15+3 = 60
D⁸(1,1)	8	15+6*+3 = 24	24+15*+ 6+3* = 48	27+10+10*+8+8+ 1 = 64 = 36+28 = 38+26	35+27+10+8 = 80
D¹⁰(1,0)	10	15*+15 = 30	24+21+15* = 60	35*+27+1+8 = 71	35+28+27+10 = 100 =74+26
D¹⁰(0,3)	10*	24*+6* = 30*	42*+15*+3* = 60*	35*+27+10*+8 = 80	64+27+8+1 = 100=64+36

Table 2: Number of Points, Lines & Planes of 3D Solid Geometry.

Solid Object	Points (Vertices)	Lines (Edges)	Planes (Faces)	Total Number (S) of Elements	Symmetry Group
Tetrahedron(†)	4	6	4	14	$T=A_4$
Cube(†)	8	12	6	26	T=S4
Octahedron(†)	6	12	8	26	O=S4
Hexagon-based pyramid	7	12	7	26	
Square-based pyramid	5	8	5	18	SU(3)
Hexagonal-polyhedron(*)	12	18	8	38	*
Dodecahedron(†)	20	30	12	62	$I=A_5$
Icosahedron(†)	12	30	20	62	$I=S_5$

Note: The Five Platonic Solids are identified with(†) sourced from Paul –Saul Sirag [8] here T is the Tetrahedral group , A4=alternating group (even permutation of 4 things), O is the octahedral group, S4= symmetric group (of permutation of 4 things), I is the icosahedral group, A5 is alternating group (of even permutations of 5 things). (*) The symmetry group of the hexagonal-polyhedron is related to the 8x8= 64 = 36+28 [= 38+26] representation of SU(3)

Conventional Bragg's law ($2a\sin\theta = n\lambda$, with $\theta = 2\pi/n$, $n = 1,2,3,4,6$) takes the form, $\mathbf{g}^2 - (\mathbf{g}.\mathbf{k} + \mathbf{k}.\mathbf{g}) = 0$, for a suitable choice of the angle between $\mathbf{k}$ (with $|\mathbf{k}| = 2\pi/\lambda$) and the reciprocal lattice vector $\mathbf{g}$ (with $|\mathbf{g}| = 2\pi n/a$) while the generalization to geno-Bragg's law involves the representation of deformation firstly by Santilli's iso-coordinate system[5]

$$k_x^2 + k_y^2 + k_z^2 \to k_x b_1^2 k_x + k_y b_2^2 k_y + k_z b_3^2 k_z = \text{invariant.}$$

$$k_x = k b_1^{-1} \sin(b_3\theta)\cos(b_1 b_2 \varphi);$$

$$k_y = k b_2^{-1} \sin(b_3\theta)\sin(b_1 b_2 \varphi);$$

$$k_z = k b_3^{-1} \cos(b_3\theta)$$

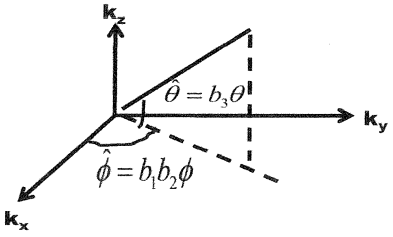

(2.2)

and secondly by treating (**k,g**) as 6-vector components of an antisymmetric 4x4 tensor,

$$\left\| G^k_{\mu\nu} \right\| \equiv \begin{pmatrix} 0 & k_1 & k_2 & k_3 \\ -k_1 & 0 & g_3 & -g_2 \\ -k_2 & -g_3 & 0 & g_1 \\ -k_3 & g_2 & -g_1 & 0 \end{pmatrix} \qquad (2.3)$$

Conventional Bragg's law follows (as shown in Appendix A of ref.[4]) from a condition on the roots of the associated eigenvalue equation

$$\text{Det}\left\| G_{\mu\nu} - \lambda\eta_{\mu\nu} \right\| \equiv \lambda^4 - (\mathbf{k}^2 - \mathbf{g}^2)\lambda^2 + (2\mathbf{k}.\mathbf{g})^2 = 0, \qquad (2.4)$$

where $\left\| \eta_{\mu\nu} \right\| \equiv diag(+1,-1,-1,-1)$ Geno-Bragg's law involves deformations characterized generally as follows

$$1/\hat{\theta} = 1/\theta_a + 1/\theta_b,\ \hat{\in}^{\pm} = (\theta_a/\theta_b \pm \theta_b/\theta_a),\ a,b = 1,2,3,4 \text{ or } 6$$

$$i.e.,\ \left.\begin{array}{l} \hat{\theta} = (\theta_a + \theta_b)/\theta_a\theta_b \\ \hat{\in}^{\pm} = (\theta_a^2 \pm \theta_b^2)/\theta_a\theta_b \end{array}\right\} \Rightarrow \left\{\begin{array}{c} \in^{+}/\hat{\theta} = (\theta_a^2 + \theta_b^2)/(\theta_a + \theta_b) \\ \in^{-}/\hat{\theta} = (\theta_a - \theta_b) \end{array}\right. \qquad (2.5)$$

and specifically corresponding to a transformation of a point-sphere into a torus,

$$0 = \theta_a^2 + \theta_b^2 + x(\theta_a\theta_b - \theta_b\theta_a) \equiv (\theta_a, \theta_b)\begin{pmatrix} 1 & -x \\ x & 1 \end{pmatrix}\begin{pmatrix} \theta_a \\ \theta_b \end{pmatrix}$$

$$\to (\theta'_a, \theta'_b)\begin{pmatrix} -1 & +x \\ x & 1 \end{pmatrix}\begin{pmatrix} \theta'_a \\ \theta'_b \end{pmatrix} \equiv -(\theta'^2_a - \theta'^2_b) + x(\theta'_a\theta'_b + \theta'_b\theta'_a) = 0 \quad (2.6a)$$

which is expressible as a transformation of the underlying metric,

$$\eta \equiv \begin{pmatrix} 1 & -x \\ x & 1 \end{pmatrix} \rightarrow \begin{pmatrix} -1 & x \\ x & 1 \end{pmatrix} = TC\eta \qquad (2.6b);$$

or equivalently,

$$0 = \theta_a^2 + \theta_b^2 + x^{-1}(\theta_a\theta_b - \theta_b\theta_a) \equiv (\theta_a, \theta_b)\begin{pmatrix} 1 & -x^{-1} \\ x^{-1} & 1 \end{pmatrix}\begin{pmatrix} \theta_a \\ \theta_b \end{pmatrix}$$

$$\rightarrow (\theta'_a, \theta'_b)\begin{pmatrix} -x^{-1} & 1 \\ 1 & x^{-1} \end{pmatrix}\begin{pmatrix} \theta'_a \\ \theta'_b \end{pmatrix} \equiv -x^{-1}(\theta'^2_a - \theta'^2_b) + (\theta'_a\theta'_b + \theta'_b\theta'_a) = 0 \quad (2.7a)$$

$$\eta \equiv \begin{pmatrix} 1 & -x^{-1} \\ x^{-1} & 1 \end{pmatrix} \rightarrow \begin{pmatrix} -x^{-1} & 1 \\ 1 & x^{-1} \end{pmatrix} = \eta DT \qquad (2.7b)$$

such that when x=1, one gets the Lie-admissible algebraic relation

$$TC\eta - \eta DT = 0 \quad (C \neq D \neq I) \qquad (2.8)$$

where, $C = \begin{pmatrix} 0 & 1 \\ 1 & 0 \end{pmatrix} \equiv \sigma_1, T = \begin{pmatrix} 0 & -1 \\ 1 & 0 \end{pmatrix} \equiv i\sigma_2, D \equiv \begin{pmatrix} -1 & 0 \\ 0 & 1 \end{pmatrix} \equiv -\sigma_3.$

The characterization of geno-space-time which we are after in this paper is obtained from eq.(2.3) by treating **(r,ct)** like **(k,g)** as a 6-vector via the replacement:

$$\left\|G^k_{\mu\nu}\right\| \equiv \begin{pmatrix} 0 & k_1 & k_2 & k_3 \\ -k_1 & 0 & g_3 & -g_2 \\ -k_2 & -g_3 & 0 & g_1 \\ -k_3 & g_2 & -g_1 & 0 \end{pmatrix} \rightarrow \begin{pmatrix} 0 & x_1 & x_2 & x_3 \\ -x_1 & 0 & ct_3 & -ct_2 \\ -x_2 & -ct_3 & 0 & ct_1 \\ -x_3 & ct_2 & -ct_1 & 0 \end{pmatrix} \equiv \left\|G^r_{\mu\nu}\right\| \quad (2.8)\text{in which}$$

$r = \sqrt{x_1^2 + x_2^2 + x_3^2}, t = \sqrt{t_1^2 + t_2^2 + t_3^2}$ are, respectively, the radii of spheres in 3D **r**-space and 3D **t**-space, the latter being quantized in units of the Planck time (to make it completely analogous to the reciprocal lattice vector, **g**). Accordingly, we observe that a discrete set of linear times (t_a, t_b, ...) can be transformed into a corresponding discrete cycles of iso-times ($\hat{\mathbf{t}}$) via a Mobius (1790-1868) transformation[9]:

$$:\frac{\mathbf{t}}{\mathbf{t_a}} = \mathbf{i}\frac{\mathbf{1} - \hat{\mathbf{t}}/\mathbf{t_a}}{\mathbf{1} + \hat{\mathbf{t}}/\mathbf{t_a}} \Rightarrow \frac{\hat{\mathbf{t}}}{\mathbf{t_a}} = \frac{\mathbf{t}/\mathbf{t_a} - \mathbf{i}}{\mathbf{t}/\mathbf{t_a} + \mathbf{i}} \qquad (2.9)$$

which shows (see, Fig. 4) that, typically, the (circular) boundary $\left|\hat{\mathbf{t}}\right| = \mathbf{t_a}$ in $\hat{\mathbf{t}}$ **-plane** is a (non-unitary) image of the line, $\left|\mathbf{t} - \mathbf{it_a}\right| = \left|\mathbf{t} + \mathbf{it_a}\right|$, in complex t-plane, and similarly for the sequence of boundaries with $\mathbf{t_a}$ replaced by $\mathbf{t_b}$. ...

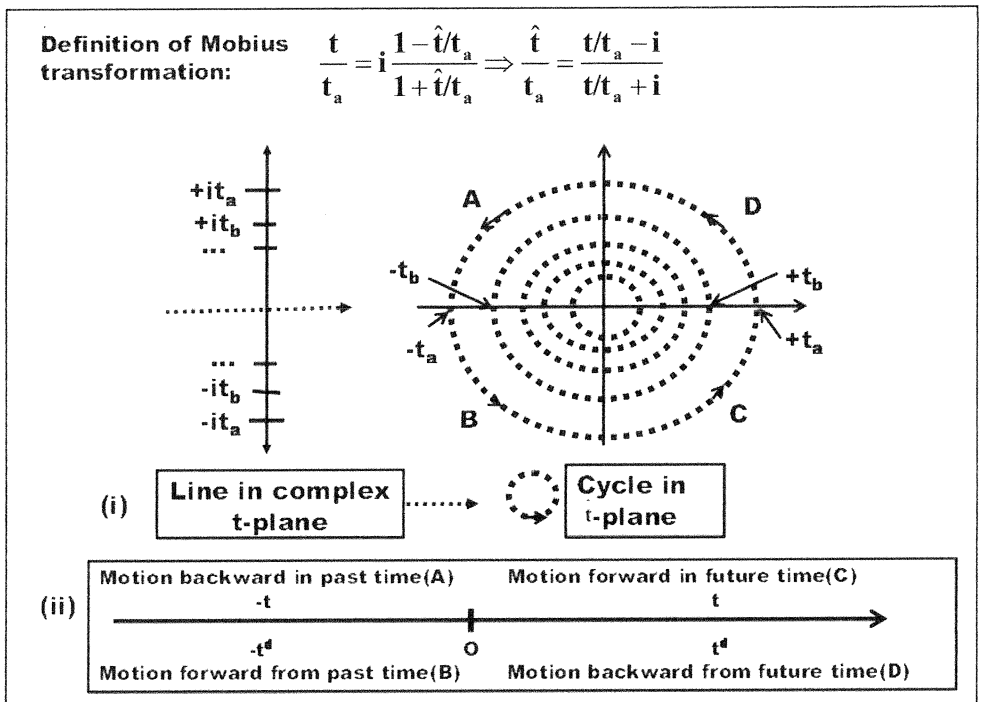

Fig.4: (i) Mobius transformation of a (discrete set of time) line into a (discrete set of isotime) cycles & (ii) correlation of the four quadrants (A,B,C,D) in iso-time plane with Santilli's four arrows of time[5,6], which underscores the need for isodual conjugation in addition to the conventional time reversal for the representation of all four directions.

In the above sense, the notion of cyclic time goes beyond the conventional (Edington's) two arrows of time but is correlated with Santilli's four directions of time known as isotimes, genotimes. and genohypertimes[5,6]. which are elaborated in algebraic geometric terms as shown in Fig. 5 by the progressive generalizations of Euclidean metric tensor of 3D space[5] as follows:

$$I=\begin{pmatrix}1&0&0\\0&1&0\\0&0&0\end{pmatrix}\rightarrow\begin{pmatrix}\hat{I}_1^{>}&0&0\\0&\hat{I}_2^{>}&0\\0&0&\hat{I}_3^{>}\end{pmatrix}=\begin{pmatrix}(\hat{I}_{11}^{>},\hat{I}_{12}^{>}...\hat{I}_{1m}^{>})&0&0\\0&(\hat{I}_{21}^{>},\hat{I}_{22}^{>}...\hat{I}_{2m}^{>})&0\\0&0&(\hat{I}_{31}^{>},\hat{I}_{32}^{>}...\hat{I}_{3m}^{>})\end{pmatrix}=1/\hat{T}^{>}$$

$$I=\begin{pmatrix}1&0&0\\0&1&0\\0&0&0\end{pmatrix}\rightarrow\begin{pmatrix}\hat{I}_1^{<}&0&0\\0&\hat{I}_2^{<}&0\\0&0&\hat{I}_3^{<}\end{pmatrix}=\begin{pmatrix}(\hat{I}_{11}^{<},\hat{I}_{12}^{<}...\hat{I}_{1m}^{<})&0&0\\0&(\hat{I}_{21}^{<},\hat{I}_{22}^{<}...\hat{I}_{2m}^{<})&0\\0&0&(\hat{I}_{31}^{<},\hat{I}_{32}^{<}...\hat{I}_{3m}^{<})\end{pmatrix}=1/\hat{T}^{<},\quad(2.10)$$

with $\hat{I}^{>}=\left({}^{<}I\right)^{+}$.

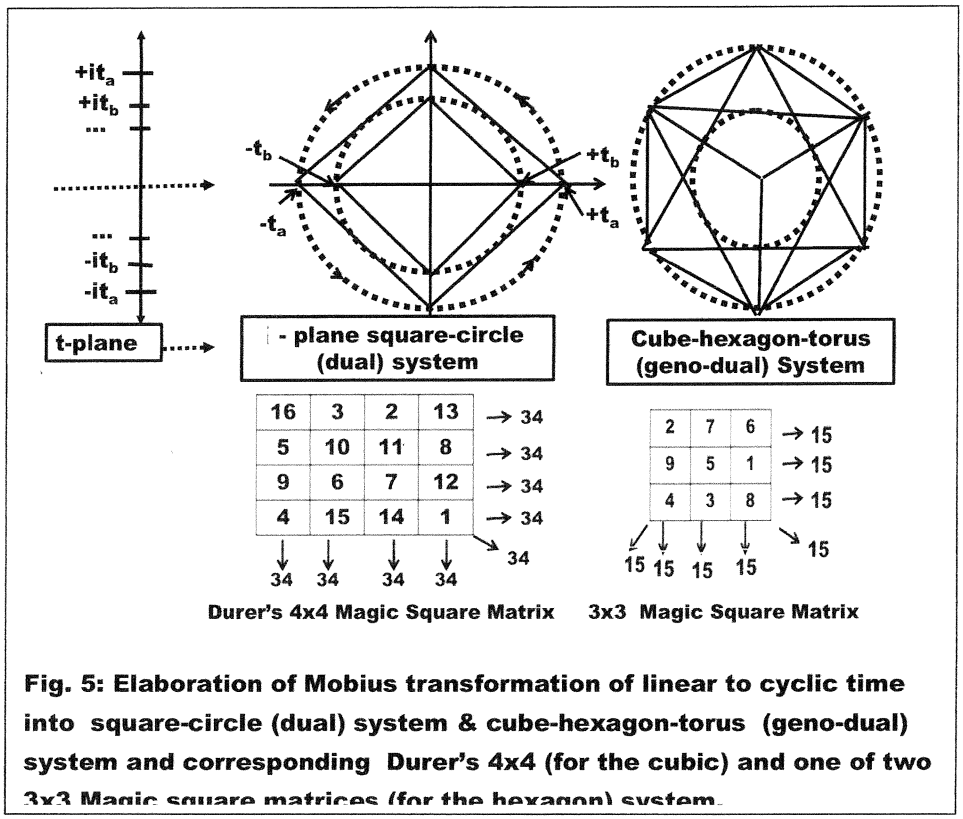

Fig. 5: Elaboration of Mobius transformation of linear to cyclic time into square-circle (dual) system & cube-hexagon-torus (geno-dual) system and corresponding Durer's 4x4 (for the cubic) and one of two 3x3 Magic square matrices (for the hexagon) system.

However, since there is presently only mathematical prescription[5,6] for constructing the generalized "units", $I^{>}$ and ${}^{<}I$, the constraints due to geno-Bragg's law on the metric tensor may be used as a guide to represent them in 3-dimensional space in terms of the 3x3 magic square matrix:

$$\hat{I}^{>} \propto \begin{pmatrix} 2 & 7 & 6 \\ 9 & 5 & 1 \\ 4 & 3 & 8 \end{pmatrix}, \quad \hat{I}^{<} \equiv (\hat{I}^{>})^{+} \propto \begin{pmatrix} 2 & 9 & 4 \\ 7 & 5 & 3 \\ 6 & 1 & 8 \end{pmatrix} \quad (2.11)$$

with $Trace(\hat{I}^{>}) = \frac{1}{2}n(n+1) = 15, (\text{for } n = 3)$. such that Bragg's law holds in the standard form $2\vec{k}.\vec{g}_n - \vec{g}_n^2 = 0$ for a wave vector, $\vec{k} = (2\pi\sqrt{15}/\lambda)(1,1,1)$ and each $\vec{g}_n = (3/2\sqrt{15})p_n$, ($n$=1,2,…,8), with $p_1 = (2,7,6)$, $p_2 = (9,5,1)$, $p_3 = (4,3,8)$, $p_4 = (2,9,4)$, $p_5 = (7,5,3), p_6 = (6,1,8)$, $p_7 = (2,5,8), p_8 = (6,5,4)$ corresponding to the three rows & column vectors as wells as the two diagonals of $I^{>}$ which we have related to the cube-hexagon holographic systems in Fig. 6.

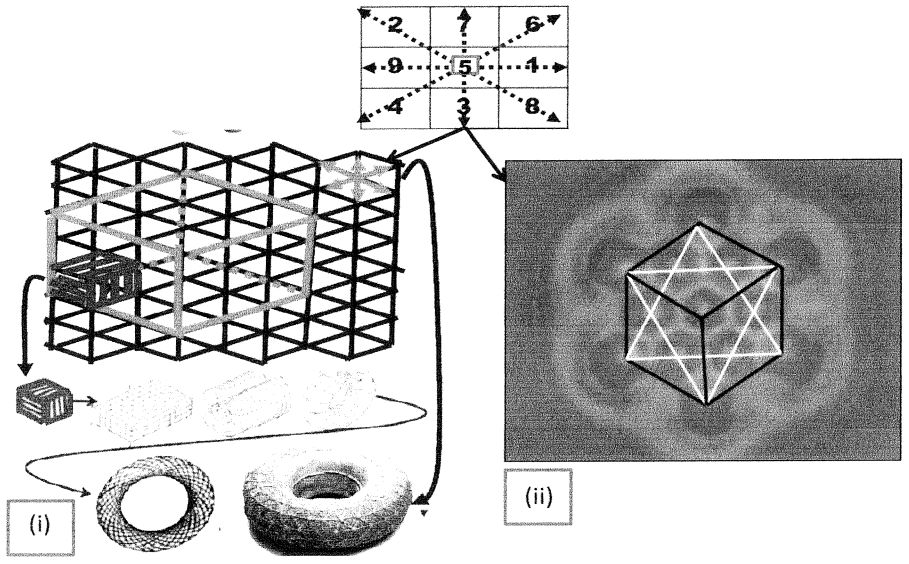

Fig. 6: Relation of the 3x3 magic square (above) to (i) Cube-hexagon holographic system and its topological folding into torus with cubic or hexagonal grids[see, ref.[10]), and to (ii) a cube-hexagon elaboration of the nanographene molecule with carbon-carbon bonds of different length and order imaged using the new technique by Gross et al[11].

The observation of the 4x4 square matrix pattern indicated in Fig.2 may now be regarded as an experimental justification for the mathematical identification of the generalized "units" in Eq.(2.11). This not only serves as a motivation for possible 10x10 matrix representation of geno-Bragg's law for cube-hexagon lattice in terms of magic square matrices in Fig. 7 but also for elaboration of Enistein's general relativity theory to geno-Einstein theory to which we now turn.

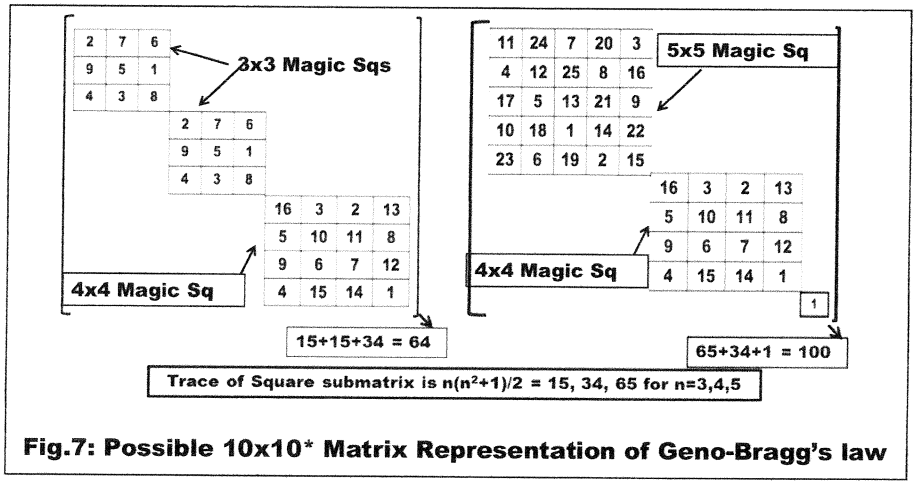

Fig.7: Possible 10x10* Matrix Representation of Geno-Bragg's law

3. GENO- EINSTEIN'S GENERAL RELATIVITY THEORY

It is well-known[12] that Einstein's general relativity field equation for the gravitational field has the form

$$G_{\mu\nu} \equiv R_{\mu\nu} - \tfrac{1}{2} R g_{\mu\nu} = -\kappa \Theta_{\mu\nu}, \qquad (3.1)$$

where $R_{\mu\nu\rho\sigma}$ is the curvature tensor defined by a metric tensor $g_{\mu\nu}$; and $R_{\mu\nu} = g^{\rho\sigma} R_{\mu\nu\rho\sigma}$ is the Ricci tensor with $R = g^{\rho\sigma} R_{\rho\sigma}$ and $\kappa = 8\pi G/c^4$; while $\Theta_{\mu\nu}$ is a *symmetric* energy-momentum tensor whose conservation is given by

$$\partial^{\nu} \Theta_{\mu\nu} = 0 \Rightarrow G_{\mu\nu,\nu} = 0 \qquad (3.2)$$

Because a straightforward addition of an *antisymmetric* electromagnetic field tensor $(F_{\mu\nu} = -F_{\nu\mu})$ to the underlying *symmetric* metric tensor $g_{\mu\nu}$, is trivially eliminated in quadric form of the line element, $g_{\mu\nu} dx^{\mu} dx^{\nu}$ in the classical O(3,1) theory, a progressive generalization of the classical theory is required.

In order to bring Einstein's general relativity theory within the purview of geno-Bragg's law[4] it is necessary to apply the characterization of the deformations of two Bragg angles in Eq.(2.5) to a differential deformation when the Bragg angles depend on a common local variable, such as the temperature of a (quaicrystalline) medium, by separating the expression for

$$\hat{\in}^{-} = (\theta_a / \theta_b - \theta_b / \theta_a)$$

into a pair of differential equation, or what is equivalent, lifting the transformation from a point-sphere into a torus in velocity space(cf Eqs.(2.6a,b) & (2.7a,b)) as follows:

$$0 = c^2 + \dot{r}^2 \equiv \begin{pmatrix} c & \dot{r} \end{pmatrix} \begin{pmatrix} 1 & 0 \\ 0 & 1 \end{pmatrix} \begin{pmatrix} c \\ \dot{r} \end{pmatrix}$$

$$\vdots$$

$$\rightarrow \begin{pmatrix} c & \dot{r} \end{pmatrix} \begin{pmatrix} 1 & -dc/d\dot{r} \\ -dc/d\dot{r} & -1 \end{pmatrix} \begin{pmatrix} c \\ \dot{r} \end{pmatrix} \equiv (c^2 - \dot{r}^2) - 2\frac{dc}{d\dot{r}} c\dot{r} = 0$$

$$\text{i.e.,} \quad \frac{d\dot{r}}{dc} = \frac{2c\dot{r}}{c^2 - \dot{r}^2} \tag{3.3a}$$

$$\therefore \Rightarrow \begin{cases} \dfrac{d\dot{r}}{d\beta} = 2\kappa c\dot{r} \\ \dfrac{dc}{d\beta} = \kappa(c^2 - \dot{r}^2) \text{ (Riccati's equation)} \end{cases} \tag{3.3b}$$

where c and $\dot{r}$ are treated as functions of a common local variable, such as the temperature parameter $\beta = 1/k_B T$. However, to re-interpret (3.3a) as geno-Bragg's law, it is necessary to characterize the slope $d\dot{r}/dc$ in $(c, \dot{r})$-space by angles in velocity space via the ("supersymmetric") transformation $(c, \dot{r}) \rightarrow (\vec{c}, \dot{\vec{r}}) \equiv (\vec{c}, \vec{v})$ generating a six-vector that defines an antisymmetric tensor analogous to Maxwell's electric and magnetic field vectors $(\vec{E}, \vec{B}) \leftrightarrow (\vec{c}, \vec{v})$. An effective speed of light($\hat{c}$) associated with the above "deformation" of the conventional Minkowski space is then determined by the following determinant equation:

$$\left\| \begin{pmatrix} \hat{c} & c_x & c_y & c_z \\ -c_x & -\hat{c} & v_z & -v_y \\ -c_y & -v_z & -\hat{c} & v_x \\ -c_z & v_y & -v_x & -\hat{c} \end{pmatrix} \right\| \equiv \hat{c}^4 + (\vec{c}^2 - \vec{v}^2)\hat{c}^2 - (\vec{c}.\vec{v})^2 = 0. \tag{3.4a}$$

As a consequence, if we define a deformation index, $\hat{c}/c_0 \equiv n$, so as to recover Einstein's special relativity principle in the form

$$\vec{c}^{\,2} - \vec{v}^{\,2} = c_0^2 \qquad (3.4b)$$

we then deduce from Eq.(3.4a) a new representation of Eq.(3.3a) in the form:

$$\tfrac{1}{2}\frac{dv}{dc} = \frac{\vec{c}.\vec{v}}{\vec{c}^{\,2} - \vec{v}^{\,2}} = \tfrac{1}{2}n^2(n^2+1) = F(n)$$
$$= 1, 10, 45, 136, 325, 666 \qquad (3.5)$$

corresponding to the Bragg angles $\theta_n = 2\pi/n$, for n=1, 2, 3, 4, 5, 6. Such a quartic expression $F(n)$ may be said to define a *geno-Higg'sfunction* that characterizes the standard cubic form $\partial F_{\pm}/\partial n \equiv F_{\pm}^{'}(n) \sim n^3 + An + B = 0$ of "cusp catastrophe" manifold[13], underlying Higg's ϕ^4 field[14] for mass generation through spontaneous symmetry breaking, where(for n=1,2,3,4,5)

$$\partial F(n)/\partial n \sim n^3 + An + B = \tfrac{1}{2}n(n^2+1) = 1, 5, 15, 34, 65. \qquad (3.6)$$

correspond to the traces of the respective *nxn* magic squares. Consequently, as earlier suggested with respect to the experimental observation in Fig. 2 and Table1, Eq.(3.6) provides a possible realization of 10x10 representation of the underlying geno-Bragg's law for a cube-hexagon lattice structure in terms of magic square matrices as indicated earlier in Fig. 7..

In terms of masses, we replace Eq(3.4a) by

$$\left\| \begin{pmatrix} \hat{m} & m_{cx} & m_{cy} & m_{cz} \\ -m_{cx} & -\hat{m} & m_{vz} & -m_{vy} \\ -m_{cy} & -m_{vz} & -\hat{m} & m_{vx} \\ -m_{cz} & m_{vy} & -m_{vx} & -\hat{m} \end{pmatrix} \right\| \equiv \hat{m}^4 + (\vec{m}_c^{\,2} - \vec{m}_v^{\,2})\hat{m}^2 - (\vec{m}_c.\vec{m}_v)^2 = 0. \quad (3.7)$$

$$n^4 + n^2\left(\frac{\vec{m}_c^{\,2} - \vec{m}_v^{\,2}}{m_0^2}\right) = \frac{(m_c m_v)^2}{m_0^2}., \text{ with } \frac{\hat{m}}{m_0} = n \qquad (3.8)$$

which reduces when we put $\vec{m}_c^{\,2} - \vec{m}_v^{\,2} = \pm m_0^2$ (allowing $\pm$ signs)to the expression:

$$\frac{(\vec{m}_c\vec{m}_v)}{m_0^2} \equiv \frac{\vec{m}_c}{m_0}.\frac{\vec{m}_v}{m_0} = \tfrac{1}{2}n^2(n^2 \pm 1) = F_{\pm}(n)$$
$$\equiv \begin{matrix} + \\ - \end{matrix}\begin{cases} 1, 10, 45, 136, 325, 666 & \text{for n} = 1,...,6 \\ 0, 9, 36, 120, 300, 630, & \text{for n} = 1,...,6 \end{cases} \qquad (3.9)$$

We observe that for n=1, the negative sign characterizes a massless particle (which may be identified with the Goldstone boson) while the positive sign characterizes massive particles related by the formula:

$$m_p m_\mu = m_0^2 \equiv (m_n/3)^2 \qquad (3.10)$$

which is satisfied by the neutron mass, $m_n = 940\ MeV/c^2$, proton mass $m_p = 938\ MeV/c^2$, and the muon mass, $m_\mu = 106\ MeV/c^2$. The realization of the n = 2 positive sign and the implication for geno-renormalization of mass has been discussed in ref.[4]..

It is of interest to observe that the other values of n in Eq,(3.9), characterize Hawking's expression for the entropy of a black hole given, according to Jeremy Dunning-Davies[15], by

$$S = k_B M^2/\sigma_m \qquad (3.11)$$

where, $\sigma_m = (c\hbar/G)^{1/2} = 2\text{x}105(\text{gm}) \equiv n(n^2-1)\,(\text{gm})$ for $n = 6$, and M is the irreducible mass of the black hole.

Furthermore, a progressive generalization to an O(4,2) (conformal including scale) invariant theory requires, by analogy with Eq.(2.3), the incorporation of a dilatation and conformal currents,

$$D_\mu = x^\nu \Theta_{\mu\nu};\quad K_{\mu\nu} = (2x_\mu x_\lambda - g_{\mu\lambda}x^2)\Theta_\nu{}^\lambda \qquad (3.12)$$

in the definition of a geno-Einstein field tensor

$$\|G_{\mu\nu}\| \equiv \begin{pmatrix} 0 & \Theta_{01} & \Theta_{02} & \Theta_{03} \\ -\Theta_{01} & 0 & D_3 & -D_2 \\ -\Theta_{02} & -D_3 & 0 & D_1 \\ -\Theta_{03} & D_2 & -D_1 & 0 \end{pmatrix} \qquad (3.13)$$

so that

$$\partial^\mu D_\mu = \Theta_{\mu\mu} = 0;\ \partial^\nu K_{\mu\nu} = x^\delta \Theta_{\mu\mu} = 0; \qquad (3.14a)$$

$$\text{Det}\,\|G_{\mu\nu} - \lambda\eta_{\mu\nu}\| \equiv \lambda^4 - (R_{\mu\nu\rho\sigma}G^{\mu\rho}G^{\nu\sigma})\lambda^2 + (\in_{\mu\nu\rho\sigma} G^{\mu\rho}G^{\nu\sigma})^2 = 0, \qquad (3.14b)$$

where $\|\eta_{\mu\nu}\| \equiv diag(+1,-1,-1,-1)$. The analog of geno-Bragg's law becomes

$$R_{\mu\nu\rho\sigma}G^{\mu\rho}G^{\nu\sigma} - 2 \in_{\mu\nu\rho\sigma} G^{\mu\rho}G^{\nu\sigma} = \begin{cases} \mathbf{J}^2 \\ \mathbf{B}^2 \end{cases} \Rightarrow \begin{cases} \mathbf{J}^2 - \mathbf{B}^2 \pm 2\mathbf{B}.\mathbf{J} = 0 \\ \mathbf{B}^2 - \mathbf{J}^2 \pm 2\mathbf{J}.\mathbf{B} = 0 \end{cases} \qquad (3.15)$$

under the dual transformation $(\mathbf{J} \to \mathbf{B},\ \mathbf{B} \to -\mathbf{J})$. Consequently, such an interpretation of geno-Einstein's tensor relating it to geno-Bragg's law leads to a natural realization of geno-Einstein's equation in London's superfluid model of a superconductor (p.412-414 of ref.[16]) in terms of Feynman's wavefunction (Anderson[17]) for a superfluid in which the superfluid velocity **J** is given in the presence of an electromagnetic vector potential, **A**, by the London equation:

$$\mathbf{J} = -(2e\hbar/mc)\mathbf{A}, \quad \mathbf{B} = \mathrm{curl}\mathbf{A} \equiv \mathrm{curl}(\zeta\mathbf{J}), \quad \zeta = (mc/2|e|\hbar) \quad (3.16)$$

which leads to the Meissner effect in a superconductor (p. 412 of ref.[16]).

Moreover, we could express the conformal current for the geno-Einstein's tensor (3.13), in the form

$$K_\mu \equiv x^\nu (M_{\mu\nu} + g_{\mu\nu} D), \qquad (3.16)$$

where $M_{\mu\nu} = x_\mu p_\nu - x_\nu p_\mu$, and observe that it is the real space analog of Maxwell's equation

$$J_\mu = \partial^\mu (F_{\mu\nu} - g_{\mu\nu}\varphi) \qquad (3.17)$$

where $\varphi \equiv \partial^\rho A_\rho = 0$ in London gauge, to arrive at the corresponding relations:

$$0 = x^\mu K_\mu \Leftrightarrow \partial^\mu J_\mu = 0 \qquad (3.18)$$

between algebraic geometric elements (points, line and planes) of geno-Einstein's (space-time) geometry and the physical variables (particle, fields and currents) of Maxwell-type lattice gauge field, as envisaged in LOOP quantum gravity[18].

Finally, in order to avoid the restriction of scale and conformal invariance to massless fermion fields in (Lorentz-invariant) O(3,1) theory, one needs to replace the Dirac current $J_\mu = \gamma_\mu$ for fermions by a tensor current,

$$K_{\mu\nu} \Leftrightarrow J_{\mu\nu} \equiv \gamma_\mu \gamma_\nu + M^{-1}(\gamma_\mu p_\nu + p_\nu \gamma_\nu) \qquad (3.19)$$

where $J_{0\mu}$ is the most general parity-conserving current in the O(4,2) algebra of Dirac's γ – matrices, and M is a 3x3 mass matrix charactering an SU(3) triplet, so that, for coupling to U(1) gauge field, A^μ, of the minimal form $J_{0\mu}A^\mu$, geno-Einstein's field theory is indeed a cube-hexagon $O(4,2)\times SU(3)\times U(1)$ lattice gauge theory, for which scale invariance ($\partial^\mu D_\mu = \Theta_{\mu\mu} = 0$) and conformal invariance for scale invariance $(\partial^\nu K_{\mu\nu} = 2x_\lambda \Theta_\nu{}^\lambda = 0)$ are non-trivial.

4. DISCUSSION AND CONCLUSION

.In this paper, we have shown how the elaboration of the conventional Bragg's law of diffraction to geno-Bragg's law in order to account for the observed diffraction patterns of cube-hexagon quasicrystal structures and a conical glass of water .could be applied to the reconstruction of Einstein's general relativity theory as a lattice gauge theory under the title "geno-Einstein's general relativity theory. Taken together with the heuristic application gravitational lensing and to geno-mass renormalization in ref 4, we conclude that further investigation of the implications of geno-Einstein's theory deserves attention.

Acknowledgements

The author wishes to acknowledge the support of the Santilli Foundation and for stimulating correspondence with Professor Christian Corda.

REFERENCES

[1] D. Shechtman, I. blech, D. Gratias and J.W. Cahn, Metallic phase with long-range orientational order and no translational symmetry, Phys. Rev. Lett. 53[20] 1951-1954 (1984); See also C. Pay-Gomez, S. Lidin (2001) — Structure of $Ca_{13}Cd_{76}$: a novel approximant to the MCd5.7 quasicrystals‖, *Angewandte Chemie* ***40, pp***4037-4039

[2] L. Pauling, "Apparent icosahedral symmetry is due to directed multiple twinning of cubic crystals," *Nature* 317 (1985) 512; International Union of Crystallography, "Report of the executive committee for 1991,"*Acta Cryst. A* 48, 922 (1992); see p. 928.

[3] A.O.E. Animalu made this observation at the reception dinner at the International Conference on Numerical Analysis and Applied Mathematics (ICNAM), Kos, Greece (2012).

[4] A.O.E. Animalu Geno-Bragg's Law and 10*x10 Representation of the SU(3) Symmetry of Quasicrystal Structures, Journal of Computational Methods in Science and Engineering, **13**, 1-17 (2013).

[5] R.M. Santilli, Rendiconti Circolo Matematico di Palermo, Supplemento **42**, 7 (1996); see also R.M. Santilli, R. M. Santilli, Nuovo Cimento **51**, 570 (1967), available in free download from the link
http://www.santilli-foundation.org/docs/Santilli-54.pdf;
and also R.M. Santilli, Hadronic J. 1, 574 (1978);
R.M. Santilli, Lie-admissible invariant representation of irreversibility for matter and antimatter at the classical and operator levels, Nuov. Cim **B121,** 443 (2006) available in free pdf download from
http://www.santilli-foundation.org/docs/Lie-admiss-NCB-I.pdf;
See also R.M. Santilli, Elements of Hadronic Mechanics, Vols. I and II (Ukraine Academy of Sciences, Kiev. 2nd edition 1995 available at
http://www.santilli-foundation.org/docs/Santilli-300.pdf
http://www.santilli-foundation.org/docs/Santilli-301.pdf

[6] Anil A. Bhalekar, Santilli's Revelation of Four Directions of Arrows of Time to be presented at ICNAAM 2013, Rhodes, Greece, 21-26 September 2013

[7] G. Zweig, *Origins of the Quark Model*, DOE R & D Report(CALT-68-805) (1980); M. Gell-Mann and Y. Ne'eman, cited in Y. Ne'eman *Algebraic Theory of Particle Physics* (W.A.Benjamin,1963) p. 31

[8] Paul-Saul Sirag *Group Theoretical Aspects of the Meru Project* (Meru Foundation Rev. 1.0, Dec. 1989.

[9] E.G. Phillips, Functions of A Complex Variable with Applications (Oliver & Boyd, Edingburgh & London, N.Y.: Interscience Publishers Inc) p. 50 (1958)

[10] Leo Gross, Fabian Mohn, Enrique Guitián, Diego Peña, Nikolaj Moll, Bruno Schuler, André Gourdon, Alejandro Criado, Gerhard Meyer, **Bond-Order Discrimination by Atomic Force Microscopy**, *Science* **337**, 1326 (2012

[11] AO.E. Animalu and C. Acholonu, Hyperspace and the Torus Revisited, *An African perspective of the Theory of Everything*, African J. of Physics Vol. 3,30-50 (2010); M. Kaku *Hyperspace: A Scientific Odyssey Through Parallel Universes, Time Warps, and the 10th Dimension*

[12] T. Frankel, Gravitational Curvature; An Introduction to Einstein's Theory (W.H. Freeman & Co, San Fransisco) (1979) A. Einstein, Relativity The Special & the General Theory (University Paperbacks, U.P. 10) (Methuen: London)

[13] J. Guckenheimer and P.Holmes, Nonlinear Oscillations, Dynamical Systems. And Bifurcations of Vector Fields (Springer-Verlag, 1986); T. Poston and I. Stewart, Catastrophe Theory and its Applications (Pitman, London 1978) p. 174

[14] P Higgs, Phys. Rev Lett 13, 508 (1964).

[15] Jeremy Dunning-Davies in *Black Holes and Their Entropy,* Hadronic J. Vol. 34, p. 109-124 (2011).

[16] A.O.E. Animalu, Intermediate Quantum Theory of Crystalline Solids (Prentice-Hall) (1977).

[17] P.W. Anderson, How Josephson Discovered his Effect , Physics Today p. 23-29.November (1970); A.O.E. Animalu, Josephson Current in Tunneling Between Coupled Superconductors, Phys. Rev. B 8, 4420-4421 (1973).

[18] A. Ashtekar (2008) "Loop Quantum Cosmology: An Overview' Gen. Rel. Gravt. 41:707-741, 2009.arXiv:gr-qc0812.0177

DYNAMIC ISO-TOPIC LIFTING WITH APPLICATION TO FIBONACCI'S SEQUENCE AND MANDELBROT'S SET

Nathan O. Schmidt
Department of Mathematics, Boise State University
1910 University Drive
Boise, ID 83725 USA
nathanschmidt@u.boisestate.edu

Received October 23, 2013

Abstract

In this exploration, we introduce and define "dynamic iso-spaces", which are cutting-edge iso-mathematical constructions that are built with "dynamic iso-topic liftings" for "dynamic iso-unit functions". For this, we consider both the continuous and discrete cases. Subsequently, we engineer two simple examples that engage Fibonacci's sequence and Mandelbrot's set to define a "Fibonacci dynamic iso-space" and a "Mandelbrot dynamic iso-space", respectively. In total, this array of resulting iso-structures indicates that a new branch of iso-mathematics may be in order.

Keywords: Geometry and topology; Santilli iso-number; Santilli iso-space; Dynamic iso-space; Fractal geometry; Fibonacci sequence; Mandelbrot set.

Copyright © 2013 by Hadronic Press, Inc., Palm Harbor, FL 34684, USA

1 Introduction

A *gigantic* problem of pure mathematics, in the context of number theory, is to establish a *universal* number classification system for describing the physical laws of nature, such as the identification of all sets that occur with numeric field axioms. During his relentless pursuit of this problem, scientific pioneer R.M. Santilli successfully circumvented the original five number field axioms [1] to create the new field of iso-mathematics [2, 3, 4, 5], which became the foundation of hadronic mechanics [6].

Since its initiation, Santilli's iso-mathematics [2, 3, 4, 5] has continued to gain momentum in application and popularity, but this emergent discipline is—to say the least—*vast*, relatively adolescent, and is currently not considered to be "mainstream" in the community of science, technology, engineering, and mathematics. Therefore, the iso-mathematics realm remains largely unexplored, with unknown bounds on its utilization potential.

In this paper, we venture into iso-mathematics [2, 3, 4, 5] by considering iso-spaces that systematically *change*. In Section 2, we introduce the notion of *dynamic iso-topic liftings* by assembling definitions for *continuous dynamic iso-spaces* and *discrete dynamic iso-spaces*. Afterwards, we give two examples that demonstrate how dynamic iso-spaces can be lifted for fractal structures in Section 3. Finally, we conclude our exploration with Section 4, where we recapitulate the results with brief discussion and outlook on future modes of research.

2 Dynamic iso-spaces

Here, we introduce and define the dynamic iso-space with its dynamic iso-topic lifting. For this, we follow Santilli's methodology [2, 3, 4, 5] and consider the following procedure:

1. Let S be a space.

2. Let $S_{\hat{t}}$ be an iso-space that results from the iso-topic lifting $S \to S_{\hat{t}}$ for the iso-unit $\hat{t} > 0$ with the corresponding inverse $\hat{\tau} = \frac{1}{\hat{t}} > 0$, such that
$$\begin{aligned} f(\hat{t}): \quad S \quad &\to \quad S_{\hat{t}} \\ f^{-1}(\hat{t}): \quad S_{\hat{t}} \quad &\to \quad S, \end{aligned} \tag{1}$$
so clearly S and $S_{\hat{t}}$ are locally iso-morphic.

3. **Dynamic iso-space.** Now, we wish to show that $S_{\hat{t}}$ is an iso-space that is characterized by constant change, meaning that $S_{\hat{t}}$ is a dynamic iso-space. Hence, we will show that $S_{\hat{t}}$ varies in accordance to some function; here, this positive-definite function will serve as the *dynamic iso-unit* that varies because its parameter varies.

4. Thus, let $r > 0$ be the parameter that varies as $r \to \infty$ for the *generic form* of the *dynamic iso-unit function*

$$\hat{t} \equiv \hat{\delta}(r) > 0, \ r \to \infty, \tag{2}$$

to consequently define the dynamic iso-space

$$S_{\hat{t}} \equiv S_{\hat{\delta}(r)}. \tag{3}$$

5. **Continuous dynamic iso-space.** First, we will show that the $S_{\hat{\delta}(r)}$ of eq. (3) can be rewritten and defined as a *continuous* dynamic iso-space if its corresponding dynamic iso-unit function is continuous as its parameter r varies; for this, the constraint is that r must take on the values of an infinite continuous sequence of positive-definite numbers. Hence, for example, if $\mathbb{R}^+$ is the set of all positive-definite real numbers, then let $r \in \mathbb{R}^+$ be the positive-definite, real-valued, varying parameter for the *continuous dynamic iso-unit function*

$$\hat{t} \equiv \hat{\delta}_{\mathbb{R}^+}(r) \equiv 2\pi r > 0, \ r \in \mathbb{R}^+, \ r \to \infty_{\mathbb{R}^+}, \tag{4}$$

to consequently define the continuous dynamic iso-space

$$S_{\hat{t}} \equiv S_{\hat{\delta}_{\mathbb{R}^+}(r)}, \tag{5}$$

where we rewrite eq. (1) to encompass the continuous dynamic structure of eqs. (4–5) as

$$\begin{array}{rccc} f(\hat{\delta}_{\mathbb{R}^+}(r)): & S & \to & S_{\hat{\delta}_{\mathbb{R}^+}(r)} \\ f^{-1}(\hat{\delta}_{\mathbb{R}^+}(r)): & S_{\hat{\delta}_{\mathbb{R}^+}(r)} & \to & S \end{array} \tag{6}$$

so S and $S_{\hat{\delta}_{\mathbb{R}^+}(r)}$ remain locally iso-morphic as $r \to \infty_{\mathbb{R}^+}$. Note that the 2π circumference scaling of eq. (4) is arbitrary for this example, as we can make eq. (4) anything we want as long as the resulting iso-unit $\hat{t}$ is positive-definite and varies continuously as $r \to \infty_{\mathbb{R}^+}$.

6. **Discrete dynamic iso-space.** Second, we will show that the $S_{\hat{\delta}(r)}$ of eq. (3) can be rewritten and defined as a *discrete* dynamic iso-space if its corresponding dynamic iso-unit function is discrete as its parameter r varies; for this, the constraint is that r must take on the values of an infinite discrete sequence of positive-definite numbers. Hence, for example, if $\mathbb{N}$ is the set of all natural numbers (positive integers), then let $r \in \mathbb{N}$ be the positive-definite, natural-valued, varying parameter for the *discrete dynamic iso-unit function*

$$\hat{t} \equiv \hat{\delta}_{\mathbb{N}}(r) \equiv 2\pi r > 0,\ r \in \mathbb{N},\ r \to \infty_{\mathbb{N}}, \tag{7}$$

to consequently define the discrete dynamic iso-space

$$S_{\hat{t}} \equiv S_{\hat{\delta}_{\mathbb{N}}(r)}, \tag{8}$$

where we rewrite eq. (1) to encompass the discrete dynamic structure of eqs. (7–8) as

$$\begin{array}{rccc} f(\hat{\delta}_{\mathbb{N}}(r)): & S & \to & S_{\hat{\delta}_{\mathbb{N}}(r)} \\ f^{-1}(\hat{\delta}_{\mathbb{N}}(r)): & S_{\hat{\delta}_{\mathbb{N}}(r)} & \to & S \end{array} \tag{9}$$

so S and $S_{\hat{\delta}_{\mathbb{N}}(r)}$ remain locally iso-morphic as $r \to \infty_{\mathbb{N}}$. Again, note that the 2π circumference scaling of eq. (7) is arbitrary for this example, as we can make eq. (7) anything we want as long as the resulting iso-unit $\hat{t}$ is positive-definite and varies discretely as $r \to \infty_{\mathbb{N}}$.

At this point, the results of eqs. (1–9) indicate the existence of a new family of iso-spaces called dynamic iso-spaces, where a member of this family (continuously or discretely) deforms in accordance to Santilli's topological-preservations as r varies. Hence, we establish the following:

Lemma 1. *A space S is locally iso-morphic to the dynamic iso-space $S_{\hat{\delta}(r)}$ under the topologically-preserving dynamic iso-topic lifting $S \to S_{\hat{\delta}(r)}$ for the dynamic iso-unit function $\hat{\delta}(r) > 0$ with inverse $\hat{\delta}^{-1}(r) = \frac{1}{\hat{\delta}(r)} > 0$, where the positive-definite parameter r varies indefinitely.*

Lemma 2. *A dynamic iso-space $S_{\hat{\delta}(r)}$ is a continuous dynamic iso-space if the dynamic iso-unit function $\hat{\delta}(r)$ is continuous as its parameter r varies.*

Lemma 3. *A dynamic iso-space $S_{\hat{\delta}(r)}$ is a discrete dynamic iso-space if the dynamic iso-unit function $\hat{\delta}(r)$ is discrete as its parameter r varies.*

3 Application Examples

Here, we provide two short examples that engage the dynamic iso-space concept. For this, we opt that both applications include fractals.

3.1 Fibonacci dynamic iso-space

First, we introduce and define a Fibonacci dynamic iso-space, which is a specific type of discrete dynamic iso-space. The well-known Fibonacci sequence is [7]

$$F = \{0, 1, 1, 2, 3, 5, 8, ...\}. \tag{10}$$

Hence, we identify the nth Fibonacci number in the sequence F with the "Fibonacci function" $F(n)$, which returns the initial values

$$\begin{array}{l} F(0) = 0,\ F(1) = 1,\ F(2) = 1,\ F(3) = 2,\ F(4) = 3, \\ F(5) = 5,\ F(6) = 8,\ \ldots\ . \end{array} \tag{11}$$

Now suppose that we begin with the positive-definite $r = F(1)$ and let $r \in F - \{0\}$ discretely varies or "jumps" according to Fibonacci's eqs. (10–11)—so in this Fibonacci case, as $r \to \infty_{Fib}$, r takes on only Fibonacci numbers (excluding zero), which satisfies the discrete iso-unit constraints that $F - \{0\}$ must be an infinite discrete sequence positive-definite numbers. Thus, the discrete dynamic iso-unit function of eq. (7) can be rewritten to define the *Fibonacci dynamic iso-unit function* as

$$\hat{t} \equiv \hat{\delta}_{Fib}(r) \equiv 2\pi r > 0,\ r \in F - \{0\},\ r \to \infty_{Fib}, \tag{12}$$

to consequently define the Fibonacci dynamic iso-space

$$S_{\hat{t}} \equiv S_{\hat{\delta}_{Fib}(r)} \tag{13}$$

with the Fibonacci dynamic iso-topic liftings

$$\begin{array}{rrcl} f(\hat{\delta}_{Fib}(r)): & S & \to & S_{\hat{\delta}_{Fib}(r)} \\ f^{-1}(\hat{\delta}_{Fib}(r)): & S_{\hat{\delta}_{Fib}(r)} & \to & S. \end{array} \tag{14}$$

Here, we observe that $\hat{t}$ strictly acquires "Fibonacci circumference" values for the dynamic lifting because r is always treated as a "Fibonacci radius", which indicates that $S_{\hat{\delta}_{Fib}(r)}$ iteratively deforms as $r \to \infty_{Fib}$, where S and $S_{\hat{\delta}_{Fib}(r)}$ remain locally iso-morphic.

At this point, we've completed our first fractal example because we've successfully defined a Fibonacci dynamic iso-space.

3.2 Mandelbrot dynamic iso-space

Second, we introduce and define a Mandelbrot dynamic iso-space, which is a specific type of discrete dynamic iso-space because we obtain each value, one-by-one, as we systematically generate Mandelbrot's set by iterating his complex quadratic polynomial [8, 9]

$$z_{n+1} = z_n^2 + c, \tag{15}$$

where $z_n, z_{n+1}, c \in \mathbb{C}$ are complex numbers. Thus, imagine that we select some c and z_0 and continuously iterate eq. (15) to obtain the discrete Mandelbrot sequence

$$M = \{z_0, z_1, z_2, z_3, z_4, z_5, ...\}. \tag{16}$$

Hence, similarly to the Fibonacci case of eq. (11), we identify the nth Mandelbrot number in the sequence M with the "Mandelbrot function" $M(n)$ that depends on c, which returns the initial values

$$\begin{aligned} &M(0) = z_0,\ M(1) = z_1,\ M(2) = z_2,\ M(3) = z_3,\ M(4) = z_4, \\ &M(5) = z_5,\ \ldots\ . \end{aligned} \tag{17}$$

Now we need positive-definite values for our dynamic iso-units, so how do we translate the *complex-valued* (and possibly negative-valued) results of Mandelbrot's eq. (17) as we did to Fibonacci's eq. (11)? Well, there are multiple ways to approach this rich problem, so honestly at this point it is a matter of preference. Thus, for the sake of example simplicity, we opt to use the real-valued modulus

$$|z_n| = \sqrt{z_{n_{\mathbb{R}}}^2 + z_{n_{\mathbb{I}}}^2} \tag{18}$$

for the nth iterate of eq. (17) because it is positive-definite. Consequently, we list the moduli of eqs. (16) and (17) as

$$M_{Mod} = \{|z_0|, |z_1|, |z_2|, |z_3|, |z_4|, |z_5|, ...\} \tag{19}$$

and

$$\begin{array}{rcl} M_{Mod}(0) & = & |z_0|,\ M_{Mod}(1) = |z_1|,\ M_{Mod}(2) = |z_2|,\ M_{Mod}(3) = |z_3|, \\ M_{Mod}(4) & = & |z_4|,\ M_{Mod}(5) = |z_5|,\ \ldots\ , \end{array} \tag{20}$$

respectively.

Next, suppose that we begin with the positive-definite $r = M_{Mod}(0)$ and let $r \in M_{Mod}$ discretely vary according to Mandelbrot's moduli of eqs. (19–20)—so in this selected Mandelbrot case, as $r \to \infty_{Man}$, r takes on only the moduli of Mandelbrot numbers, which satisfies the discrete iso-unit constraints that M_{Mod} must be an infinite discrete sequence of positive-definite numbers. Thus, the discrete dynamic iso-unit function of eq. (7) can be rewritten to define the *Mandelbrot dynamic iso-unit function* as

$$\hat{t} \equiv \hat{\delta}_{Man}(r) \equiv 2\pi r > 0,\ r \in M_{Mod},\ r \to \infty_{Man}, \tag{21}$$

to consequently define the Mandelbrot dynamic iso-space

$$S_{\hat{t}} \equiv S_{\hat{\delta}_{Man}(r)} \tag{22}$$

with the Mandelbrot dynamic iso-topic liftings

$$\begin{array}{rccc} f(\hat{\delta}_{Man}(r)): & S & \to & S_{\hat{\delta}_{Man}(r)} \\ f^{-1}(\hat{\delta}_{Man}(r)): & S_{\hat{\delta}_{Man}(r)} & \to & S. \end{array} \tag{23}$$

Here, we observe that $\hat{t}$ strictly acquires "Mandelbrot circumference" values for the dynamic lifting because r is always treated as a "Mandelbrot radius", which indicates that $S_{\hat{\delta}_{Man}(r)}$ iteratively deforms as $r \to \infty_{Man}$, where S and $S_{\hat{\delta}_{Man}(r)}$ remain locally iso-morphic.

At this point, we've completed our second fractal example because we've successfully defined one version of a Mandelbrot dynamic iso-space.

4 Conclusion

The results of this work include original definitions and lemmas for continuous and discrete dynamic iso-spaces, and example constructions of Fibonacci and Mandelbrot dynamic iso-spaces. These dynamic iso-spaces may serve as important tools for future analysis and exploration. But there is still much work to do, as we must continue to relentlessly scrutinize, challenge, and upgrade this emerging framework via the scientific method. In particular, we suggest that in order to test the validity of our results and advance the general capability and applicability of these dynamic iso-systems to subsequent levels, a thorough and rigorous iso-mathematical investigation should be conducted along this research trajectory. For this, we must prove the said lemmas and expand the framework by instantiating additional pertinent families of dynamic iso-structures, and furthermore the dynamic geno-structures, dynamic hyper-structures, and dynamic iso-dual-structures.

References

[1] A. Cayley. *The Collected Mathematical Papers of Arthur Cayley...*, volume 6. The University Press, 1893.

[2] R. M. Santilli. Isonumbers and genonumbers of dimensions 1, 2, 4, 8, their isoduals and pseudoduals, and "hidden numbers" of dimension 3, 5, 6, 7. *Algebras, Groups and Geometries*, 10:273, 1993.

[3] R. M. Santilli. Rendiconti circolo matematico di palermo. *Supplemento*, 42:7, 1996.

[4] C. X. Jiang. Fundaments of the theory of Santillian numbers. *International Academic Presss, America-Europe-Asia*, 2002.

[5] C. Corda. Introduction to Santilli iso-numbers. In *AIP Conference Proceedings-American Institute of Physics*, volume 1479, page 1013, 2012.

[6] R. M. Santilli. Hadronic mathematics, mechanics and chemistry. *Volume I, II, III, IV, and V, International Academic Press, New York*, 2008.

[7] P. Singh. The so-called Fibonacci numbers in ancient and medieval India. *Historia Mathematica*, 12(3):229–244, 1985.

[8] B. B. Mandelbrot. *The fractal geometry of nature*. Times Books, 1982.

[9] B. B. Mandelbrot. *Fractals and chaos: the Mandelbrot set and beyond*, volume 3. Springer, 2004.

ACTIVE SITES, COMPLEXITY STRUCTURES AND HYPERSTRUCTURES IN CATALYSTS

M. Piumetti
Department of Applied Science and Technology
Politecnico di Torino, 10129 Torino, Italy
marco.piumetti@polito.it
N. Lygeros
LGPC (UMR 5285), Université de Lyon
69616, Villeurbanne, France
nlygeros@gmail.com

Received October 20, 2013

Abstract

This paper focuses on the problem of active sites in heterogeneous catalysis through a review based on three examples from the literature, namely metal nanoparticles, zeolites and transition metal oxides (redox MvK-type mechanism). Self-organizing phenomena in catalysis may reflect various complexity structures, including the self-repair and reorganization of active sites, the mutual interactions between neighbouring sites, the mass transfer limitations (i.e. shape selective control), the dynamic active networks of "sites-joined", and so on. These phenomena may give rise to non-linear dynamics in catalytic processes. The latter typically result in a non-linear combination of distinct complexity structures and hence catalytic behaviours may appear with multicomponent systems, as zeolites and mixed oxides. Thus, the algebraic hyperstructures are introduced as a model to describe the complexity of catalysis. The solid catalyst acts as a hyperoperator computing a non-linear combination of complexity structures, namely multivalued operation ($\circ$). This hyperoperation is weak associative since the complexity structures (sets) contain the n-polytopes as common elements. As a result, the complexity structures in catalysis belong to Hv-structures, the largest class of hyperstructures which satisfy the weak properties.

Keywords: Catalytically active sites; self-organizing phenomena; complexity structures; hyperstructures; Hv-structures.

Copyright © 2013 by Hadronic Press, Inc., Palm Harbor, FL 34684, USA

1 Introduction

The active sites represent the "heart" of a catalyst and hence it is not surprising that a large number of theoretical studies and experiments in the field of heterogeneous, homogeneous and enzymatic catalysis focus on the characterisation of active centres present on the catalyst surface.

In recent years, considerable progress has been made in the characterization of catalytic reactions at solid surfaces. Indeed, thanks to the development of *in-situ* spectroscopies and to advanced scanning probe techniques, it has been possible to study active sites under working conditions and to investigate the elementary processes underlying a reaction on an atomic scale [1]. As a result, many investigations have confirmed that active sites are dynamic entities that can continuously change their physico-chemical properties depending on the reaction conditions [1,2]. Dynamic STM analysis also revealed that active centers may include more than one single site to form "reactive networks" [3-5].

A "real" catalyst surface is structurally and compositionally complex and multifunctional interface, exposing various adsorption/reaction sites. Thus, the surface properties have their relevant consequences on the chemical reactivity [6,8]. Moreover, there is an important aspect contributing to the gap between surface science and catalysis, that is related to the reaction mechanism and can be denoted as "chemical complexity". Catalytic reactions may involve mixtures of several reactants and/or intricate reaction networks with multiple steps and pathways [9,10]. Typically, the more complex the reaction mechanism, the slower the turnover rate as the elementary reaction steps involve more complex molecular rearrangements [11]. The catalyst has to regenerate itself through the desorption of products and the self-repair of active sites after each catalytic cycle.

During a reaction, the catalyst surface typically receives a mix of fluctuating molecules (i.e. reactants, products, poisons, etc.) and hence many active centres (or regions) on the surface may interact with each other through mass/heat transport phenomena and surface strain [2,7]. This suggests that solid catalysts operate through sophisticated self-organizing phenomena, in which both structural parameters and kinetic effects play a role [6].

The concept of "self-organization" indicates the order formation in both thermodynamically closed and open chemical systems [2]. Closed systems tend to reach the equilibrium conditions by reducing their free energy,

although kinetic constrains may limit the attainment of equilibrium. On the contrary, open systems far from the equilibrium (i.e. reactions at steady-state flow conditions) exhibit the interaction between chemical kinetics and transport phenomena. Moreover, there is an unexpected relation between the chemical kinetics and the space-time structures of reaction systems. These systems belong to the class of irreversible processes creating entropy and may be described through kinetic equations with broken time symmetry instead of canonical equations [12].

Non-equilibrium systems were first studied by I. Prigogine [13] who denoted them as "dissipative structures" and were later incorporated in the framework of synergetics by H. Haken [14]. Specifically, Prigogine showed the complexity of time in non-equilibrium systems, through the concepts of symmetry breaking, irreversibility and time's arrow. Consequently, catalytic reactions cannot be reduced to classical dynamics or quantum mechanics in deterministic, time-reversible descriptions [12]. However, it is impossible to know exactly the spatio-temporal self-organizing phenomena occurring in systems far from equilibrium due to fundamental limitations having their origins in the mathematical structures [8]. Noteworthy, the causality condition on a space-time appears inaccessible by strictly deterministic processes and the complexity of time is still greater than one can imagine in a linear framework.

Such effects have been experimented with CO oxidation over Pt single crystal surfaces by G. Ertl [2,8,16]. Indeed, under certain external conditions (i.e. p_{CO} and temperature) the Pt surface can alternate between two states, showing regular oscillations in reaction rates. However, at high CO pressure values ($p_{CO} > 5 \cdot 10^{-5}$ mbar) a new irregular behaviour occurs, giving rise to chaotic phenomena.

Self-organization phenomena appear in different regions of the solid surface and the interactions which determine the values of relevant kinetic constants and transport coefficients mainly depend on short-range forces [8,15].

In open systems where different entities, such as atoms, molecules, defects, and so on are able to move and interact with each other, phenomenological rate equations of the concentrations of the reactant species are usually derived from material, energy or momentum balance equations, leading to reaction-diffusion dynamics. Consequently, the resulting spatio-temporal concentration patterns are no longer governed by atomic dimensions but

through the so-called diffusion length. Thus, the temporal evolution of the resulting concentration patterns in open systems far from the equilibrium can be described through a set of non-linear partial differential equations, combining the chemical kinetics with the diffusion processes of the adsorbed species, as follows:

$$\partial \quad \partial = \quad , \quad + \quad \nabla 2$$

where x_i are the state variables (i.e. surface concentrations) of the reacting chemicals, F_i are the non-linear operators expressing the chemical kinetics, D_i are the diffusion coefficients and p_k are a set of parameters [16].

In fair agreement with our previous studies [17,18], in the present work we investigate the complexity of active sites in heterogeneous catalysis through a review based on three examples from the literature, namely metal nanoparticles, zeolites and transition metal oxides acting via redox MvK-type mechanism. Moreover, the hyperstructures are proposed as a model to describe the complexity of catalysis. Introduced in 1990, the Hv-structures proved to have a lot of applications in several applied sciences, such as linguistics, biology, chemistry, physics, and so on [20].

Algebraic hyperstructures are a natural extension of classical algebraic structures: in an algebraic structure, the composition of two elements is an element, while in an algebraic hypestructure, the composition of two elements (i.e. reactant molecules) is a set (i.e. the reaction products) [19,20]. Thus, it will be proved that various complexity structures in catalysis belong to the Hv-structures, the largest class of hyperstructures which satisfy the weak properties [19].

2 Metal clusters and nanoparticles

The chemical reactivity of nanostructured systems is often related to the size and shape of the metal particles (= structure-sensitive reactions), as well as to the nature of the support materials [21-24]. On the contrary, in structure-insensitive reactions all the surface sites exhibit comparable reactivity on several planes of a single crystal. For instance, hydrogenation reactions are usually structure-insensitive since they can occur in many different arrangements of surface atoms. This is mainly due to the fact that

dissociation of H_2 molecules on the metal surface shows high reaction probability on different surface sites [23].

Physico-chemical properties of nano-sized metal particles mainly change as a function of their size. Thus, the most significant consequence of decreasing the particle size is the increase in the surface/volume ratio (i.e. surface atoms of a 2 nm particle constitute about 60% of the total) [25]; the rise in the fraction of surface atoms is responsible for some changes in the structural character. Notable changes typically include: i) a decrease in the melting temperature and ii) a lowering of the interatomic separation. Indeed, small metal clusters (i.e. ranging from ca. 2 to 30 atoms) are close to molecular in their behaviour with electronic states (DOS) that are discrete or approaching discrete behaviour. On the contrary, metal nanoparticles (i.e. containing 10^3-10^7 atoms) have a continuous band of electronic energy levels and a well-defined Fermi surface [25]. These features partially explain some of the fundamental differences in the chemical reactivity between metal clusters and nanoparticles.

Typically, small particles are more reactive than larger ones, since the electronic state and defect density may change markedly at a critical size around 2 nm [26]. As a whole, a decrease in particle size will increase the number of surface atoms having low-coordination numbers, such as corners (CN = 4,5,6) and edges (CN = 7) for all particle shapes. Theoretical studies indicate that surface atoms having low coordination number (such as edges and corners) are the seat of increased chemical reactivity and are therefore the preferred active centres [27]. For instance, the relative fractions of atoms at corners (CN = 6) and edges (CN =7) in a truncated octahedron Au nanoparticle increase significantly as the particle sizes become smaller than 3-4 nm (Fig. 1A) [17]. Moreover, the relative amounts of edge, corner and terrace sites are particle shape dependent (Fig. 1B), and hence distinct geometries may lead to different chemical reactivities.

As already noted by Langmuir [28] "the surface atoms are not rigid but tend to arrange themselves so that the total energy will be a minimum. In general, this will involve a shifting on the positions of the atoms with respect to each other". Thus, the displaced atoms must return to their initial state when the reaction cycle is completed. Inward relaxation and reconstruction of catalytic surfaces are much more marked at low-coordination sites, which are more "flexible" and self-repair the sites at higher rates [29].

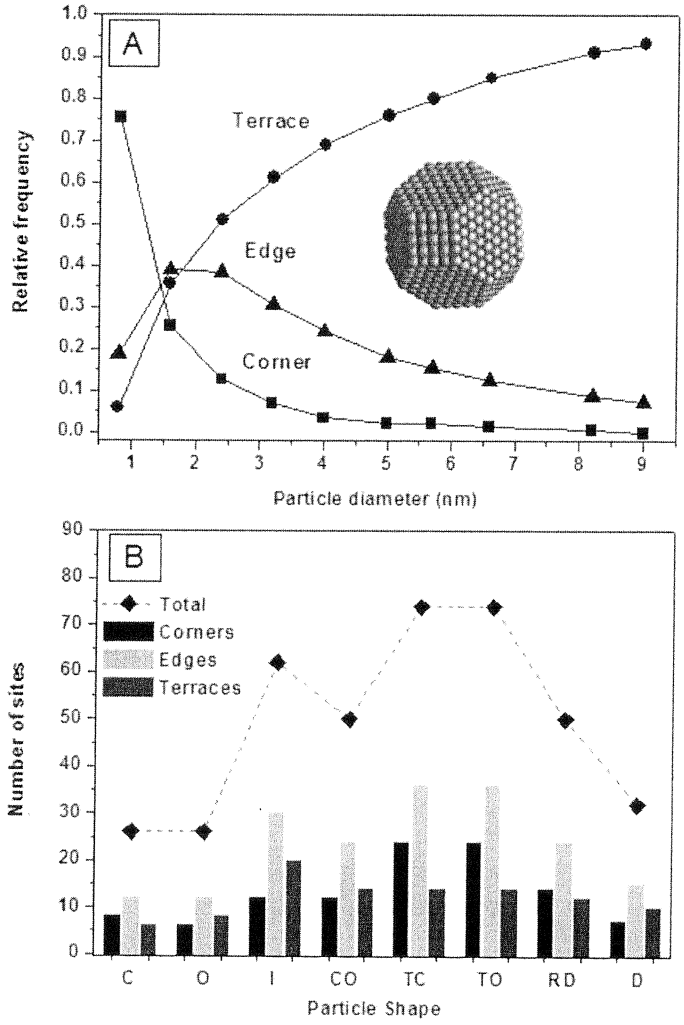

Fig. 1: Dependence of relative amounts of surface sites (normalized to exposed atoms) as a function of Au particle diameter (section A) [17]. Values calculated from ref. [25] Total numbers of edges, corners and terraces of particles having different convex shapes: (C) cube, (O) octahedron, (I) icosahedron, (CO) cuboctahedron, (TC) truncated cube, (TO) truncated octahedron, (RD) rhombic dodecahedron, (D) decahedron (Section B).

Self-repairing phenomena reflect the intrinsic property of any effective catalyst to "regenerate" the sites once the catalytic cycle has been concluded. Such mechanisms occur locally at each active site and represent the lowest level of self-organization at solid surfaces [10]. For instance, the marked ability of isolated Ti(IV) sites inside the silicalite framework (Ti-Silicalite-1 catalyst) to self-repair in a reversible (or nearly reversible) way their local environment upon interaction with adsorbates is probably the key to the reactivity of this important material used for a range of low-temperature catalytic oxidation processes with hydrogen peroxide [30].

In small metal clusters, atoms are often packed into polygonal (2-D) or polyhedral (3-D) shapes, having several planes of symmetry and high packing efficiency with characteristic numbers, namely magic numbers.

For instance, three, four, six and eight atoms are often packed into triangular, tetrahedral, octahedral and cubic arrays, respectively. The formation of a sequence of cluster magic numbers is closely related to the mechanisms of cluster formation (nucleation) and growing, which are kinetically and thermodynamically controlled and hence sensitive to experimental conditions [27]. Therefore, it is natural to expect that metal clusters with magic numbers are more abundant than others, likely because they are particularly stable, as a result of packing of atoms according to precise rules determined by electronic and/or steric principles. As the cluster size increases, the force governing their formation may switch from bonding (electronic) to packing (steric) in nature. Consequently, the assemblage of atoms to form energetically stable clusters/nanoparticles of relatively efficient packing and high symmetry reflects the presence of well-defined concentration patterns, as result of self-organization phenomena.

Depending on the surface energy of the {hkl} planes and on the adsorption bond strength of molecules from the surrounding gas-phase, metal nano-sized particles often form convex polyhedral shapes, having the Euler characteristic of the sphere (X = 2). Thus, several convex polyhedral geometries, as the regular Platonic solids, the semi-regular Archimedean solids and their dual Catalans, and other semiregular convex polyhedra (i.e. prisms, dipyramids, antiprims and trapezohedra) are frequently found in the cluster chemistry [27]. These solids are dominated by crystallographic faces, which exhibit different surface atom densities, electronic structures, bonding, chemical reactivities and thermodynamic properties [31-33].

In recent years, many studies have investigated the equilibrium shapes of fcc metal nanoparticles, such as gold, platinum and palladium showing several convex polyhedral shapes, including icosahedron and truncated icosahedron, decahedron, truncated octahedron and cuboctahedron [31-33]. For instance, Fig. 2 shows an ideal Pt nanoparticle (~2.5 nm) with a truncated octahedron shape, exhibiting corner, edge and terrace sites. This geometrical structure is typical for many metal nanoparticles, as achieved with Pt20C nanoparticles (the inset of Fig. 2).

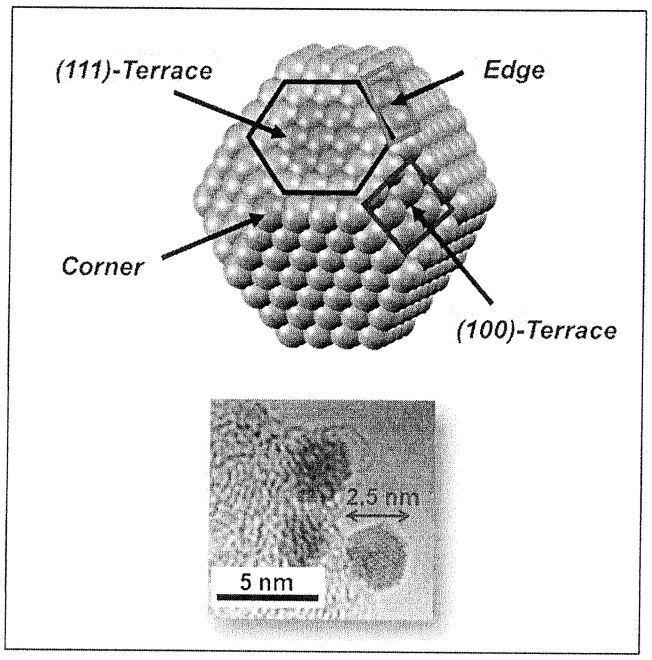

Fig. 2: Schematization of an ideal Pt-nanoparticle (~2.5 nm) with a truncated octahedron structure (above) . HRTEM micrograph of the Pt20C nanoparticles exhibiting truncated octahedron shapes (below).

Although many computational and theoretical studies agree on the energetic order of distinct particle shapes, they do not necessary agree with experimental observations. Such discrepancies between experimental data and thermodynamic modelling of small metal particles are often attributed to kinetic effects. In fact, the cooperation (or competition) between kinetic

and thermodynamic factors may lead to non-linear dynamics at solid surfaces. For instance, combined techniques revealed that icosahedral Au particles, thermodynamically more stable in small clusters, are also observed in larger nanoparticles, as a consequence of kinetic effects [31-34]. Moreover, non-convex shapes ($X \neq 2$), as Kepler-Poinsot polyhedra, may also form during reactions as a consequence of selective passivation and blocking of edge and corner sites during growth, coupled with anisotropic growth rates in different orientations [35].
All these convex and non-convex solids belong to the class of polytopes, geometrical structures with any general number of dimensions. Indeed, the term of n-polytope is used to refer to a n-dimensional structure.
The polytopes are fine as a model to describe the complexity of the geometrical structures. For instance, a polygon is a 2-polytope, a polyhedron is a 3-polytope, a polychoron is a 4-polytope and so on. In addition, the elements of a 3-polytope are its vertices (0-dimensional face), edges (1-dimensional face) and terraces (2-dimensional face).
Since metal clusters and nanoparticles are formed through the assemblage of atoms in three dimensions, they can be considered 3-polytopes. However, these clusters/nanoparticles are not static but change over time, i.e. depending on the external conditions, and hence they can be denoted as polychorons, four dimensional polytopes. Similarly, self-repairing mechanisms, occurring locally on vertices, edges and terraces during catalytic reaction, can be included in the class of polytopes variable over the time, having 1, 2 and 3-dimensional structures, respectively. As a result, the polytopes can be considered the initial set of the action of hyperstructures.

3 Multicomponent systems: zeolites

Although the first description of zeolites dates back to 250 years ago, over the last five decades there has been a growing interest in zeolite research activities. At present, almost 200 different structural types of zeolites have been recognized, differing in the size, shape and connectivity of their channels [36,37]. These materials are much more than just an ideal 3-D regular arrangement of TO_4 tetrahedral having channels and voids that hold appropriate active sites. They are multicomponent systems made up of tiny crystals of definite morphologies, containing defects of various origins and a certain nanoscopic (at unit cell level) and macroscopic (at crystal level)

distribution of active sites, either acid, basic or redox, or a combination of them [38]. The diversity of morphologies is also increased by the presence of elements other than Al for Si in the framework, which may be either aliovalent (2+ or 3+) or isovalent (4+), and the search for new materials is encouraged by the knowledge of hypothetical geometries that have been shown to be energetically possible [37]. The faujasitic zeolites X and Y provide excellent examples of many of the important types of zeolite structural chemistry. In Al-containing X and Y systems, the siting of extra-framework cations introduced either during the synthesis or subsequently by cation exchange is very important in the determination of their physico-chemical properties. Fig. 3 shows some possible extra-framework sites in zeolite Y with associated cages and channels. Cations can be located at different sites, depending on the particular zeolite framework, cation size, dehydration state and nature of adsorbed molecules. Moreover, whereas pure silica frameworks are electrically neutral, the substitution of trivalent Al for tetravalent Si ($Al^{3+} \leftrightarrow Si^{4+}$) induces a negative charge to the material that has to be balanced by positively charged extra-framework cations within the pore space. Thus, the presence of strong electric fields and controllable adsorption features within the pores will produce a unique type of material [36].

As a whole, when a guest molecule presents a polar character and/or the zeolitic framework is not purely siliceous, the electrostatic interactions among atoms and/or molecules cannot be neglected. Specifically, when a molecule is confined in the channels of a zeolite, the sorption energy depends on different energetic factors. Among these, there are the van der Waals interactions (i.e. attractive and repulsive forces), polar, field-dipolar and field gradient-quadrupole forces, sorbate-sorbate intermolecular interactions and the acid-base chemical interactions [36].

The interaction in the confined space of the pores is characterized by the geometry of the environment of the active center (i.e. van der Waals interactions) and by the chemical composition of the environment (i.e. polar and field-dipole terms). When the size of a guest molecule approaches the sizes of the zeolitic channels, it is also necessary to consider the electronic confinement, which can affect the energetic state of reactants, modifying their reactivities [36]. Moreover, the effect of field gradients, which weaken

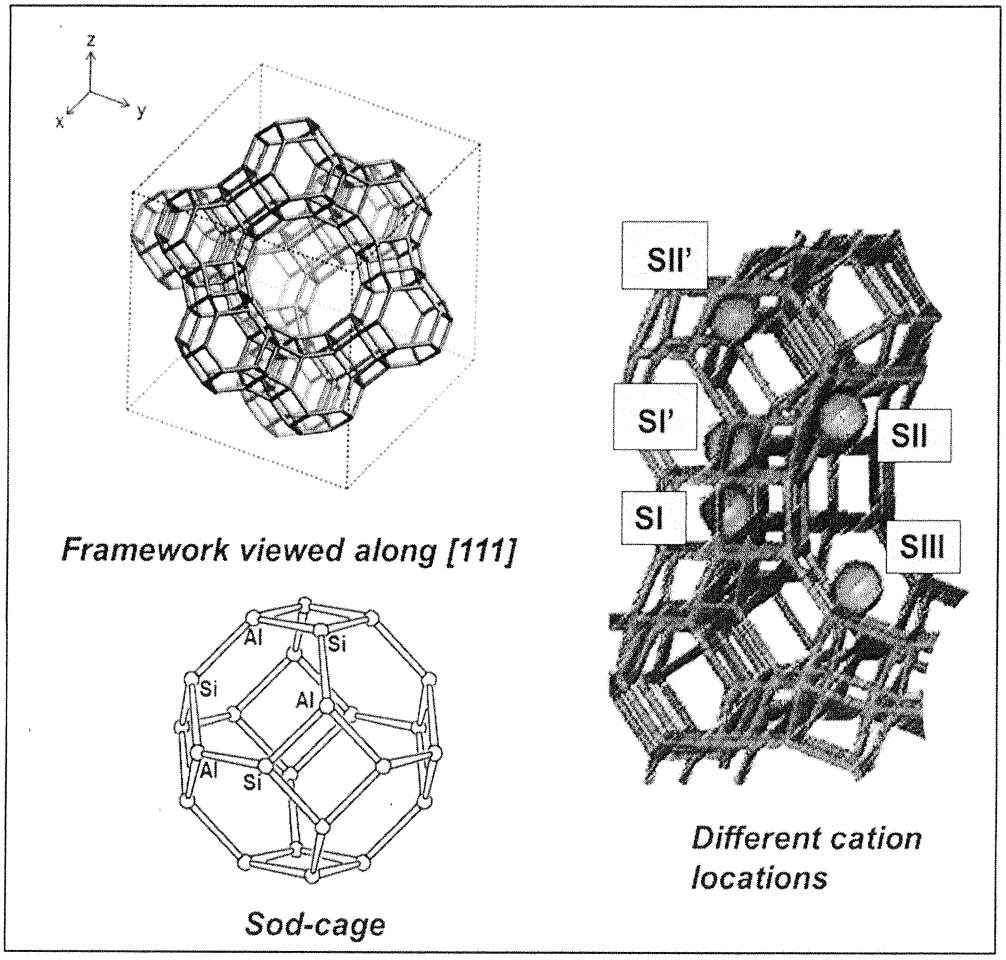

Fig. 3: Framework type of zeolite Y (left); Structures taken from C. Baerlocher W. M. Meier, D.H. Olson (ed) (2001), Atlas of zeolite framework types, 5th edn, Elsevier, Amsterdam. Extra-framework cation sites (SI, SI', SII, SII' and SIII) observed in the same material (right).

some hydrocarbon bonds, depends on the charge density (i.e. Al content), the temperature, the zeolitic structure and the polarizing effect of cations [40]. Although pure silica zeolites are highly hydrophobic, the isomorphic substitution of silicon with aluminum, and the subsequent neutralization of the framework with cations make the structure hydrophilic [37].

Indeed, zeolites containing charges are typically hydrophilic materials that, depending on the amount of extra-framework species and on the framework Si/Al ratio, can be more or less selective adsorbents for polar or non-polar compounds [36].

Zeolites are able to discriminate both reactant and product molecules by size and shape, when they have significant differences in terms of diffusivity through a given pore channel system. In addition, the relative orientation of the channels and cavities in respect to the crystal shape may affect the diffusion path of molecules through the crystals [38]. Thus, different types of shape selectivity may occur within a given zeolitic structure, namely reactant selectivity, product selectivity and transition-state selectivity [39]. The latter, in particular, takes place when the specific configuration around a transition state located in crystalline volume is such that only certain configurations are possible.

Moreover, the reaction pathway, and hence the chemical complexity, can be strongly affected by the framework geometry in the neighborhood of the active site. Thus, the steric constraints assume a significant importance for driving the reaction towards the desired products [36].Typical examples of transition-state selectivity include the inhibition of coke formation within ZSM-5 crystals and the cracking of paraffins within the pores [40,41].

The complexity of zeolites is still greater if one considers them as solid acid catalysts. Indeed, these materials typically contain Brønsted acid OH groups (i.e. SiOHAl), which are responsible for the catalytic activity of reactions catalyzed by acids, such as cracking or isomerization of hydrocarbons [38,41]. For H-forms of zeolites (i.e. H-faujasite, H-ZSM-5, H-chabazite, etc.), the cracking rates of hydrocarbons were often found to increase linearly with the framework aluminum, which corresponds to the density of Brønsted acid sites [37]. For instance, a linear increase of the activity towards the *n*-hexane cracking rate with the Al content in the framework was observed, as long as the sites could be considered as non-interacting. The acid strength of sites can be also altered by isomorphic substitution of Si for trivalent atoms other than Al. Similarly, the Si-O-T bond angle, which depends on the zeolite structure type, affects the partial charge and the acid strength of the hydroxyl protons.

In addition to the local effects, the overall composition of the zeolite framework influences the acid strength of bridging OH groups, through the

mean Sanderson electronegativity (S^m). Typically, the acid strength of Brønsted sites increases with increasing S^m of the zeolite framework, that is, with decreasing of aluminum content [37].

As it is known, the surface acidity of zeolites plays a key role in many catalytic reactions. For instance, catalytic cracking of alkanes and alkenes is a high-temperature reaction network that is acid-catalyzed and proceeds through the formation of carbocation transition states [5]. Because of the complexity of feedstocks and reaction pathways, the variety of products that can be obtained is huge.

This suggests that zeolites may display sensitivity to tiny changes in their states, and hence a small alteration in their condition at one instant may give rise to great differences in terms of reaction products.

Consequently, during a reaction various self-organizing phenomena may occur in multicomponent systems and their geometrical complexity can be described with polytopes acting in a discrete 3-D space. For instance, self-repair and reorganization of active sites on corners reflect 2-polytopes, as well as the electrostatic interactions between cations in zeolite framework and guest molecules may be described through polychorons. Similarly, mass transfer limitations (i.e. shape selective control) occur in 3-D frameworks containing well-defined pores and cavities of molecular dimensions. This means that self-organizing phenomena due to shape selective control give rise to geometrical structures consistent with polychorons.

Since self-organizing phenomena in catalysis may reflect complexity structures [18] their non-linear combination results in a hyperoperation ($\circ$), namely multivalued operation. Indeed, the catalyst may act like a hyperoperator in the sense of the theory of hypestructures [19,20]. This hyperoperator maps two reactants (x,y) of the catalytic process (H_v-structures) into the class of polytopes (a subset $x \circ y$ of H_v). Moreover, the hyperoperation is weak associative because two sets, i.e. (xy)z and x(yz), have at least one common element for all x,y,z in H_v. The weak associativity can be seen easily because different complexity structures (sets) contain n-polytopes as common elements in every catalytic reaction [19].

As a result, the complexity of heterogeneous catalysis can be fairly well described through the Hv-structures.

4 Dynamic active networks: transition metal oxides acting via redox MvK-type mechanism

Typically, oxidation reactions catalyzed by mixed oxides occur via a Mars-van Krevelen mechanism (MvK) [42] whereby the active centres are not isolated sites but ensembles of ions and electrons mutually interacting in an active network [43,44]. These catalytic systems exhibit sophisticated self-organization structures, in which dynamic networks of "sites-joined" may promote either selective or total oxidation reactions [17,45]. Indeed, the MvK-type mechanism requires that a hydrocarbon molecule (R-H) extracts lattice oxygen from the surface of the oxide catalyst ($R\text{-}H + O^{2-} \rightarrow R\text{-}O^{-} + H^{+} + 2e^{-}$), so generating oxidized products and a reduced catalyst surface. Then, lattice oxygen is replenished by the reduction of gaseous oxygen ($\frac{1}{2} O_2 + 2e^{-} \rightarrow O^{2-}$) [10]. In other words, two redox steps take place during catalytic reaction, one consisting of the injection of electrons into the catalyst, the other extracting them from the oxide.

This mechanism occurs quite frequently in selective oxidation reactions over vanadium oxides, as originally proposed by P. Mars and D. van Krevelen [41]. There is, however, evidence that also other metal oxides, such as those of Mo, Cr, and Fe operate via redox cycles [10,46].

Requirements for the MvK mechanism to take place comprise the facile redox behaviour of cations (i.e. V, Cr, Mo, etc.) and the good mobility of both electrons and lattice oxygens within the solid [43,44]. Other factors comprise the facile activation of reactants, the presence of surface defects (i.e. corners edges and terraces), the surface acid-base properties, and the temperature [43,44,46-48].

Catalytic performances of redox catalysts are also influenced by the nature of lattice oxygens. Indeed, the latter have diverse stabilities and may react differently, *i.e.* via electrophilic or nucleophilic attack. For instance, lattice O^{-2} (nucleophilic species) are usually responsible for selective oxidations, whereas electrophilic species (i.e. O_2^{-}, O_2^{-2} and O^{-}) are highly reactive and result in total oxidations [5,49,50]. Nevertheless, their properties are strongly influenced by the electronegativity of the element present in the support material (i.e. Al, Ti, Si, etc.) [51-53].

Noteworthy, the complexity of metal oxides acting via redox cycles further depends on the fact that acid-base and redox properties can be closely related to each other. For instance, it has been recently observed that the

Oxidative DeHydrogenation (ODH) of propane over mesoporous VO_x-SiO_2 catalysts with comparable vanadium content (V-SBA-15 and V-MCF ca. 2.5 % by weight) also depends on the Brønsted acidity of V species, as measured by IR spectroscopy (Fig. 4A) [54-56]. Indeed, Brønsted acidity seems to be negatively correlated with the selectivity to propene, since stronger Brønsted acid sites favour the formation of CO_x and other by-products (Fig. 4B) [57,58].

Moreover, higher selectivity to propene (selective oxidation product) was obtained over V-MCF as compared to V-SBA-15. This behaviour was related to the different porous network of the two catalysts: the structure of MCF, featuring a 3-D network with ultra-large cells (20-40 nm), favours molecular diffusion along each direction (= lower residence time), unlike cylindrical channels of SBA-15 (3-6 nm) occurring in one dimension mainly (axial diffusion). On the other hand, a non-porous sample prepared by flame pyrolysis (V-SiO_2), exhibited worse performances than mesoporous systems, confirming the important role of mesoporosity in oxidation processes [54-56].

Therefore, multiple causes affect the catalytic performance of redox systems, having ensembles of atoms (ions) and electrons mutually interacting in dynamic active networks. On the other hand, both structural and chemical complexity are closely related in transition metal oxide catalysts operating through a Mvk mechanism and this further suggests that such redox catalysts are very sensitive to the reaction conditions.

Moreover, several studies revealed that oxidation reactions at solid surfaces may change their reaction mechanism as a function of temperature [47]. G.I. Golodets et al. [49] proposed a classification of the oxidation mechanisms as function of temperature, according to which the redox MvK-type mechanism takes place in the temperature range between 300 and 500 °C, being replaced at higher temperatures by radical processes in the gas-phase. Below about 100 °C oxidation reactions may occur through peroxidic mechanisms, in which adsorbed radicals are directly involved. Golodets also identified a "transitional" region at moderate temperatures (in the range between 100 and 300 °C), where complex surface re-oxidation mechanisms are involved and the latter should be responsible for the formation of total oxidation products [47].

All these findings revealed that self-organizing phenomena may occur at the surface of metal oxides during oxidation reactions. Their geometrical structures can be described by means of 3-polytopes taking place both in space and time. On the other hand, a fractal approach (3 + *e* dimensions, where *e* represent the dimension of the boundary) is likely more appropriate to describe theoretically the dynamic active networks operating in metal oxide catalysts.

5 Concluding remarks

The principles of non-linear dynamics govern self-organization phenomena in catalytic reactions. The latter typically occur in open systems, far from the equilibrium conditions, and hence the resulting spatio-temporal phenomena can be described through non-linear differential equations, combining both the chemical kinetics and the diffusion processes.

Self-organizing phenomena in heterogeneous catalysis reflect different complexity structures, including the self-repair and reorganization of active sites, the mutual interactions between neighbouring sites, the mass transfer limitations (i.e. shape selective control), the dynamic active networks of "sites-joined", and so on. Thus, the observed self-organization processes at catalyst surfaces are related to spatio-temporal structures, in which both the structural and chemical complexity are closely related to each other.

As a whole, the catalysis process results in a non-linear combination of distinct complexity structures and hence catalytic behaviours may appear with multicomponent systems, such as zeolites or transition metal oxides acting via redox MvK-type mechanism. This also suggests the possibility of having non-reproducible reactions, i.e. in terms of reaction pathways and products.

In agreement with the theory of hyperstructures, the catalyst acts as a hyperoperator computing a non-linear combination (namely multivalued operation, $\circ$) of different complexity structures.

During the reaction (= Hv-structure), the catalyst allows reactants (i.e. x,y) to be mapped into the class of polytopes (a subset $x \circ y$ of H_v). The hyperoperation is weak associative because different complexity structures (sets) contain n-polytopes as common elements. This allows the condition required for the existence of the Hv-structures to be satisfied. Polytopes, with any general number of dimensions, have been introduced to describe

the complexity of the geometrical structure that is the initial set of the action of hypestructures. Therefore, the algebraic hyperstructures (namely H_v-structures) are fine as a model to describe the complexity of catalysis.

Acknowledgements
The authors are grateful to Prof. Gerhard Ertl (Fritz-Haber Institute of the Max Plank Society, Berlin) for many helpful discussions during the preparation of this work. We thank Dr. Patrick Gelin (Lyon) for providing data about Pt-nanoparticles (Fig. 2).

References
[1] M. Che, J.C. Védrine, *Characterization of Solid Materials and Heterogeneous Catalysts,* Wiley-VCH, Weinheim, 2012.
[2] G. Ertl, *Reactions at Solid Surfaces,* Wiley-VCH, Hoboken, 2009.
[3] O. Deutschman, H. Knözinger, K. Kochloefl, T. Turek, *Ullman's Encyclopedia of Industrial Chemistry,*, Wiley-VCH, Weinheim, 2012.
[4] T. Mitsui, M. K. Rose, E. Fomin, D. F. Ogletree, M. Salmeron, Nature **422** (2003), 705-707.
[5] G. Ertl, H. Knözinger, F. Schüth, J. Weitkamp, *Handbook of Heterogeneous Catalysis* (2nd ed.), Wiley-VCH, Weinheim, 2008.
[6] J. Libuda, S. Schauermann, M. Laurin, T. Schalow, H. J. Freund, Monatshefte fur Chemie **136** (2005), 59-75.
[7] J. Libuda, T. Schalow, B. Brandt, M. Laurin, S. Schauermann, Microchimic Acta **156** (2007), 9-20.
[8] G. Ertl G, Angew. Chem. Int. Ed. Engl. **29**(11) (1990), 1219-1227.
[9] J. Libuda, H. J. Freund, J. Phys. Chem. B **106** (2002), 4901-4915.
[10] R. A. van Santen, M. Neurock, *Molecular Heterogeneous Catalysis,* Wiley-VCH, Verlag, 2006.
[11] G. A. Samorjai, A. M. Contreras, M. Montano, R. M. Rioux, PNAS **103** (2006), 10577-10583.
[12] I. Prigogine, Ann. N.Y. Acad. Sci. **988** (2003), 128-132.
[13] G. Nicolis, I. Prigogine, *Self-Organization in Non-Equilibrium Systems,* Wiley-VCH, New York, 1977.
[14] H. Haken, *Synergetics: An Introduction*, Springer-Verlag, Berlin-Heidelberg-New York, 1977.
[15] I. Prigogine, Science, **421**(4358) (1978), 777-785.

[16] G. Ertl, Angew. Chem. Int. Ed., **47** (2008), 3524-3535.
[17] M. Piumetti, F. Freyria, B. Bonelli, Chimica Oggi-Chemistry Today, **31**(4) (2013), 55-58.
[18] M. Piumetti, N. Lygeros, Chimica Oggi-Chemistry Today, (accepted).
[19] T. Vougiouklis, *New Frontiers in Hyperstructures*, Hadronic Press, Palm Harbor, 1996.
[20] B. Davvaz, R. M. Santilli T. Vougiouklis, Proc. 3th Int. Conf. Treat. Irrev. Proc.. (Kathmandu University, Nepal) 2011, 1-12.
[21] C. Mager-Maury, C. Chizallet, P. Sautet, P. Raybaud, ACS Catal, **2** (2012), 1346-1357.
[22] A. S. Barnard, Y. Chen, J. Mater. Chem., **21** (2011), 12239-12245.
[23] G. A. Somorjai, J. Y. Park, Catal. Letters, **115** (2007), 87-98.
[24] C. H. Hu, C. Chizallet, C. Mager-Maury, M. Corral-Valero, P. Sautet, H. Toulhoat, P. Raybaud, J. Catal, **274** (2010), 99-110.
[25] J. M. Thomas, R. Raja, Top. Catal., **53** (2010), 848-858.
[26] M. Haruta, CATTECH, **6**(3) (2002), 102-115.
[27] D. L. Feldheim, C. A. Foss, *Metal Nanoparticles,* Marcel Dakker, New York, 2002.
[28] I. Langmuir, J. Am. Chem. Soc., **38** (1916), 2221-2295.
[29] G. A. Somorjai, Langmuir, **7** (1991), 3176-3182.
[30] C. Lambert, S. Bordiga, D. Arduino, A. Zecchina, F. Geobaldo, G. Spanò, F. Genoni, G. Petrini, A. Carati, F. Villain, G. Vlaic, J. Phys. Chem B, **102** (1998), 6382-6390.
[31] A. S. Barnard, Accounts Chem. Res., **45** (2012), 1688-1697.
[32] A. S. Barnard, L. S. Curtiss, ChemPhysChem, **7** (2006), 1544-1553.
[33] A. S. Barnard, J. Phys. Chem. B, **110** (2006), 24498-24504.
[34] C. Mager-Maury, G. Bonnard, C. Chizallet, P. Sautet, P. Raybaud, ChemCatChem, **3** (2011), 200-207.
[35] A. S. Barnard, 2013, Personal Communication.
[36] A. Corma, J. Catal., **216** (2003), 298-312.
[37] J. Čejka, A. Corma, S. Zones, *Zeolites and Catalysis*, Wiley-VCH, Weinheim, 2010.
[38] J. Čejka, G. Centi G, J. Perez-Pariente, W. J. Roth, Catal. Today, **179** (2012), 2-15.
[39] A. Corma, Chem. Rev., **95** (1995), 559-614.
[40] A. Corma, Curr. Opin. In Solid State Mater. Sci., **2** (1997), 63-75.

[41] M. Brändle, J. Sauer, J. Am. Chem. Soc., **120** (1998), 1556-1570.
[42] P. Mars, D. van Krevelen, Chem. Eng. Sci. Spec. Suppl., **3** (1954), 41-59.
[43] J. C. Védrine, G. Coudurier, J. M. Millet, Catal. Today, **33** (1997), 3-13.
[44] J. C. Védrine, Top. Catal., **21** (2002), 97-106.
[45] W. R. Ashby, E:CO, **6** (2004), 102-106.
[46] B. K. Hodnett, *Heterogeneous Catalytic Oxidation,* Wiley-VCH, New York, 2000.
[47] M. Ruitenbeek, A. J. van Dillen, F. M. F. de Groot, I. E. Wachs, J. W. Geus, D. C. Koningsberger, Top. Catal., **10** (2000), 241-254.
[48] J. C. Védrine, J. M. Millet, J. C. Volta, Catal. Today, **32** (1996), 115-123.
[49] G.I. Golodets, Eds. G. Centi, F. Trifirò, *Stud. Surf. Sci. Catal. "New Developments in Selective Oxidation",* **693** (1990), 55.
[50] K. D. M. Harris, P. P. Edwards, *Turning Points in Solid-State Materials and Surface Science,* RCS Publishing, Cambridge, 2008.
[51] D. Kulkarni, I. E. Wachs, Appl. Catal. A: Gen., **237** (2002), 121-137.
[52] D. E. Fein, I. E. Wachs, J. Catal., **210** (2002), 241-254.
[53] X. Wang, I. E. Wachs, Catal. Today, **96** (2004), 211-222.
[54] M. Piumetti, B. Bonelli, P. Massiani, Y. Millot, S. Dzwigaj, M. Armandi, L. Gaberova, E. Garrone, Micropor. Mesopor. Mater., **142** (2011), 45-54.
[55] M. Piumetti, B. Bonelli, M. Armandi, L. Gaberova, S. Casale, P. Massiani, E. Garrone, Microporous Mesoporous Mater., **133** (2010), 36-44.
[56] M. Piumetti, B. Bonelli, P. Massiani, S. Dzwigaj, I. Rossetti, S. Casale, M. Armandi, C. Thomas, E. Garrone, Catal. Today, **179** (2012), 140-148.
[57] M. Piumetti, M. Armandi, E. Garrone, B. Bonelli, Microporous Mesoporous Mater., **164** (2012), 111-119.
[58] I. Rossetti, G. F. Mancini, P. Ghigna, M. Scavini, M. Piumetti, B. Bonelli, F. Cavani, A. Comite, J. Phys. Chem. C, **116** (2012), 22386-22398.

DARK ENERGY, INERTIA AND MACH'S PRINCIPLE

C. Sivaram
Indian Institute of Astrophysics
Bangalore – 560 034, India
sivaram@iiap.res.in

Kenath Arun
Christ Junior College
Bangalore – 560 029, India
kenath.arun@cjc.christcollege.edu

Received November 6, 2013

Abstract

Mach's Principle says that a particle's inertia is due to some interaction of that particle with all the other masses in the universe. Here we explore the possibility of the gravitational interaction energy of the background quantum vacuum energy playing the role of a global Higg's field (described by a varying cosmological constant) entirely contributing to the local inertial masses of particles in the spirit of Mach's principle.

Keywords: Dark Energy; Inertia; Mach's principle; Quantum vacuum energy; Global Higg's field; Varying cosmological constant.

Copyright © 2013 by Hadronic Press, Inc., Palm Harbor, FL 34684, USA

1 Introduction

Mach's Principle implies that the local standards of non-acceleration are determined by some average of the motions of all the masses in the universe. As a result, it even implies interactions between inertia and electromagnetism. [1]

In the case of electromagnetic field, as is well known, an accelerated moving charge exerts a different electromagnetic force than a charge at rest (i.e. Coulomb field). This electromagnetic field, of a moving charge, falls of as $1/r$ rather than $1/r^2$! [2]

Thus we have for the force, for charges q_1 and q_2 separated by r :

$$F_{em} = \frac{kq_1q_2}{r^2} + \frac{kq_1q_2}{rc^2}a \tag{1}$$

For large r, the $1/r$ term dominates. So we have:

$$F_{em} \approx \frac{kq_1q_2}{rc^2}a \tag{2}$$

Now in the case of gravity similar force has been proposed (that is Einstein-Sciama force) for mass m_1 and m_2 separated by r : [3]

$$F_{Grav} = \frac{Gm_1m_2}{r^2} + \frac{Gm_1m_2}{rc^2}a \tag{3}$$

And again for large r, the $1/r$ term dominates. That is:

$$F_{Grav} \approx \frac{Gm_1m_2}{rc^2}a \tag{4}$$

So if at all gravitational forces contribute to local inertia, this term dominates. So we do not consider the static $1/r^2$ term but only the $1/r$ term while considering the Machian effects of distant masses.

2 Effect of distant mass

Thus we can write for the cumulative effect of all distant masses m_i on the local mass m ,

$$F_{Grav} = \sum_i \frac{Gm_i}{rc^2}ma \tag{5}$$

which is summed over all the masses m_i

We can write for

$$\sum m_i = \int_{Vol} \rho dV \tag{6}$$

ρ is the average density of matter in the universe
a is the acceleration
c is the velocity of light

From this we have:

$$F_{Grav} = \frac{G}{c^2}\left[\int_{Vol} \frac{\rho dV}{r}\right] ma = \frac{G}{c^2}\left[\int_0^{R_H} \frac{\rho}{r}\left(4\pi r^2 dr\right)\right] ma \tag{7}$$

(The integration is carried out over the Hubble volume)

This gives:

$$F_{Grav} = \frac{2\pi G \rho R_H^2}{c^2} ma = \frac{2\pi G\rho}{H_0^2} ma \tag{8}$$

Where

$$H_0^2 = \left(\frac{c}{R_H}\right)^2 = \frac{8\pi G \rho_C}{3} \tag{9}$$

and ρ_C is the critical density

Therefore we have:

$$F_{Grav} = 0.75ma \tag{10}$$

3 Dark energy dominated universe

If the universe is vacuum dominated or dark energy dominated [4], the simplest case being that of a cosmological constant, Λ term, for which we have:

$$\rho = \frac{\Lambda c^2}{8\pi G}; H_0^2 = \frac{\Lambda c^2}{3} \tag{11}$$

This when substituted in equation (8) gives:

$$F = \frac{2\pi G\left(\frac{\Lambda c^2}{8\pi G}\right)}{\frac{\Lambda c^2}{3}} ma = 0.75ma \tag{12}$$

This indicates that gravitating vacuum energy (DE) could contribute up to 75% of the inertial mass of particles.

The quantum vacuum energy density for the curved space (of constant curvature) is given by: [5, 6]

$$\rho_{Vac} = \frac{\hbar c}{4\pi}\Lambda \int_0^{k_{\max}} k dk + \hbar c \Lambda^2 \int_0^{k_{\max}} \frac{dk}{k} + \hbar c \Lambda^3 \int_0^{k_{\max}} \frac{dk}{k^3} + \ldots \quad (13)$$

Since $\Lambda \approx 10^{-56} cm^{-2}$, the terms with higher powers of Λ are much smaller. They become significant only at Planck scale. Therefore we have: [7]

$$\rho_{Vac} = \frac{\hbar c}{4\pi}\Lambda \int_0^{k_{\max}} k dk \quad (14)$$

If $k_{\max} = \left(\frac{c^3}{\hbar G}\right)^{1/2}$ is the Planck cut off wavenumber $\sim \frac{1}{L_{pl}}$

$$\rho_{Vac} = \frac{\hbar c}{8\pi}\Lambda\left(\frac{c^3}{\hbar G}\right) = \frac{\Lambda c^4}{8\pi G} \quad (15)$$

Using this in the equation (7) we have

$$F = \frac{G}{c^2}\left[\frac{\hbar c}{4\pi}\Lambda \int_0^{k_{\max}} k dk \Big/ c^2\right]\left[\int_0^{R_H} \frac{4\pi r^2 dr}{r}\right] ma \quad (16)$$

This gives:

$$F = \left(\Lambda R_H^2\right) ma \quad (17)$$

This implies that $\Lambda R_H^2 \sim 1$, in order that all the local inertia is accounted for by the total gravitational interaction energy of the background vacuum energy up to Hubble radius.

This very important relation $\left(\Lambda R_H^2 \sim 1\right)$ is consistent with the present observations, that is:

$$\Lambda = \frac{1}{R_H^2} \approx 10^{-56} cm^{-2} \quad (18)$$

Where

$$R_H = cH_0 = 10^{28} cm \quad (19)$$

4 Epoch dependent effects

From equation (11) and (18) we have the dependence of dark energy density on the Λ term as $\rho \propto \Lambda$, and $\Lambda \sim R_H^{-2} \propto (1+z)^2$. Therefore we have:

$$\rho_\Lambda = \rho_{\Lambda_0}(1+z)^2 \tag{20}$$

(where ρ_{Λ_0} is the present value of dark energy density)

Where as the matter density goes as:

$$\rho_m = \rho_{m_0}(1+z)^3 \tag{21}$$

(where ρ_{m_0} is the present value of matter density)

At a particular redshift, say, $z = z_0$, both matter and DE would have been equally significant.

$$\rho_{\Lambda_0}(1+z_0)^2 = \rho_{m_0}(1+z_0)^3 \tag{22}$$

$$(1+z_0) = \frac{\rho_{\Lambda_0}}{\rho_{m_0}} \approx 3 \tag{23}$$

That is $z_0 \approx 2$ (24)

This is consistent with observations as it has been observed that Λ is dominant even at about 8 billion years ago corresponding to $z_0 \approx 2$. [8]

If Λ were not dependent on R_H (and hence z), the redshift where both matter and DE were equally significant would be given by:

$$\rho_{\Lambda_0} = \rho_{m_0}(1+z)^3 \tag{25}$$

$z_0 \approx 0.44$, which is not quite consistent with observation.

At primordial nucleosynthesis, that is at $z \approx 10^9$, the energy densities are given by: [9]

$$\begin{aligned} \rho_\Lambda &\approx 10^{18}\rho_{\Lambda_0} \\ \rho_m &\approx 10^{27}\rho_{m_0} \\ \rho_R &\approx 10^{36}\rho_{R_0} \end{aligned} \tag{26}$$

Thus at nucleosynthesis, the dark energy density was several orders lower than radiation energy density. So it will not affect element abundance.

At recombination, that is $z \approx 10^3$ the energy densities are given by:

$$\begin{aligned} \rho_\Lambda &\approx 10^6 \rho_{\Lambda_0} \\ \rho_m &\approx 10^9 \rho_{m_0} \\ \rho_R &\approx 10^{12} \rho_{R_0} \end{aligned} \tag{27}$$

So ρ_m and ρ_R at recombination are several orders higher than ρ_Λ. So it will not much affect CMBR.

Only at around $z \approx 2$, ρ_Λ would dominate.

5 Alternate approach

Yet another way of arriving at the result, $\Lambda \sim 1/R_H^2$ is to invoke the fact that according to general relativity, the maximum force is given by: [10]

$$F_{\max} = \frac{GM^2}{R_{\min}^2} \tag{28}$$

Where

$$R_{\min} \approx \frac{GM}{c^2} \tag{29}$$

(that is, an object cannot be localised to $R < R_{\min}$)

This implies that:

$$F_{\max} = \frac{c^4}{G} \tag{30}$$

This is independent of mass!

Applying this result (which holds independent of scale) over the entire Hubble radius gives for the cosmic energy density the relation:

$$\varepsilon = \frac{c^4}{GA} = \frac{c^4}{G\left(4\pi R_H^2\right)} \tag{31}$$

Where $A \approx 4\pi R_H^2$ is the area of the Hubble surface.

The usual energy density implied by the cosmological constant is also given by:

$$\varepsilon = \frac{\Lambda c^4}{4\pi G} \tag{32}$$

Comparing equations (31) and (32) again implies:

$$\Lambda \sim \frac{1}{R_H^2} \tag{33}$$

Perhaps the first papers in which a time varying cosmological constant (DE or quintessence) were considered, i.e. Λ varying as $1/R_H^2$ with epoch was ref. [11, 12].

Also, a time dependent vacuum energy with, $\Lambda \propto t^{-2}$ was obtained from a theory of unification of gravity with other interactions, where it was shown that the quantum vacuum energy (due to a Higgs field) owing to spontaneous symmetry breaking of a generalised gauge theory, in the early universe, varies with epoch as t^{-2}.

An exact solution was given as: [13]

$$R = R_0 \cosh^{3/2} \sqrt{\Lambda} t \tag{34}$$

And this paper, written in 1975 was perhaps the very first solution which gives an inflationary exponential expansion driven by a large cosmological vacuum energy in the early universe.

In all the early papers, Λ was $\Lambda_{Pl}\left(\sim 10^{66} cm^{-2}\right)$ at $10^{-43} s$ (i.e. Planck time) and dropped down as t^{-2}, that is:

$$\Lambda_{present} \left(\approx \Lambda_{Pl} \left(\frac{t_{Pl}}{t_H} \right)^2 \right) \approx 10^{-56} cm^{-2} \tag{35}$$

($t_H \sim 10^{17} s$ is the Hubble time)

Which is just the value deduced for the dominant dark energy density at present. For a summary of these early papers on dark energy by one of the present authors see ref. [14]

In conclusion, it is conceivable that the gravitational interaction energy of the background quantum vacuum energy playing the role of a global Higg's field (described by a varying cosmological constant) entirely contributes to the local inertial masses of particles in the spirit of Mach's principle.

Reference

[1] W. Rindler, *Essential Relativity*, Springler-Verlag, New York (1977)
[2] J.D. Jackson, *Classical Electrodynamics*, Wiley, New York (1975)
[3] M. Gasperini, Gravitation and the Einstein-Sciama force. Lettere Al Nuovo Cimento, 21 (1978), 285-287

[4] D.N. Spergel, et al, First Year Wilkinson Microwave Anisotropy Probe (WMAP) Observations: Determination of Cosmological Parameters. Astrophys. J. Suppl. 148 (2003), 175-194
[5] C. Sivaram, Uncertainty principle limits on the cosmological constant. Int. J. Theor. Phys. 25 (1986), 825-827
[6] C. Sivaram, The Planck length as a cosmological constraint. Astrophys. Space Sci. 127 (1986), 133-137
[7] C. Sivaram, Evolution of the Universe through the Planck epoch. Astrophys. Space Sci., 125 (1986), 189-199
[8] M. Hicken, et al, Improved Energy constraints from ~100 new CfA Supernova Type Ia light curves. Astrophys. J. 700 (2009), 1097-1140
[9] E.W. Kolb and M.S. Turner, *The Early Universe*, Addison-Wesley, Redwood City (1990)
[10] C. Sivaram and V. de Sabbata, Universality of charge arising from torsion. Found. Phys. Lett. 6 (1993), 201-206
[11] C. Sivaram and K.P. Sinha, Strong (f) gravity, Dirac's large numbers hypothesis and the early hadron era of the big-bang universe. J. Indian Inst. Sci. 57 (1975), 257-269
[12] C. Sivaram and K.P. Sinha, f-gravity and Dirac's large numbers hypothesis. Phys. Lett. B, 60 (1976), 181-182
[13] K.P Sinha, C. Sivaram and E.C.G. Sudershan, The superfluid vacuum state, time-varying cosmological constant, and nonsingular cosmological models. Found. Phys. 6 (1976), 717-726
[14] C. Sivaram, A Brief History of Dark Energy. Astrophys. Space Sci. 319 (2009), 3-4

HADRONIC JOURNAL 36, 205 -210 (2013)

MAGNETIC EFFECT OF NON-COMMUTATIVITY

B.G. Sidharth
G.P. Birla Observatory & Astronomical Research Centre
B.M. Birla Science Centre
Adarsh Nagar, Hyderbad – 500 063 India

C.V. Aditya
University of Stuttgart, Germany

Received November 26, 2013

Abstract

The covariant formulation of electromagnetism refers to ways of writing the laws of electromagnetism in particular, Maxwell's equations and the Lorentz force in a form which is "manifestly covariant" i.e. in terms of covariant four-vectors and tensors, in the formalism of special relativity. This present paper deals with modification of Maxwell's equations in relation to non-commutative spacetime. We conclude that such non-commutativity leads to extra electromagnetic effects and indicate a physical verification in the case of Graphene.

Copyright © 2013 by Hadronic Press, Inc., Palm Harbor, FL 34684, USA

1 NON-COMMUTATIVE MAXWELL'S EQUATION

Maxwell's equation in covariant format can be written as

$$\partial^{\mu} F_{\mu\nu} = \frac{4\pi}{c} j_{\nu} \tag{1}$$

This particular equation is in an abridged form with $\mu, \nu = 1, 2, 3, 4$.

$$\partial_{\mu}(\partial_{\mu} A_{\nu} - \partial_{\nu} A_{\mu}) = \frac{4\pi}{c} j_{\nu} \tag{2}$$

$$\partial_{\mu}\partial_{\mu} A_{\nu} - \partial_{\mu}\partial_{\nu} A_{\mu} = \frac{4\pi}{c} j_{\nu} \tag{3}$$

We now try to see the form which equation (1) or equation (2) to (4) take in the case of non-commutative spacetime. Non-commutative spacetime has been widely discussed in the literature (Cf.ref.[1] and several references therein). In this case, as shown in detail elsewhere [1, 2], we have with $p_{\mu} \doteq \partial_{\mu}$

$$p_{\mu} p^{\mu} = D_{\mu\mu} - \Gamma^{\mu}_{\lambda\mu} \partial_{\mu} \tag{4}$$

$$p_{\mu} p^{\nu} = D_{\mu\nu} - \Gamma^{\mu}_{\lambda\mu} \partial_{\nu} \tag{5}$$

where $D_{\mu\nu}$ denotes the double partial derivative and Γ is a suitable Christoffel symbol.
As we can see, if the last term on the right side is zero then we return to the usual continuous spacetime. It was shown that the last term occurs below the Compton wavelength [1]. Now we substitute (4) and (5) in equation (3) and try to analysis the physical behaviour. We have

$$(D_{\mu\mu} - \Gamma^{\mu}_{\lambda\mu} \partial_{\mu}) A_{\nu} - (D_{\mu\nu} - \Gamma^{\mu}_{\lambda\mu} \partial_{\nu}) A_{\mu} = \frac{4\pi}{c} j_{\nu} \tag{6}$$

$$(D_{\mu\mu} A_{\nu} - D_{\mu\nu} A_{\mu}) = \frac{4\pi}{c} j_{\nu} + (\Gamma^{\mu}_{\lambda\mu} \partial_{\mu} A_{\nu} - \Gamma^{\mu}_{\lambda\mu} \partial_{\nu} A_{\mu}) \tag{7}$$

$$(D_{\mu\mu} A_{\nu} - D_{\mu\nu} A_{\mu}) = \frac{4\pi}{c} j_{\nu} + \Gamma^{\mu}_{\lambda\mu} (\partial_{\mu} A_{\nu} - \partial_{\nu} A_{\mu}) \tag{8}$$

$$\partial^{\mu} F_{\mu\nu} = \frac{4\pi}{c} j_{\nu} + \Gamma^{\mu}_{\lambda\mu} F_{\mu\nu} \tag{9}$$

This can be written as

$$\partial^{\mu} F_{\mu\nu} = \frac{4\pi}{c} j_{\nu} + A_{\lambda} \epsilon F_{\mu\nu} \tag{10}$$

where ε in (10) is a dimensionless number which is equal to one for our non-commutative case (4) and equals zero for the usual commutative case and has been introduced for clarity. In the usual commutative space and time $\varepsilon = 0$ and we get back the usual covariant Maxwell's equations given in (1). So now there are additional terms in the Maxwell equations.
Now let us try to derive these equations for two dimensions. We will see that this is a non-trivial case. We get

$$\partial^{1} F_{14} = \frac{4\pi}{c} j_{4} + A_{2} \varepsilon F_{14} \tag{11}$$

$$\partial^{2} F_{24} = \frac{4\pi}{c} j_{4} + A_{1} \varepsilon F_{24} \tag{12}$$

$$\partial^{4} F_{42} = \frac{4\pi}{c} j_{2} + A_{1} \varepsilon F_{12} \tag{13}$$

$$\partial^{1} F_{12} = \frac{4\pi}{c} j_{2} + A_{4} \varepsilon F_{12} \tag{14}$$

$$\partial^{2} F_{21} = \frac{4\pi}{c} j_{1} + A_{4} \varepsilon F_{21} \tag{15}$$

$$\partial^{4} F_{41} = \frac{4\pi}{c} j_{1} + A_{2} \varepsilon F_{41} \tag{16}$$

Now from covariant electrodynamics we know that $F_{\mu\nu}$ is the electromagnetic tensor and is given by [3]

$$F_{\mu\nu} = \begin{array}{c} \\ \mu \downarrow \end{array} \begin{array}{c} \nu \rightarrow \\ \begin{pmatrix} 0 & -cB_z & cB_y & -E_x \\ cB_z & 0 & -cB_x & -E_y \\ -cB_y & cB_x & 0 & -E_z \\ E_x & E_y & E_z & 0 \end{pmatrix} \end{array} \tag{17}$$

This electromagnetic tensor will give Maxwell's equations. We can see that the electromagnetic tensor is asymmetric. Now from the different components from (11)-(16) given by using equation (17) we get

$$\frac{\partial E_x}{\partial x} = 4\pi\frac{\partial \rho}{\partial t} + \varepsilon A_y E_x \tag{18}$$

$$\frac{\partial E_y}{\partial y} = 4\pi\frac{\partial \rho}{\partial t} + \varepsilon A_x E_y \tag{19}$$

$$-\frac{\partial E_y}{\partial t} = 4\pi j_y - \varepsilon A_x E_y \tag{20}$$

$$\frac{\partial B_z}{\partial x} = 4\pi j_y + \varepsilon A_t B_z \tag{21}$$

$$\frac{\partial B_z}{\partial y} = 4\pi j_x + \varepsilon A_t B_z \tag{22}$$

$$-\frac{\partial E_x}{\partial t} = 4\pi j_x - \varepsilon A_y E_x \tag{23}$$

2 Results and Discussions

So from equations (18) to (23) we can see that there are extra terms in the Maxwell equations and if $\varepsilon = 0$ then we get the usual Maxwell's equations. Thus we can see that introduction of non-commutative spacetime leads to extra effects in Maxwell's equations (18) to (23) which indicate an extra electromagnetic field. Furthermore, as noted by one of the authors, and as can be seen from (18) to (23), the extra magnetic effect can be not just of the stationary type, that is it allows for the possibility of radiation [4].
In commutative spacetime $\varepsilon = 0$ and the extra magnetic effects will disappear. To get more insight into the extra magnetic effect we observe an alternate way of expressing the non-commutativity above. This is with a minimum spacetime extension which also leads to non-commutative geometry [1].
We have now a relation such that

$$[x, y] = l^2\Theta \tag{24}$$

where x and y are coordinates and l is the minimum extension and Θ are matrices. Because of the non-commutative geometry (24) it is known that there is the generation of a magnetic field which was shown independently by one of the authors and Saito [5, 6], with the relation

$$Bl^2 = hc/e \tag{25}$$

In other words, the non-commutativity of spacetime generates the extra electromagnetic effects.

3 TWO DIMENSIONAL GRAPHENE

The best example of the foregoing is the recent understanding of spacetime in Graphene [7] which approximates the above 2D scenario. The authors concluded that electron spin is attributed to the discreteness of spacetime which resembles a chess board and this type of a discrete partition of spacetime will lead to the generation of a magnetic field which may even effects the intrinsic behaviour of the electron.
Here spacetime is discrete and during the hopping of electrons there is change in spin direction which shows that the space is not smooth and this give rise to some sort a of magnetic field which can cause the change of spin in the electron during hopping. So we can see that this behaviour of electron spin can be analogous to the above with appearance of magnetic field in non-commutative spacetime.

References

[1] Sidharth, B.G. (2008). *The Thermodynamic Universe* (World Scientific, Singapore, 2008).

[2] Sidharth, B.G. (2001). *Chaotic Universe: From the Planck to the Hubble Scale* (Nova Science, New York, 2001).

[3] Panofsky, W.K.H., and Phillips, M. (1962). *Classical Electricity and Magnetism* (Addison-Wesley Publishing Company U.S.A, 1962) pp.324-339.

[4] Sidharth, B.G. (2012). *Prespacetime Journal* 3 (2) February 2012.

[5] Sidharth, B.G. (2003). *Nuovo Cimento B* 118B, (1), pp.35-40.

[6] Saito, T. (2000). *Gravitation and Cosmology* 6, No.22, pp.130-136.

[7] Mecklenburg, M., and Regan, R.C. (2011). *Phy.Rev.Lett.* 106,116803.

MADELBROT ISO-SETS: ISO-UNIT IMPACT ASSESSMENT

Reza Katebi
Department of Physics, California State University
Fullerton, 800 North State College Boulevard
Fullerton, CA 92831 USA
rkatebi.gravity@gmail.com
Nathan Schmidt
Department of Mathematics, Boise State University
1910 University Drive
Boise, ID 83725 USA
nathanschmidt@u.boisestate.edu

Received November 19, 2013

Abstract

In this introductory work, we use Santilli's iso-topic lifting as a cutting-edge platform to explore Mandelbrot's set. The objective is to upgrade Mandelbrot's complex quadratic polynomial with iso-multiplication and then computationally probe the effects on this revolutionary fractal. For this, we define the "iso-complex quadratic polynomial" and engage it to generate a locally iso-morphic array of "Mandelbrot iso-sets" by varying the iso-unit, where the connectedness property is topologically preserved in each case. The iso-unit broadens and strengthens the chaotic analysis, and authorizes an enhanced classification and demystification such complex systems because it equips us with an additional degree of freedom: the new Mandelbrot iso-set array is an improvement over the traditional Mandelbrot set because it is significantly more general. In total, the experimental results exemplify dynamic iso-spaces and indicate two modes of topological effects: scale-deformation and boundary-deformation. Ultimately, these new and preliminary developments spark further insight into the emerging realm of iso-fractals.

Keywords: Geometry and topology; Chaos theory; Complex systems; Santilli iso-number; Fractal; Iso-fractal; Mandelbrot set; Mandelbrot iso-set.

Copyright © 2013 by Hadronic Press, Inc., Palm Harbor, FL 34684, USA

1 Introduction

The Mandelbrot set is often considered to be the most famous fractal. It is a mathematical set of points in a Euclidean complex space $\mathbb{C}$, with a distinctive boundary that characterizes a fractal structure with self-similarity [1, 2]. The set is closely related to Julia sets [3] and is named after the French mathematician Benoit Mandelbrot, the pioneer who analyzed and popularized it [1, 2]. Images of Mandelbrot's set are created by iteratively sampling complex numbers and determining, for each one, if the result tends towards infinity when a particular mathematical operation is iterated on it [1, 2]. For each complex number, the real and imaginary components serve as 2D image coordinates in $\mathbb{C}$ [4], where the pixels are colored to encode the sequence divergence rate [1, 2]. In particular, the Mandelbrot set is the set of values of $c \in \mathbb{C}$ for which the orbit of 0 under iteration of Mandelbrot's complex quadratic polynomial [1, 2]

$$z_{n+1} = z_n^2 + c, \tag{1}$$

remains bounded, where $z_n, z_{n+1}, c \in \mathbb{C}$ are complex numbers. That is, c is part of the Mandelbrot set if, when starting with $z_0 = 0$ and applying the iteration repeatedly, the absolute value of z_n remains bounded however large n gets [1, 2]. Mandelbrot initially hypothesized that the connectedness property is not preserved for his set, but after further experimentation he later revised his conjecture and claimed that the set is connected [5]. Subsequently, Douady and Hubbard proved that indeed Mandelbrot's set is connected [5, 6]. Beyond the discipline of mathematics, the Mandelbrot set has become prominent in various art forms due to its aesthetic appeal [7, 8, 9] and, moreover, because it is an emergent complex structure that arises from the application of *simple* rules [1, 2].

So why are the Mandelbrot set and other such fractals important subjects to study in science and mathematics? Well, it turns out that *fractal geometry* is the language of chaos theory [4, 10], and fractal/chaotic patterns are *abundant* in the physical, chemical, and biological expressions of nature [8, 11, 12]. Moreover, fractal geometry and chaos theory are a relatively new discipline [4]. Chaos theory examines the behavior of dynamical systems that are *highly sensitive* to initial conditions [11, 13]. In a chaotic dynamical system, *miniscule* differences in initial conditions yield *widely*

diverging outcomes, thereby generally rendering long-term predictions impossible [11, 13]. For this, additional examples of chaos and fractals are also observed in lightning discharges [14, 15, 16, 17], weather patterns [18, 19, 20], aquatic ecosystems [21, 22], population biology [23], the biological allometric scaling laws [24, 25, 26, 27, 28], cancers and genetics [29, 30], viruses and pathogens [31, 32], the human brain [33, 34, 35], earthquakes [36, 37, 38], volcanoes [39, 40, 41], the global stock market [42, 43], and more. Certainly, fractals such as the Mandelbrot set must play a fundamental role in classifying and demystifying such *complex* systems—but how?

In this paper, we resume the iso-fractal developments of [4] and attack this complex problem by utilizing the power of Santilli's new iso-topic lifting [44, 45, 46, 47, 48, 49] to probe Mandelbrot's set [1, 2]. For this, we launch with Section 2, where we deploy Santilli's iso-numbers [44, 45, 46, 47, 48, 49] to upgrade Mandelbrot's complex quadratic polynomial—eq. (1)—with iso-multiplication to construct the *iso-complex quadratic polynomial*, which is used to construct a *Mandelbrot iso-set*. For this, we identify the procedure and results for the *main* computational experiment that assesses the impact of Santilli's iso-unit [44, 45, 46, 47, 48, 49] for various Mandelbrot iso-sets, where the connectedness property is preserved. Afterwards, in the *extended* experiment of Section 3, we expand the examination and outcomes to include a Mandelbrot iso-complex polynomial of degree k along with a version based on the tangent trigonometric function. Finally, we conclude with Section 4, where we briefly recapitulate this mode of research and suggest future actions to take.

2 Main Experiment

Here, motivated by the iso-fractal initiation of [4], we engage Santilli's iso-numbers [44, 45, 46, 47, 48, 49] to explore Mandelbrot's set [1, 2] in Euclidean complex space. In the procedure of Section 2.1, we attack our objective by upgrading Mandelbrot's complex quadratic polynomial—eq. (1)—with Santilli's iso-multiplication [44, 45, 46, 47, 48, 49] to construct the iso-complex quadratic polynomial, which is used to construct a Mandelbrot iso-set. Afterwards, in Section 2.2, we examine the computational results for an array of Mandelbrot iso-sets with distinct iso-topic liftings to assess the impact of varying the iso-units.

2.1 Main Procedure

In this section, the iso-complex quadratic polynomial for the experiment is assembled as follows:

1. First, in accordance to Santilli's iso-number methodology [44, 45, 46, 47, 48, 49], we select the positive-definite iso-unit $\hat{r} > 0$ with the corresponding inverse $\hat{\kappa} = \frac{1}{\hat{r}} > 0$.

2. Second, given that $\mathbb{C}$ is the set of all complex numbers, then we demonstrate that $\mathbb{C}$ is iso-topically lifted via $\mathbb{C} \to \mathbb{C}_{\hat{r}}$ to establish $\mathbb{C}_{\hat{r}}$, which is the set of all iso-complex numbers [4, 44, 45, 46, 47, 48, 49]. Thus, if $z_1, z_2 \in \mathbb{C}$ are complex numbers, then the corresponding iso-complex numbers $\hat{z}_1, \hat{z}_2 \in \mathbb{C}_{\hat{r}}$ are directly related via [4, 44, 45, 46, 47, 48, 49]

$$\begin{array}{rcl} \hat{z}_1 & = & z_1 \times \hat{r} \\ & & , \ \forall z_1, z_2 \in \mathbb{C} \to \forall \hat{z}_1, \hat{z}_2 \in \mathbb{C}_{\hat{r}}, \\ \hat{z}_2 & = & z_2 \times \hat{r} \end{array} \tag{2}$$

   where the conventional complex multiplication $\hat{z}_1 \times \hat{z}_2$ is upgraded with the iso-multiplication [4, 44, 45, 46, 47, 48, 49]

$$\hat{z}_1 \ \hat{\times} \ \hat{z}_2 = \hat{z}_1 \times \hat{\kappa} \times \hat{z}_2 = \hat{z}_1 \times \frac{1}{\hat{r}} \times \hat{z}_2. \tag{3}$$

3. Third, given the iso-multiplication of eq. (3), we deduce the iso-square via the expansion

$$\begin{array}{rcl} \hat{z}_n^2 & = & \hat{z}_n \ \hat{\times} \ \hat{z}_n \\ & = & (z_n \times \hat{r}) \times \hat{\kappa} \times (z_n \times \hat{r}) \\ & = & (z_n \times \hat{r}) \times \frac{1}{\hat{r}} \times (z_n \times \hat{r}) \\ & = & z_n \times z_n \times \hat{r}. \end{array} \tag{4}$$

4. Fourth, we prove that the axiom of the multiplicative units of eqs. (2–4) is confirmed by the expressions [4, 44, 45, 46, 47, 48, 49]

$$1 \ \hat{\times} \ \hat{z}_n = 1 \times \hat{\kappa} \times \hat{z}_n = \hat{z}_n \times \frac{1}{\hat{r}} \times 1 = \hat{z}_n \ \hat{\times} \ 1, \ \forall \hat{z}_n \in \mathbb{C}_{\hat{r}}. \tag{5}$$

5. Fifth, we establish that eqs. (2–5) are characterized by the iso-topic lifting and its inverse [4, 44, 45, 46, 47, 48, 49]

$$\begin{aligned} f(\hat{r}): \quad \mathbb{C} \quad &\rightarrow \quad \mathbb{C}_{\hat{r}} \\ f^{-1}(\hat{r}): \quad \mathbb{C}_{\hat{r}} \quad &\rightarrow \quad \mathbb{C}, \end{aligned} \tag{6}$$

respectively, where indeed $\mathbb{C}$ and $\mathbb{C}_{\hat{r}}$ are *locally iso-morphic*.

6. Finally, we engage eqs. (2–6) to upgrade eq. (1) to define the iso-complex quadratic polynomial as

$$\hat{z}_{n+1} \equiv \hat{z}_n^2 + \hat{c} \equiv (\hat{z}_n \hat{\times} \hat{z}_n) + \hat{c} \equiv (z_n \times z_n \times \hat{r}) + (c \times \hat{r}) \equiv z_{n+1} \times \hat{r}, \tag{7}$$

where $\hat{z}_n, \hat{z}_{n+1}, \hat{c} \in \mathbb{C}_{\hat{r}}$ are iso-complex numbers and $z_n, z_{n+1}, c \in \mathbb{C}$ are the corresponding complex numbers. Hence, we can computationally generate a Mandelbrot iso-set by systematically iterating eq. (7)! Here, we note that the restricted iso-unit case of $\hat{r} = 1$ for eq. (7) yields the conventional Mandelbrot set of eq. (1) with the standard multiplicative unit, therefore the Mandelbrot iso-set array includes the Mandelbrot set as an element so they are connected.

Thus, given that the Mandelbrot set generated by eq. (1) has been proven to have the connectedness property by Douady and Hubbard [5, 6], and given that the iso-topic lifting of eqs. (2–6) is topologically-preserving to the Mandelbrot set, then we deduce that a Mandelbrot iso-set generated by eq. (7)—which is locally iso-morphic—*must inherit the connectedness property*. Here, we *hypothesize* that the Julia set for a given point in a Mandelbrot iso-set is connected, but this notion of "Julia iso-sets" is beyond the limited scope of this paper and will thus be a subject for future research.

At this point, we've successfully upgraded Mandelbrot's complex quadratic polynomial [1, 2] of eq. (1) with Santilli's iso-multiplication [4, 44, 45, 46, 47, 48, 49] to synthesize the iso-complex quadratic polynomial of eq. (7), which is used to generate Mandelbrot iso-sets.

2.2 Main Results

In total, we computationally experimented with the 5 distinct iso-units:

$$\hat{r} \in \{\frac{1}{2}, \frac{3}{4}, 1, \frac{4}{3}, 2\}. \tag{8}$$

In eq. (8), we observe that $\frac{1}{2}$ is the inverse of 2, 1 is the inverse of 1, and $\frac{3}{4}$ is the inverse of $\frac{4}{3}$, so these iso-unit values are in fact *dual*. Our objective is to insert the various iso-units of eq. (8) into the iso-complex quadratic polynomial of eq. (7) to observe the effect of Santilli's iso-topic lifting [4, 44, 45, 46, 47, 48, 49] on Mandelbrot's set [1, 2].

For our experimental control case, we started with $\hat{r} = 1$ and generated the Mandelbrot set—see the *middle* graphic in Figure 1. Afterwards, we varied the iso-unit for $\hat{r} \neq 1$, such that $\hat{r} = \frac{1}{2}, \frac{3}{4}, \frac{4}{3}, 2$, to generate the Mandelbrot iso-sets—see the *non-middle* graphics in Figure 1. In this preliminary assessment, we observe that the iso-unit variation impact results of Figure 1 indicate that Santilli's iso-topic lifting [4, 44, 45, 46, 47, 48, 49] yields—at minimum—*two* general topological effects:

1. **scale-deformation**, where the fractal is magnified ("zoom-in") or de-magnified ("zoom-out"); and

2. **boundary-deformation**, where the relative position of the fractal boundaries and sequence divergence rates are restructured.

Effects 1 and 2 prove the iso-mathematical existence of the proposed Mandelbrot iso-sets, which are indeed *locally iso-morphic* to the Mandelbrot set. Moreover, these computational results are an experimental implementation of the discrete dynamic iso-spaces in [50], where the iso-unit is treated as a dynamic iso-unit function of a parameter that varies by taking on discrete values.

3 Extended Experiment: Procedure and Results

Here, inspired by the procedure and outcomes of Section 2, we further probe the Mandelbrot iso-set array by experimenting with two alternative variations of the iso-complex polynomial of eq. (7) to open up additional iso-fractal cases for investigation.

First, for the *degree-k Mandelbrot iso-set* experimental case, we replace the $\hat{z}_n^2$ of eq. (7) with the generalization $\hat{z}_n^k$ to define the *degree-k Mandelbrot iso-complex polynomial*

$$\hat{z}_{n+1} \equiv \hat{z}_n^k + \hat{c}, \tag{9}$$

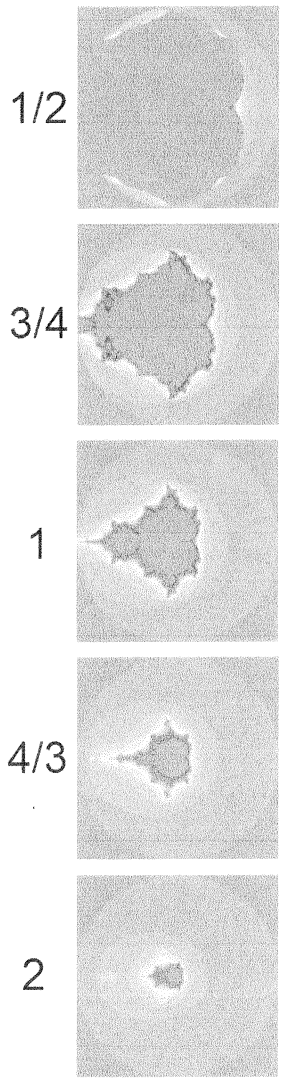

Fig. 1: A depiction of the iso-unit impact variation for the *main* computational experiment. In the *left* column, the varying iso-units of eq. (8) are listed. In the *right* column, the middle graphic is the Mandelbrot set and the non-middle graphics are the Mandelbrot iso-sets that are generated by eq. (7). Observe that Santilli's iso-topic lifting [44, 45, 46, 47, 48, 49] yields two general topological effects: scale-deformation and boundary-deformation.

such that $k > 0$ is a positive-definite natural number. Subsequently, for eq. (9), we set $k = 3$ and re-execute the computational experiment with the same 5 distinct iso-unit parameters of eq. (8): the resulting degree-3 Mandelbrot iso-sets are displayed in the *left* column of Figure 2, which are indeed *locally iso-morphic* to each other. Here, similar to the computational results of Section 2.2, we observe the two general topological effects: scale-deformation and boundary-deformation.

Second, for the *tangent Mandelbrot iso-set* experimental case, we replace the $\hat{z}_n^2$ of eq. (7) with the variation $\tan(\hat{z}_n^2)$ to define the *tangent Mandelbrot iso-complex polynomial*

$$\hat{z}_{n+1} \equiv \tan(\hat{z}_n^2) + \hat{c}. \tag{10}$$

Subsequently, for eq. (10), we re-execute the computations with the same 5 distinct iso-unit parameters of eq. (8): the resulting tangent Mandelbrot iso-sets are displayed in the *right* column of Figure 2, which are indeed *locally iso-morphic* to each other. Here, similar to the computational results of the degree-3 Mandelbrot iso-set case, we observe the two general topological effects: scale-deformation and boundary-deformation.

Thus, in total, the extended outcomes of eqs. (9–10) and Figure 2 indicate that it is possible to develop theoretical and experimental computations for generating such Mandelbrot iso-set variations.

4 Conclusion

The outcomes of this investigation reveal and assess the preliminary impact of Santilli's iso-unit [44, 45, 46, 47, 48, 49] on Mandelbrot's set [1, 2]. More precisely, we were inspired by the iso-fractal developments of [4] and deployed iso-topic liftings [44, 45, 46, 47, 48, 49] to transform Mandelbrot's complex quadratic polynomial into an iso-complex quadratic polynomial, which thereby enabled us to forge the new Mandelbrot iso-set—the Mandelbrot set and a given Mandelbrot iso-set are locally iso-morphic. Subsequently, the initial results of the computational experiments revealed that varying the iso-units causes two general topological effects: scale-deformation and boundary-deformation. For this, we noted that this experiment is an implementation of discrete dynamic iso-spaces [50].

The main results of Section 2.2 clearly indicate that the Mandelbrot set is a specific type of Mandelbrot iso-set when the iso-unit $\hat{r}$ is *not* iso-topically

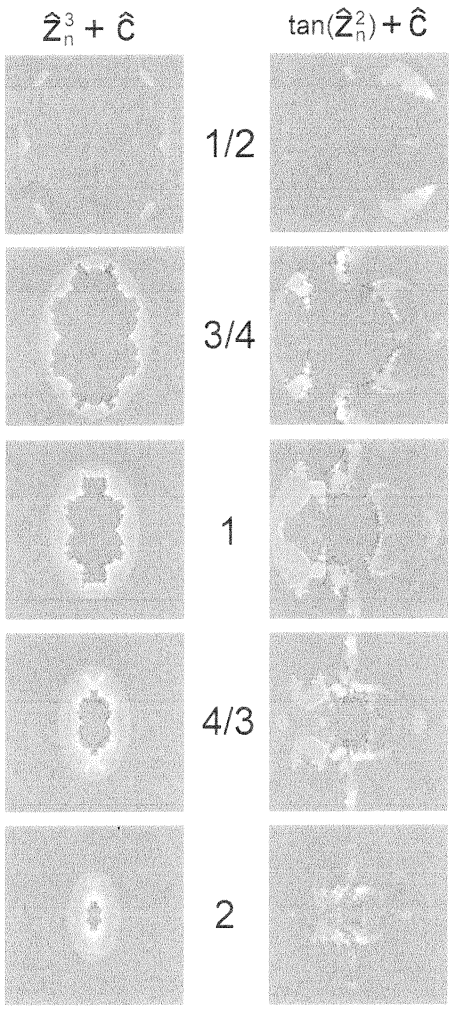

Fig. 2: A depiction of the iso-unit impact variation for the *extended* computational experiment. In the *left* column, the *degree-k Mandelbrot iso-sets* generated by $\hat{z}_n^k + \hat{c}$ in eq. (9) for $k = 3$ are listed. In the *middle* column, the varying iso-units of eq. (8) are listed. In the *right* column, the *tangent Mandelbrot iso-sets* generated by $\tan(\hat{z}_n^2) + \hat{c}$ in eq. (10) are listed. Again, in both experimental cases, observe that Santilli's iso-topic lifting [44, 45, 46, 47, 48, 49] yields two general topological effects: scale-deformation and boundary-deformation.

lifted and thus restricted to the conventional case $\hat{r} = 1$; one could classify the Mandelbrot set as the "base case" of the Mandelbrot iso-set array. Thus, the iso-topic liftings [44, 45, 46, 47, 48, 49] preserve *all* of the Mandelbrot set's characteristics and extend them. For this, the iso-topic liftings [44, 45, 46, 47, 48, 49] enable us to vary $\hat{r}$, which serves as an additional degree of freedom for iso-fractal construction and analysis, and therefore authorizes an enhanced classification and demystification methodology for such chaotic systems because we can take into further account the iso-unit impact of the scale-deformations and boundary-deformations. Hence, we recapitulate these outcomes and implications by pointing out that: *the Mandelbrot iso-set is an improvement over the Mandelbrot set* because the iso-topic liftings [44, 45, 46, 47, 48, 49] render it to be *significantly more general.*

The extended results of Section 3 further probed the Mandelbrot iso-set array by experimenting with two alternative variations of the iso-complex polynomial: the degree-k Mandelbrot iso-set and the tangent Mandelbrot iso-set. Here, the two experimental cases proved the existence of such iso-fractals, which are indeed locally iso-morphic to each other under the topological-preservations of the iso-topic liftings [44, 45, 46, 47, 48, 49], where again, we observed the two said modes of topological deformation effects.

In our opinion, the examination and results indicate an exciting and promising future for this mode of cutting-edge research: the territory of iso-fractals is a vast, uncharted frontier. Ultimately, the implications of this venture are significant because they advance the borderland of iso-mathematics to new trajectories of thought, inquiry, and experimentation. Hence, for future research, we plan to conduct additional related surveys of iso-mathematics that investigate novel patterns for advancement, with the intent to simplify and classify these emerging, developing iso-fractals. More precisely, in future work, we plan to identify the area and Hausdorff dimension [51] of the Mandelbrot iso-set and develop Julia iso-sets to test our connectedness hypothesis in a more generalized iso-fractal framework.

5 Acknowledgment

We wish to thank the anonymous referees for the constructive criticisms and comments that enhanced the quality and application of this paper.

References

[1] B. B. Mandelbrot. *The fractal geometry of nature.* Times Books, 1982.

[2] B. B. Mandelbrot. *Fractals and chaos: the Mandelbrot set and beyond*, volume 3. Springer, 2004.

[3] I. D. Entwistle. Julia set art and fractals in the complex plane. *Computers & Graphics*, 13(3):389–392, 1989.

[4] N. O. Schmidt and R. Katebi. Initiating Santilli's iso-mathematics to triplex numbers, fractals, and Inopin's holographic ring: preliminary assessment and new lemmas. *Hadronic Journal (in press)*, 36, 2013.

[5] O. Knill. Harvard mathematics archive - the Mandelbrot set, 2005.

[6] A. Douady and J. H. Hubbard. Exploring the Mandelbrot set. The Orsay notes.

[7] B. B. Mandelbrot. Fractals and an art for the sake of science. *Leonardo. Supplemental Issue*, pages 21–24, 1989.

[8] J. Briggs. *Fractals: The patterns of chaos: A new aesthetic of art, science, and nature.* Simon and Schuster, 1992.

[9] J. J. Ventrella. Evolving the Mandelbrot set to imitate figurative art. In *Design by Evolution*, pages 145–167. Springer, 2008.

[10] H. O. Peitgen, H. Jürgens, and D. Saupe. *Chaos and fractals: new frontiers of science.* Springer, 2004.

[11] E. N. Lorenz. *The essence of chaos.* Routledge, 1995.

[12] G. W. Flake. *The computational beauty of nature: Computer explorations of fractals, chaos, complex systems and adaption.* The MIT Press, 1998.

[13] S. H. Kellert. *In the wake of chaos: Unpredictable order in dynamical systems.* University of Chicago Press, 1993.

[14] A. A. Tsonis and J. B. Elsner. Fractal characterization and simulation of lightning. *Beiträge zur Physik der Atmosphäre*, 60:187–192, 1987.

[15] J. Sanudo, J. B. Gómez, F. Castano, A. F. Pacheco, and et al. Fractal dimension of lightning discharge. *Nonlinear Processes in Geophysics*, 2(2):101–106, 1995.

[16] G. Milikh and J. A. Valdivia. Model of gamma ray flashes due to fractal lightning. *Geophysical Research Letters*, 26(4):525–528, 1999.

[17] J. A. Riousset, V. P. Pasko, P. R. Krehbiel, R. J. Thomas, and W. Rison. Three-dimensional fractal modeling of intracloud lightning dis-

charge in a New Mexico thunderstorm and comparison with lightning mapping observations. *Journal of Geophysical Research: Atmospheres (1984–2012)*, 112(D15), 2007.

[18] A. A. Tsonis and J. B. Elsner. Chaos, strange attractors, and weather. *Bulletin of the American Meteorological Society*, 70:14–23, 1989.

[19] R. F. Cahalan and J. H. Joseph. Fractal statistics of cloud fields. *Monthly Weather Review*, 117(2):261–272, 1989.

[20] J. B. Elsner and K. P. Georgakakos. Estimating the dimension of weather and climate attractors: important issues about the procedure and interpretation. *Journal of the Atmospheric Sciences*, 50(15), 1993.

[21] S. B. Grant, C. Poor, and S. Relle. Scaling theory and solutions for the steady-state coagulation and settling of fractal aggregates in aquatic systems. *Colloids and Surfaces A: Physicochemical and Engineering Aspects*, 107:155–174, 1996.

[22] J. Huisman and F. J. Weissing. Biodiversity of plankton by species oscillations and chaos. *Nature*, 402(6760):407–410, 1999.

[23] P. Philippe. Chaos, population biology, and epidemiology: some research implications. *Human Biology*, 65(4):525, 1993.

[24] G. B. West, J. H. Brown, and B. J. Enquist. A general model for the origin of allometric scaling laws in biology. *Science*, 276(5309):122–126, 1997.

[25] G. B. West, J. H. Brown, and B. J. Enquist. The fourth dimension of life: fractal geometry and allometric scaling of organisms. *Science*, 284(5420):1677–1679, 1999.

[26] R. Wu, C. X. Ma, R. C. Littell, and G. Casella. A statistical model for the genetic origin of allometric scaling laws in biology. *Journal of Theoretical Biology*, 219(1):121–135, 2002.

[27] G. B. West and J. H. Brown. The origin of allometric scaling laws in biology from genomes to ecosystems: towards a quantitative unifying theory of biological structure and organization. *Journal of Experimental Biology*, 208(9):1575–1592, 2005.

[28] L. Demetrius. The origin of allometric scaling laws in biology. *Journal of Theoretical Biology*, 243(4):455–467, 2006.

[29] P. Duesberg. Chromosomal chaos and cancer. *Scientific American Magazine*, 296(5):52–59, 2007.

[30] G. A. Calin, C. Vasilescu, M. Negrini, and G. Barbanti-Brodano. Genetic chaos and antichaos in human cancers. *Medical Hypotheses*, 60(2):258–262, 2003.

[31] P. Yam. Noisy nucleotides. DNA sequences show fractal correlations. *Scientific American*, 267(3):23–4, 1992.

[32] L. Bos and et al. *Plant viruses, unique and intriguing pathogens: a textbook of plant virology.* Backhuys Publishers, 1999.

[33] X. Nan and X. Jinghua. The fractal dimension of EEG as a physical measure of conscious human brain activities. *Bulletin of Mathematical Biology*, 50(5):559–565, 1988.

[34] S. L. Free, S. M. Sisodiya, M. J. Cook, D. R. Fish, and S. D. Shorvon. Three-dimensional fractal analysis of the white matter surface from magnetic resonance images of the human brain. *Cerebral Cortex*, 6(6):830–836, 1996.

[35] D. S. Bassett, A. Meyer-Lindenberg, S. Achard, T. Duke, and E. Bullmore. Adaptive reconfiguration of fractal small-world human brain functional networks. *Proceedings of the National Academy of Sciences*, 103(51):19518–19523, 2006.

[36] H. J. Xu and L. Knopoff. Periodicity and chaos in a one-dimensional dynamical model of earthquakes. *Physical Review E*, 50(5):3577, 1994.

[37] C. H. Scholz. Earthquakes as chaos. *Nature*, 348(6298):197–198, 1990.

[38] M. Sahimi, M. C. Robertson, and C. G. Sammis. Fractal distribution of earthquake hypocenters and its relation to fault patterns and percolation. *Physical Review Letters*, 70(14):2186, 1993.

[39] S. L. Harris. *Agents of chaos: earthquakes, volcanoes, and other natural disasters.* Mountain Press Publishing Company, 1990.

[40] D. L. Turcotte. *Fractals and chaos in geology and geophysics.* Cambridge University Press, 1997.

[41] U. Kueppers, D. Perugini, and D. B. Dingwell. Explosive energy during volcanic eruptions from fractal analysis of pyroclasts. *Earth and Planetary Science Letters*, 248(3):800–807, 2006.

[42] B. LeBaron. Chaos and nonlinear forecastability in economics and finance. *Philosophical Transactions of the Royal Society of London. Series A: Physical and Engineering Sciences*, 348(1688):397–404, 1994.

[43] E. E. Peters and et al. *Fractal market analysis: applying chaos theory*

to investment and economics, volume 24. Wiley New York, 1994.

[44] R. M. Santilli. Isonumbers and genonumbers of dimensions 1, 2, 4, 8, their isoduals and pseudoduals, and "hidden numbers" of dimension 3, 5, 6, 7. *Algebras, Groups and Geometries*, 10:273, 1993.

[45] R. M. Santilli. Rendiconti circolo matematico di palermo. *Supplemento*, 42:7, 1996.

[46] C. X. Jiang. Fundaments of the theory of Santillian numbers. *International Academic Presss, America-Europe-Asia*, 2002.

[47] R. M. Santilli. Hadronic mathematics, mechanics and chemistry. *Volume I, II, III, IV, and V, International Academic Press, New York*, 2008.

[48] C. Corda. Introduction to Santilli iso-numbers. In *AIP Conference Proceedings-American Institute of Physics*, volume 1479, page 1013, 2012.

[49] C. Corda. Introduction to Santilli iso-mathematics. In *AIP Conference Proceedings-American Institute of Physics*, 2013.

[50] N. O. Schmidt. Dynamic iso-topic lifting with application to Fibonacci's sequence and Mandelbrot's set. *Hadronic Journal (in press)*, 36, 2013.

[51] Mitsuhiro Shishikura. The Hausdorff dimension of the boundary of the Mandelbrot set and Julia sets. *Annals of Mathematics*, pages 225–267, 1998.

ISO-GALOIS FIELDS

Arun S. Muktibodh
Department of Mathematics
Mohota College of Science
Nagpur-440009
India
amukti2000@yahoo.com

Received November 13, 2013

Abstract

Rugero Maria Santilli [8], [9], [10] and [11] defined iso-fields of characteristic zero. In this paper we extend this definition to define Iso-Galois fields which are essentially of non-zero characteristic. Iso-Galois fields of first and second kind are also defined with specific examples. We have also proved some results regarding the structure of these constructs.

keywords:- Isounit, Isofield, Galois field and Iso-Galois field.

Copyright © 2013 by Hadronic Press, Inc., Palm Harbor, FL 34684, USA

1 Introduction

During a talk at the conference *Differental Geometric Methods in Mathematical Physics* held in Clausthal, Germany, in 1980, Ruggero Maria Santilli submitted new numbers based on certain axiom preserving generalization of the multiplication, today known as *isotopic numbers* or *isonumbers* in short. This generalization induced the so-called isotopies of the conventional multiplication with consequential generalization of the multiplicative unit, where the Greek word "isotopy" suggested the meaning "same topology". Subsequently, Rugero Maria Santilli submitted a new conjugation, under the name *isoduality* which yields an additional class of numbers, today known as *isodual isonumbers.*

The discovery of isonumbers was made with the specific need of quantitative representation of the transition from :

a) *exterior dynamical problem*, i.e., particles moving in the homogeneous and isotropic vacuum (empty space) with consequential local-differential and potential-cannonical equations of motion, to

b) the *interior dynamical problem*, i.e., extended and therefore deformable particles moving within an inhomogeneous and anisotropic physical medium, with consequential equations of motion of the most general known nonlinear, nonlocal-integral and nonpotential-noncanonical type.

We appraise the readers with some basic ideas of Santilli's isofields and some related results.

1.1 Santilli's Isofield

Definition 1.1. *Given a field F with elements $\alpha, \beta, \gamma, \ldots$, sum $\alpha + \beta$, multiplication $\alpha\beta$, and respective units 0 and 1, "Santilli's isofields" are rings of elements $\hat{\alpha} = \alpha\hat{1}$ where α are elements of F and $\hat{1} = \hat{T}^{-1}$ is a positive-definite $n \times n$ matrix generally outside F equipped with the same sum $\hat{\alpha} + \hat{\beta}$ of F with related additive unit $\hat{0} = 0$ and a new multiplication $\hat{\alpha} * \hat{\beta} = \hat{\alpha}\hat{T}\hat{\beta}$, under which $\hat{1} = \hat{T}^{-1}$ is the new left and right unit of F in which case $\hat{F}$ satisfies all axioms of a field.*

The 'isofields' $\hat{F} = \hat{F}(\hat{\alpha}, +, \hat{\times})$ are given by elements $\hat{\alpha}, \hat{\beta}, \hat{\gamma} \ldots$ characterized by one-to-one and invertible maps $\alpha \to \hat{\alpha}$ of the original element

$\alpha \in F$ equipped with two operations $(+, \hat{\times})$, the conventional addition $+$ of F and a new multiplication $\hat{\times}$ called "isomultiplication" with corresponding conventional additive unit 0 and a generalized multiplicative unit $\hat{1}$, called "multiplicative isounit" under which all the axioms of the original field F are preserved.

If the conventional field is chosen to be alternative under the operation of conventional multiplication then the resulting isofield is also isoalternative under isomultiplication.
If the given algebraic structure is a noncommutative division ring (e.g. ring of quaternions) then the resulting isoalgebraic structure is also noncommutative under the isomultiplication.

This new algebraic structure has revolutionized contemporary mathematics and found its applications in so far unexplored (unexplained) and unknown territories of quantum mechanics and quantum chemistry.
The resulting new theory of numbers has become the basis of recent studies of **nonlinear-nonlocal, non-Hamiltonian systems** in nuclear particle and statistical physics. Santilli iso-numbers, which are the mathematical basis of Hadronic Mechanics, are also introduced and reviewed in [2].

Isofields are of two types, **isofield of first kind**; wherein the isounit does not belong to the original field, and **isofield of second kind**; wherein the isounit belongs to the original field. The elements of the isofield are called as **isonumbers**. This leads to number of new terms and parallel developments of conventional mathematics.

We mention two important propositions by Santilli [10].

Proposition 1.1. *The necessary and sufficient condition for the lifting (where the multiplication is lifted but elements are not)* $F(a, +, \times) \longrightarrow (\hat{F}, +, \hat{\times}), \hat{\times} = \times\hat{T}\times, \hat{1} = \hat{T}^{-1}$ *to be an isotopy (that is for* $\hat{F}$ *to verify all axioms of the original field F) is that* $\hat{T}$ *is a non-null element of the original field* F.

e.g. We can start with the field of real numbers $\Re$ and construct an isotopic field $\hat{\Re}$ with a new multiplicative identity as $\hat{1} = \frac{1}{2}$ where $\hat{T} = 2$ as the isounit. So, if $a \in \Re$ then $\hat{a} = a.\frac{1}{2}$. Thus the product of two iso numbers $\hat{a}$ and $\hat{b}$ will be $\hat{a}\hat{\times}\hat{b} = \frac{a}{2}.2.\frac{b}{2} = \frac{ab}{2} = \widehat{ab}$.

Proposition 1.2. *The lifting (where both the multiplication and the elements are lifted)*
$F(a, +, \times) \longrightarrow (\hat{F}, +, \hat{\times}), \hat{a} = a \times \hat{1}, \hat{\times} = \times\hat{T}\times, \hat{1} = \hat{T}^{-1}$ *constitutes an isotopy even when the multiplicative isounit* $\hat{1}$ *is not an element of the original field.*

The following three theorems [5] directly follow from the definition of isofield.

Proposition 1.3. *If* $(F, +, \times)$ *is a field and* $(\hat{F}, \hat{+}, \hat{\times})$ *is the corresponding isofield such that the isounit* $\hat{I} \in F$ *then* $(F, +, \times) \cong (\hat{F}, \hat{+}, \hat{\times})$.

Clearly, the map $x \longmapsto \hat{x}$ is an isomorphism.

Proposition 1.4. *If* $(F, +, \times)$ *is a field and* $(\hat{F}, \hat{+}, \hat{\times})$ *is the corresponding isofield such that the isounit* $\hat{I} \notin F$ *then* $(F, +, \times)$ *is isotopic to* $(\hat{F}, \hat{+}, \hat{\times})$.

Proposition 1.5. *Isofield corresponding to a non-commutative field is isotopic to the original field.*

The noncommutative ring of Quaternions is an example of this type.

1.2 Galois fields

Finite fields were first introduced by Galois in 1830 in his proof of the unsolvability of the general quintic equation. Hence finite fields are also called as Galois fields. When Cayley invented matrices a few decades later, it was natural to investigate groups of matrices over finite fields. In fact, the groups of matrices over the finite fields have become the most important class of groups. Finite fields have vast applications in computer science, coding theory, information theory, and cryptography.

Thus, Galois fields are finite fields. Finite fields are of nonzero characteristic. Every finite field is of prime-power order, and for every power of a prime there is a unique Galois field of this order.
Santilli's isofields are defined for the fields of characteristic zero, and hence for infinite fields.
Our main purpose is to apply Santilli's ideas to the fields of non-zero characteristic and seek for further development in this direction.
In this paper we answer the open problems posed in [5],

- Can we construct finite isofields of first kind ?
- Can we construct finite isofields of second kind ?

in the affirmative.

2 Iso-Galois fields

Definition 2.1. *If F is an iso-field and F is finite, then F is called an Iso-Galois field.*

Definition 2.2. *Let F be a Galois field. If G is an Iso-Galois field of F wherein the prescribed multiplicative identity is from the field F itself, then the Iso-Galois field G is called an* ***Iso-Galois field of second kind.***

Definition 2.3. *Let F be a Galois field. If G is an Iso-Galois field of F wherein the prescribed multiplicative identity is not from the field F, then the Iso-Galois field G is called an* ***Iso-Galois field of first kind.***

If G is an Iso-Galois field constructed from the field F then we call the field F as the **trivial iso-field**.

3 Iso-Galois fields of second kind

Consider a Galois field F_8 as a set of following matrices of integers modulo 2.

$$(0)=\begin{pmatrix}0&0&0\\0&0&0\\0&0&0\end{pmatrix},(1)=\begin{pmatrix}1&0&0\\0&1&0\\0&0&1\end{pmatrix},(2)=\begin{pmatrix}0&1&0\\0&0&1\\1&1&0\end{pmatrix},(3)=\begin{pmatrix}0&0&1\\1&1&0\\0&1&1\end{pmatrix},$$
$$(4)=\begin{pmatrix}1&1&0\\0&1&1\\1&1&1\end{pmatrix},(5)=\begin{pmatrix}0&1&1\\1&1&1\\1&0&1\end{pmatrix},(6)=\begin{pmatrix}1&1&1\\1&0&1\\1&0&0\end{pmatrix},(7)=\begin{pmatrix}1&0&1\\1&0&0\\0&1&0\end{pmatrix}$$

For an isofield it will be sufficient to consider the multiplication table of non-zero elements of F_8.

$\cdot$	(1)	(2)	(3)	(4)	(5)	(6)	(7)
(1)	1	2	3	4	5	6	7
(2)	2	3	4	5	6	7	1
(3)	3	4	5	6	7	1	2
(4)	4	5	6	7	1	2	3
(5)	5	6	7	1	2	3	4
(6)	6	7	1	2	3	4	5
(7)	7	1	2	3	4	5	6

Let us choose the iso-element $\hat{T}=(4)\equiv 4\in F_8$ in the above composition table. Then the iso-unit element is $\hat{1}=\frac{1}{\hat{T}}=\frac{1}{4}=4^{-1}=5$. By using the fact that for $a\in F_8$, $\hat{a}=a\cdot\frac{1}{\hat{T}}=a\cdot 5$. We construct the corresponding isonumbers. Thus,
$\hat{2}=2\cdot\frac{1}{4}=2\cdot 5=6$. Similarly, $\hat{3}=7$, $\hat{4}=1$, $\hat{3}=7$, $\hat{4}=1$, $\hat{5}=2$, $\hat{6}=3$ and $\hat{7}=4$.
We now construct the corresponding composition table for the isonumbers using the fact that the isomultiplication $\hat{\times}$ is defined as $\hat{a}\hat{\times}\hat{b}=\hat{a}\hat{T}\hat{b}$.
e.g. $\hat{6}\hat{\times}\hat{7}=6\cdot 4\cdot 7=1$ using above composition table. Thus the corresponding isomultiplication table (or iso-composition table) for isonumbers will be;

$\hat{\times}$	$\widehat{(1)}$	$\widehat{(2)}$	$\widehat{(3)}$	$\widehat{(4)}$	$\widehat{(5)}$	$\widehat{(6)}$	$\widehat{(7)}$
$\widehat{(1)}$	4	5	6	7	1	2	3
$\widehat{(2)}$	5	6	7	1	2	3	4
$\widehat{(3)}$	6	7	1	2	3	4	5
$\widehat{(4)}$	7	1	2	3	4	5	6
$\widehat{(5)}$	1	2	3	4	5	6	7
$\widehat{(6)}$	2	3	4	5	6	7	1
$\widehat{(7)}$	3	4	5	6	7	1	2

Note that the numbers in the iso-composition table are isonumbers.

Remark. *1. The function $f : F_8 \to F_8$ defined by $f(x) = 5x$ is not an isomorphism. However,*
2. The isofunction $\hat{f} : x \to \hat{x}$ is an isomorphism.

We generalize these observations in the following Theorem.

Theorem 3.1. *If F is a Galois field such that $\hat{F}$ is an Iso-Galois field of second kind, where $\hat{T} \in F$ is an isoelement and $\hat{x} = \hat{T}^{-1}x$, $x \in F$ then the function $f : F \to F$ defined by $x \mapsto \hat{T}^{-1}x$ is not an isomorphism but is an isotopism, whereas the isofunction $\hat{f} : F \to \hat{F}$ is an isomorphism.*

Proof. It is easy to verify that the function f is a translation from F to F and hence is not an isomorphism. It is an isotopism because we have prescribed a new identity and the result follows from [5].
If we consider the isofunction $\hat{f} : F \to \hat{F}$ then for $x, y \in F$, $\hat{f}(x.y) = \hat{T}^{-1}x.y$ whereas $\hat{f}(x)\hat{\times}\hat{f}(y) = \hat{x}\hat{\times}\hat{y} = \hat{T}^{-1}x.\hat{T}.\hat{T}^{-1}y = \hat{T}^{-1}x.y$. Thus $\hat{f}(x.y) = \hat{f}(x)\hat{\times}\hat{f}(y)$. □

Theorem 3.2. *If F is a Galois field of order p^m and n is the number of involutions in F then there exist $p^m - n - 1$ number of distinct Iso-Galois fields of kind two of F.*

Proof. The multiplicative group of F will obviously contain $p^m - 1$ number of non-zero elements. Every involution and its inverse will obviously give

rise to the same Iso-Galois field of second kind. Therefore the total number of distinct Iso-Galois fields would be $p^m - n - 1$. □

4 Iso-Galois fields of First kind

Consider a Galois field F of order 16 represented by the polynomials $a + bx + cx^2 + dx^3$, a, b, c and d are integers modulo 2. The polynomials are generated by the powers of x using the rule $x^4 = 1 + x$.
The elements of the field are; $(0) = (0,0,0,0)$, $(1) = (1,0,0,0)$, $(2) = (0,1,0,0)$, $(3) = (0,0,1,0)$, $(4) = (0,0,0,1)$, $(5) = (1,1,0,0)$, $(6) = (0,1,1,0)$, $(7) = (0,0,1,1)$, $(8) = (1,1,0,1)$, $(9) = (1,0,1,0)$, $(10) = (0,1,0,1)$, $(11) = (1,1,1,0)$, $(12) = (0,1,1,1)$, $(13) = (1,1,1,1)$, $(14) = (1,0,1,1)$, $(15) = (1,0,0,1)$ with the following composition table for multiplication;

·	1	2	3	4	5	6	7	8	9	10	11	12	13	14	15
1	1	2	3	4	5	6	7	8	9	10	11	12	13	14	15
2	2	3	4	5	6	7	8	9	10	11	12	13	14	15	1
3	3	4	5	6	7	8	9	10	11	12	13	14	15	1	2
4	4	5	6	7	8	9	10	11	12	13	14	15	1	2	3
5	5	6	7	8	9	10	11	12	13	14	15	1	2	3	4
6	6	7	8	9	10	11	12	13	14	15	1	2	3	4	5
7	7	8	9	10	11	12	13	14	15	1	2	3	4	5	6
8	8	9	10	11	12	13	14	15	1	2	3	4	5	6	7
9	9	10	11	12	13	14	15	1	2	3	4	5	6	7	8
10	10	11	12	13	14	15	1	2	3	4	5	6	7	8	9
11	11	12	13	14	15	1	2	3	4	5	6	7	8	9	10
12	12	13	14	15	1	2	3	4	5	6	7	8	9	10	11
13	13	14	15	1	2	3	4	5	6	7	8	9	10	11	12
14	14	15	1	2	3	4	5	6	7	8	9	10	11	12	13
15	15	1	2	3	4	5	6	7	8	9	10	11	12	13	14

The set $F_1 = \{0, 1, 6, 11\}$ forms a subfield of F. We consider an element $\hat{T} = 2$ such that $\hat{T}$ does not belong to F_1 and form an Iso-Galois field of F_1. The isoelement $\hat{1} = \frac{1}{\hat{T}} = \hat{T}^{-1} = 2^{-1} = 15$. The numbers of F_1 are converted

to following isonumbers as $\hat{1} = 15$, $\hat{6} = 6.15 = 5$ and $\hat{11} = 11.15 = 10$. Thus the isofield is $\hat{F}_1 = \{0, 15, 5, 10\}$ with the following composition table for isomultiplication.

$\hat{\times}$	15	5	10
15	15	5	10
5	5	10	15
10	10	15	5

e.g the isoproduct of 5 and 10 is given by $5.\hat{T}.10 = 5.2.10 = 15$.
Similarly, if $\hat{T} = 7$ then $\hat{1} = \frac{1}{\hat{T}} = 7^{-1} = 10$. The numbers of F_1 are converted to following isonumbers as $\hat{1} = 10$, $\hat{6} = 6.10 = 15$ and $\hat{11} = 11.10 = 5$. Thus the isofield is $\hat{F}_1 = \{0, 10, 15, 5\}$ with the following composition table for isomultiplication.

$\hat{\times}$	10	15	5
10	10	15	5
15	15	5	10
5	5	10	15

Theorem 4.1. *If F is a Galois field of order p^n and F_1 is a subfield of F of order p^m such that $F \setminus F_1$ has r number of involutions, then there exist $p^m - p^n - r$ number of distinct Iso-Galois fields of first kind of F_1.*

Proof. F_1 is a subfield of F implies $m|n$. Let $n = m + r$. Then
$o(F \setminus F_1) = p^n - p^m = p^{m+r} - p^m = p^m(p^r - 1) \ldots (1)$.
Case I : If $p = 2$ then $(1) \Rightarrow o(F \setminus F_1)$ is even.
Case II ; If $p \neq 2$ then $p^r - 1$ is even and again $o(F \setminus F_1)$ is even.
Also, if $x \in F \setminus F_1$ then x^{-1} also belongs to $F \setminus F_1$. Thus, each $x \in F \setminus F_1$ gives rise to one isofield of first kind of F_1. Now, if x is an involution then $x = x^{-1}$ and hence x and x^{-1} will give rise to same isofield. If there are r number of involutions in $F \setminus F_1$ then the number of elements which give rise to distinct isofields will be $p^n - p^m - r$. Hence the result. □

References

[1] R. H. Bruck, *A Survey of Binary Systems*, Springer Verlag, (1958).

[2] Christian Corda, *Introduction to Santilli iso-numbers* American Institute of Physics, AIP Conf. Proc. 1479, 1013 (2012); doi: 10.1063/1.4756316.

[3] Chun-Xuan Jiang, *Foundations of Santilli's Isonumber Theory, with applictions to New Cryptograms, Fermat's Theorem and Goldbach's Conjecture*, International Academic Press, America-Europe-Asia, 2002.

[4] J. K. Kadeisvili and N. Kamiya, *A characterization of Isofields and their isoduals*, Hadronic J. 16, 155-172,(1993).

[5] A. S. Muktibodh, *Foundations of Isomathematics*, American Institute of Physics, AIP Conference Proceedings 1558, 707 (2013); doi: 10.1063/1.4825589.

[6] Ruggero Maria Santilli, *isonumbers and genonumbers of dimension 1,2,4,8, their isoduals and pseudoduals, and "hidden numbers" of dimension 3,5,6,7*, algebras, groups and geometries 10, 273-322 (1993).

[7] R. M. Santilli, *Foundations of Hadronic Chemistry*, Kluwer Academic Publisher, Dordrecht, 2001.

[8] R. M. Santilli, Isotopies of contemporary mathematical structures, I; Isotopies of fields, vector spaces, transformation theory, Lie Algebras, analytic mechanics and space-time symmetries, Algebras, groups and Geometries 8, 169-266 (1991).

[9] R. M. Santilli, Isotopies of contemporary mathematical structures, II; Isotopies of symplectic geometry, affine geometry, Riemanian geometry and Einstein gravitation, Algebras, Groups and Geometries, 8, 275-390 (1991).

[10] R. M. Santilli, Elements of Hadronic Mechanics, Vol. I (1995) [15a], Vol. II, second edition (1995) [15b] Academy of Sciences, Kiev, http://www.santilli-foundation.org/docs/Santilli-300.pdf http://www.santilli-foundation.org/docs/Santilli-301.pdf.

[11] R. M. Santilli, Hadronic Mathematics, Physics and Chemistry, Vols. I [4a], II [4b], III [4c], IV [4d] and V [4e] , New York : International Academic Press , also in http://www.i-b-r.org/Hadronic-Mechanics.htm.

Acknowledgements: I profoundly thank Dr. Svetlin Georgiev, France, for the fruitful interactions and discussions I had with him, during his visit to India in October 2013.

ON THE MASS-ENERGY RELATIONSHIP $E=mc^2$

John Shim
Jshim454@gmail.com

Received November 30, 2013

Abstract

This paper examines Einstein's derivations of the mass-energy relationship $E=mc^2$ using the Lorentz transformations applied to a slowly accelerating charge of mass m, and also applied to a moving system emitting photons in opposite directions. In the first case, it is shown that Einstein's use of the transformations is inconsistent with the classical definition of electrostatic force, $\vec{F}= q\vec{E}$, and that the expression given by Einstein for the kinetic energy of the charge due to its motion relative to the stationary system must be interpreted as a modification of the classical electrostatic interaction. In the second case, it is shown that Einstein's conclusion does not follow from his example, and that the Lorentz transformations give no information about the kinetic energy of the excitation energy of a system due to its motion relative to a stationary coordinate system.

Keywords: Relativity; Special Relativity; Mass-energy relationship; Mass, Energy, Lorentz transformations.

Copyright © 2013 by Hadronic Press, Inc., Palm Harbor, FL 34684, US

Einstein in 1905 gave two derivations [1,2] of the mass energy relationship $E=mc^2$. The first was based on the change in kinetic energy of a slowly accelerating charge in an electrostatic field, using the classical definition of force on an electric charge due to an electrostatic field, $\vec{F}= q\vec{E}$. Einstein treats the case of a charge ε, of mass m, under the influence of an electric field in the x-direction, X, constant along the x-axis, so that the classical law of motion, $ma_x = F_x$ becomes

$$m\, d^2x/dt^2 = \varepsilon X \qquad (1)$$

He expresses (1) in a coordinate system moving at a velocity, v, relative to the stationary field, X, and then uses the Lorentz transformations to convert the acceleration on the left side of (1) back to the stationary coordinate system.

The force definition, $\vec{F}= q\vec{E}$, of course, already incorporates the change in velocity of the charge due to the force. That is, the force defined by the right side of the equation is independent of the velocity of the charge relative to the stationary field, $\vec{E}$. Einstein assumes that, because ε, m, and X are constants in the coordinate system of the field, they are constant also in a coordinate system moving at constant velocity, v, along the x-axis. Therefore (1) is also independent of any transformation to such a coordinate system. That is, the acceleration defined by the right side of (1) is always the same. Using ξ,τ as the coordinates in the moving coordinate system, we then must have

$$d^2\xi/d\tau^2 = d^2x/dt^2 = \varepsilon X/m\ .$$

Einstein ignores this independence, expresses (1) in a coordinate system moving at a velocity, v, relative to the stationary field, as

$$m\, d^2\xi/d\tau^2 = \varepsilon X' \qquad (2),$$

and then inappropriately transforms it back into the coordinate system of the stationary field with the Lorentz transformations, using them on the only term in the expression that is transformable, which is the acceleration, $d^2\xi/d\tau^2$. His new acceleration in the stationary coordinate system then becomes

$$d^2x'/dt'^2 = (\beta^3)\, d^2x/dt^2, \qquad (\beta = 1/\sqrt{1-v^2/c^2})$$

which he incorrectly substitutes for d^2x/dt^2 in (1), treating both sides of (1) as independent from each other, and gets

$$m\,\beta^3\, d^2x/dt^2 = \varepsilon X \qquad (3)$$

He then presents this as the classical electrostatic law of motion modified by the Lorentz transformations, which it is not. The acceleration on the left side of (1) is not independent of, but rather is defined by the force on the right, so that the acceleration in (1) by definition is $\varepsilon X/m$, and cannot be modified without changing the force on the right. That is, if $d^2x/dt^2 = \varepsilon X/m$, then $\beta^3\, d^2x/dt^2 \neq \varepsilon X/m$. By modifying the acceleration on the left side of (1), Einstein necessarily changes the force on the charge from εX to $\varepsilon X\, \beta^3$, so that if we are consistent with the logic of the classical law of motion, the left side of equation (3) must represent a new force, and so (3) must be correctly written as

$$m\, d^2x/dt^2 = \varepsilon X\, \beta^3 \qquad (4)$$

The kinetic energy imparted to the charge by the force in (4) would then be

$$W = \iint_{0,0}^{x,v} \varepsilon X\, \beta^3 dx\, dv.$$

Instead of using this expression, however, Einstein treats the left and right sides of the incorrect expression (3) as independent and equal, then writes incorrectly

$$W = \int \varepsilon X \, dx = m \int_0^v \beta^3 \, v \, dv .$$

Evaluating the integral on the right side, he then gets

$$W = mc^2 (\beta - 1),$$

thereby changing the force on the charge from $F = \varepsilon X$ to $F = m\beta^3 v$.

So, by an inappropriate application of the Lorentz transformations, and a complete misinterpretation of the classical law of motion, Einstein somehow arrives at an expression for the kinetic energy of the moving charge that evidently represents, at least to some degree, an actual velocity dependence, and possibly a mass dependence, of the electromagnetic interaction not exhibited in the classical model—to me a truly remarkable result. Unfortunately, in my view, the general acceptance of Einstein's representation of this modification as a change in the mass, or effective mass, of the moving charge due merely to its motion relative to an arbitrary coordinate system has effectively prevented any investigation into its actual source, as well as implying an applicability to other forces that may or may not be correct.

In Einstein's second derivation, he examines an excited system of energy E_0 before and after emitting two light pulses of equal energy, ½ L, in opposite directions. He expresses the energy in its own coordinate system, and in a coordinate system moving at a velocity v relative to it. He then attempts to show that the kinetic energy difference before and after emission between the two coordinate systems is

$$K_0 - K_1 = L (\beta - 1) \qquad (5)$$

Using the Lorentz transformations, he determines the energy of the emitted light pulses in the moving coordinate system, and then writes the total energy in each coordinate system after emission as

$$E_0 = E_1 + L, \tag{6}$$

$$H_0 = H_1 + \beta L \tag{7}$$

He then defines the kinetic energies

$$H_0 - E_0 = K_0 + C \tag{8}$$

$$H_1 - E_1 = K_1 + C \tag{9}$$

where C is an arbitrary constant. By subtracting the two, he then obtains (5).

However, we can also write E_0 and H_0 more transparently as

$$E_0 = E_1 + E^* \text{ , and}$$

$$H_0 = H_1 + H^* \text{ ,}$$

where E^* and H^* represent the excitation energy of the system before emission as determined in the two coordinate systems. Then the expressions for K become

$$(H_1 + H^*) - (E_1 + E^*) = K_0 + C \text{ and}$$

$$H_1 - E_1 = K_1 + C ,$$

so that

$$K_0 - K_1 = H^* - E^* = L (\beta - 1) .$$

In other words, since $E^* = L$ by assumption, Einstein merely equates the potential energy of excitation as transformed to the moving coordinate system, H^*, to the light pulse energy as transformed to the moving coordinate system, $L\beta$. But we do not know the transformed value of E^*. That is, we have no way of determining whether the potential energy of this excited system behaves as a kinetic energy of mass such that $H^* = L\beta$ without measuring it, or at least by some other argument than Einstein provides here.

[1] A. Einstein, *Annalen der Physik*, 17:891, 1905. 1923 English translation

[2] A. Einstein, *Annalen der Physik*. **18**:639, 1905. 1923 English translation

FERMIODYNAMICS THROUGH GENERALIZED ELECTRODYNAMICS

Sushama V. Vaidya
Physics Department
S.B. College of Science
Aurangabad – 431001, India
sushansh@yahoo.com

M.T. Teli
Physics Department
Dr. Babasaheb Ambedkar
Aurangabad – 431004, India (Retd.)
sushansh@yahoo.com

Received December 10, 2013

Abstract

Lorentz invariant fermion theory is established through Generalized Electrodynamics. Conservation of fermion number and chirality involves scalar and pseudoscalar masses in terms of the fields which make the fermions to be binary mass compounds. The mass formula is illustrated for nucleons. The evolution of particle masses in the theory is compatible with the dynamical theory.

Keywords: Generalized Dirac-Maxwell equations, Fermiodynamics, fermion number, chirality, binary mass, dynamical theory.

Copyright © 2013 by Hadronic Press, Inc., Palm Harbor, FL 34684, US

1 Introduction

It is believed that Lorenz condition [1] closes electrodynamics and limits it to describe photons only. The condition is gauge invariant and was required for getting retarded potentials for obtaining retarded fields from inhomogeneous wave equations. A good review literature on Lorenz condition is available [2] [3] [4]. However, the inhomogeneous wave equations can be obtained *without the need* of Lorenz gauge. This is achieved by introducing electric and magnetic scalar fields in place of Lorenz conditions in the Dirac-Maxwell equations with monopoles. This approach leads to the generalized Dirac-Maxwell (GDM) equations [5], [6], [7], [8], [9] which have exhibited many interesting features. They involve four components each of electric and magnetic fields instead of three. The equations have duality symmetries not only amongst the fields but also amongst the potentials and the sources of the fields. They possess dimensional symmetry in all these quantities along with the space and time. They easily accept tensor and quaternion forms.

Recently [7] we have re-established the GDM equations by making duality symmetrization of Maxwell's equations and tensor form is obtained for them suitable for getting Power and Force laws. The generalized Poynting vector is then seen to satisfy relativistic energy-momentum relation giving rise to mass of particles directly in terms of the fields. Two Lorentz invariant masses - scalar and pseudoscalar are seen to arise to form a binary mass compound. The model is seen to fit for neutron and proton formation from bare nucleons and pions.

Consideration of lifting of the Lorenz condition has also been made by others. Lehnert and Anastasovski *et al* [10], [11], [12], [13], [14] have replaced Lorenz condition by introducing electric scalar function. Likewise, Vlaenderen and Waser [15] and Vlaenderen [16] have introduced electric scalar field into Maxwell's equations and obtained generalized Maxwell's equations without monopoles which led them to inhomogeneous wave equations for electric potentials.

The extended electrodynamics is so far devoted to the investigations concerning spin-1 bosons. Now, there is electrodynamics theory for photons and bosons. But there is no electrodynamics-type theory for spin $\frac{1}{2}$ fermions which is half the branch of particle Physics. There is Dirac equation for electrons, but it is not a field theory. Since nature loves symmetry we expect that there should be electrodynamics for fermions.

In this paper, we extend the GDM equations of generalized electrodynamics to construct and investigate spinor theory for fermions in terms of fermion fields. This will be an alternative Dirac theory for general spin $\frac{1}{2}$ fermions.

In sec. (2) we give the GDM equations at a glance as a background for the development of fermion theory. Sec. (3) expresses the GDM equations in Dirac form by treating the components of fields, potentials and the sources as components of spinors. Equations of continuity for vector as well as axial vector currents are obtained for conservation of fermion number and chirality. The conditions on the source spinors lead to the charge-mass equivalence relation. Hamiltonian obtained for the fermions identifies the fermions as compound mass particles with the scalar and pseudoscalar component masses in terms of the fields. Operators and isospin are also investigated in this section. In the sec. (4) we investigate plane wave solutions of the fermion equations where we find that there are four linearly independent components for the fermion spinors- two for up and down spin states and the remaining two for the two isospin states. In sec. (5) we establish Lorentz invariance of the fermion equations. Sec. (6) is devoted to interpret the mass of the fermions on the basis of dynamical model of superconductivity. Important findings are briefly summarized in the sec. (7).

2 Generalized Dirac-Maxwell equations (GDM) at glance

In the following and the subsequent sections, Greek indices μ,ν,λ,ρ etc. take values 0, 1, 2 and 3. Italic indices *i, j, k* etc. take values 1, 2 and 3. Natural units and Einstein's summation convention over repeated covariant and contra-variant indices are used. Bold faced letters indicate three-vectors.

The GDM equations in the extended electrodynamics in usual notations are the following [5]

$$\nabla\times\mathbf{H}-\partial_0\mathbf{E}-\nabla E_0=\mathbf{j}^{\mathrm{e}},\quad \nabla\cdot\mathbf{E}+\partial_0 E_0=\rho^{\mathrm{e}} \tag{1}$$

$$\nabla\times\mathbf{E}+\partial_0\mathbf{H}+\nabla H_0=-\mathbf{j}^{\mathrm{m}},\quad \nabla\cdot\mathbf{H}+\partial_0 H_0=\rho^{\mathrm{m}} \tag{2}$$

Their potential solutions are given by

$$\mathbf{H}=\nabla\times\mathbf{A}^{e}-\partial_0\mathbf{A}^{\mathrm{m}}-\nabla\varphi^{\mathrm{m}},\ \mathbf{E}=-\nabla\times\mathbf{A}^{\mathrm{m}}-\partial_0\mathbf{A}^{\mathrm{e}}-\nabla\varphi^{\mathrm{e}}$$

$$H_0=\nabla\cdot\mathbf{A}^{\mathrm{m}}+\partial_0\varphi^{\mathrm{m}}=\partial_\mu A^{\mathrm{m}\mu},\quad E_0=\nabla\cdot\mathbf{A}^{\mathrm{e}}+\partial_0\varphi^{\mathrm{e}}=\partial_\mu A^{\mathrm{e}\mu}, \tag{3}$$

where $A^{m\mu}=(\varphi^{m},\mathbf{A}^{m})$ and $A^{e\mu}=(\varphi^{e},\mathbf{A}^{e})$ are respectively the electric and magnetic four potentials (as indicated by the superscripts e and m) and satisfy the inhomogeneous wave equations

$$\partial^2 A^{e,m\mu} = j^{e,m\mu} \tag{4}$$

The GDM equations are fully symmetric in dimensions of space-time, source-current density vectors, potential four vectors and electromagnetic fields. Let us define a set $\{e\}$ of electrical quantities

$$\{e\} = \{E_0, \mathbf{E}, \varphi^{e}, \mathbf{A}^{e}, \rho^{e}, \mathbf{j}^{e}\}$$

and the set $\{m\}$ of magnetic quantities as

$$\{m\} = \{H_0, \mathbf{H}, \varphi^{m}, \mathbf{A}^{m}, \rho^{m}, \mathbf{j}^{m}\}$$

We then see that under the full duality transformations defined as $\{m\} \rightarrow \{e\}$ and $\{e\} \rightarrow -\{m\}$, the set of eqns. (1) and. (2) and the set of eqns. (3) are invariant.

The GDM equations are readily expressible into tensor form most suitably in terms of dyons [5] [6] [9] [17] [18] f^{μ} which are also called as Riemann-Silberstein (RS) vectors [19] defined as

$$f^{\mu} = H^{\mu} + iE^{\mu}, V^{\mu} = A^{m\mu} + iA^{e\mu} \text{ and } j^{\mu} = j^{m\mu} + ij^{e\mu} \tag{5}$$

3 The GDM Equations In Dirac Form

The GDM equations can be represented into Dirac form as

$$\hat{\partial}\phi = J \ , \ \phi = \hat{\partial}V \ , \ \partial^2 V = J \tag{6}$$

where the components of the fields, potentials and source are now the components of spinors or matrices defined as follows

$$\phi = \begin{bmatrix} H \\ E \end{bmatrix}, \quad J = \begin{bmatrix} J_m \\ J_e \end{bmatrix}, \quad V = \begin{bmatrix} V_m \\ V_e \end{bmatrix} \tag{7}$$

The four component subspinors are defined as

$$H = \begin{bmatrix} E_0 \\ \boldsymbol{H} \end{bmatrix}, \quad E = \begin{bmatrix} -H_0 \\ \boldsymbol{E} \end{bmatrix}, \quad V_m = \begin{bmatrix} \varphi_e \\ -\boldsymbol{A}_m \end{bmatrix}, \quad V_e = \begin{bmatrix} \varphi_m \\ \boldsymbol{A}_e \end{bmatrix},$$

$$J_m = \begin{bmatrix} \rho_e \\ -\boldsymbol{J}_m \end{bmatrix}, \quad J_e = \begin{bmatrix} \rho_m \\ \boldsymbol{J}_e \end{bmatrix} \tag{8}$$

The differential (Dirac) operator is given by

$$\hat{\partial} = \Gamma^{\mu} \partial_{\mu} \tag{9}$$

where Γ^{μ} are the 8x8 matrices having the representation given by

$$\Gamma^0 = \begin{bmatrix} I & 0 \\ 0 & -I \end{bmatrix}, \ \Gamma^i = \begin{bmatrix} 0 & M_i \\ M_i & 0 \end{bmatrix}, \ \Gamma^5 = \Gamma^0\Gamma^1\Gamma^2\Gamma^3 = \begin{bmatrix} 0 & -I \\ I & 0 \end{bmatrix} \tag{10}$$

with the 4x4 submatrices defined as

$$M_1 = \begin{bmatrix} \tau_2 & 0 \\ 0 & -\tau_2 \end{bmatrix}, \ M_2 = \begin{bmatrix} 0 & I \\ -I & 0 \end{bmatrix}, \ M_3 = \begin{bmatrix} 0 & \tau_2 \\ \tau_2 & 0 \end{bmatrix}, \ \tau_2 = \begin{bmatrix} 0 & 1 \\ -1 & 0 \end{bmatrix} \tag{11}$$

and I is the unit matrix of appropriate dimension.

These matrices satisfy Lie algebra

$$\left[M_i, M_j\right] = 2\varepsilon_{ijk} M_k \,, \ M_i M_j = -\delta_{ij} I + \varepsilon_{ijk} M_k \tag{12}$$

The Γ^{μ} matrices are isomorphic with the 4x4 Dirac matrices and obey Clifford algebra

$$\Gamma^{\mu}\Gamma^{\nu}+\Gamma^{\nu}\Gamma^{\mu}=2g^{\mu\nu} \tag{13}$$

$$\left(\Gamma^{0}\right)^{2}=I,\ \left(\Gamma^{i}\right)^{2}=-I \tag{14}$$

$g^{\mu\nu}$ is the fundamental metric with signature (+, −, −, −), δ_{ij} is the Kronecker delta while ε_{ijk} is the totally antisymmetric tensor with $\varepsilon_{123}=+1$.

3.1 Equations of continuity

To apply eqn. (6) to fermions we replace the electromagnetic concept of the fields by the concepts of the respective fermion fields such as lepton field, nucleon (nuclear) field for nucleons and strong (color) field for hyperons and quarks. Similarly, instead of the kinds 'electro'-'magnetic' there will be P-odd and P-even terms for subspinors. Thus the subspinors H, V_m and J_m are P-even while E, V_e and J_e are P-odd.

In the case of fermions, conservation of charge is to be considered as the conservation of fermion number which means conservation of vector current V^{μ} or equation of continuity for that current. Along with this there is also to be considered conservation of *chirality* or conservation of axial vector current A^{μ}. The field source is to be selected accordingly so as to match the simultaneous conservation of the vector V^{μ} and the axial vector A^{μ} currents which are defined as

$$V^{\mu}=\frac{1}{2}\left[\bar{\phi}\Gamma^{\mu}\phi\right],\ \text{and}\ A^{\mu}=\frac{1}{2}i\bar{\phi}\Gamma^{\mu}\Gamma^{5}\phi \tag{16}$$

Here $\bar{\phi}=\phi^{\dagger}\Gamma^{0}$ is the Dirac conjugated spinor.

We get for the desired equations of continuity

$$\partial_{\mu}\left[\bar{\phi}\Gamma^{\mu}\phi\right]=\bar{\phi}J+\bar{J}\phi=0 \tag{17}$$

and

$$\partial_\mu\left[\bar{\phi}\Gamma^\mu\Gamma^5\phi\right]=\bar{\phi}\Gamma^5 J-\bar{J}\Gamma^5\phi=0 \tag{18}$$

There is no unique solution for the source current satisfying these equations. We choose the following general one

$$J=-iM\phi \tag{19}$$

where

$$M=\tfrac{1}{2}\left[\bar{\phi}\phi+\Gamma^5\left(\bar{\phi}\Gamma^5\phi\right)\right] \tag{20}$$

(One can take + sign also on the r.h.s. of eqn. (19)).

We parameterize eqn. (20) by defining

$$\tfrac{1}{2}\bar{\phi}\phi=\tfrac{1}{2}\left(H^\dagger H-E^\dagger E\right)=\tfrac{1}{2}\left({H_0}^2-{E_0}^2-\boldsymbol{H}^2+\boldsymbol{E}^2\right)=m_1N=mN\cos\theta \tag{21}$$

and

$$\tfrac{1}{2}\bar{\phi}\Gamma^5\phi=-\tfrac{1}{2}\left(H^\dagger E+E^\dagger H\right)=\left(H_0E_0-\boldsymbol{E}\cdot\boldsymbol{H}\right)=m_2N=mN\sin\theta \tag{21a}$$

Then

$$m^2={m_1}^2+{m_2}^2=\left(\frac{1}{2}\bar{\phi}\phi\right)^2+\left(\frac{1}{2}\bar{\phi}\Gamma^5\phi\right)^2,\quad \tan\theta=\frac{m_2}{m_1} \tag{22}$$

and so

$$M=\left(m_1+m_2\Gamma^5\right)N=m\exp\left(\Gamma^5\theta\right)N \tag{23}$$

The angle θ is the phase associated with the particle and N is the fermion number density per unit volume. For convenience we shall take $N=1$.
Eqns. (20), (21) and (22) then reduce to

$$\tfrac{1}{2}\bar{\phi}\phi=m_1=m\cos\theta\ ,\quad \tfrac{1}{2}\bar{\phi}\Gamma^5\phi=m_2=m\sin\theta \tag{24}$$

$$M = \left(m_1 + m_2\Gamma^5\right) = m\exp\left(\Gamma^5\theta\right) \tag{24a}$$

Substituting this solution into the GDM eqn. (6) we obtain it in the Dirac form as

$$\left(\hat{\partial} + iM\right)\phi = 0 \tag{25}$$

3.2 Hamiltonian and particle mass

Now we have to identify the meaning of various terms in eqn. (25). By writing the operator $\hat{\partial}$ as $\hat{\partial} = i\hat{p}$ we identify the Hamiltonian as

$$H = \boldsymbol{\sigma}\cdot\boldsymbol{p} + \Gamma^0 M = H^\dagger, \quad \boldsymbol{\sigma} = \Gamma^0\boldsymbol{\Gamma} \tag{26}$$

The Hamiltonian is hermitian and is the generalization of Dirac's Hamiltonian. There is doubling of the dimensions of the matrices involved. Its energy eigenvalues are real and are given by

$$\varepsilon^2 = \boldsymbol{p}^2 + \left(m_1^{\,2} + m_2^{\,2}\right) = \boldsymbol{p}^2 + m^2 \tag{27}$$

where m^2 is given by eqn, (22)

This equation identifies m_1, m_2 and m as masses with m_1 and m_2 respectively as scalar and pseudoscalar components of the compound mass m. According to eqn. (21) and (21a), the mass m_1 occurs due to the asymmetry between the norms of the subspinors H and E while the mass component m_2 occurs due to the breaking of the orthogonality between these subspinors.

Using the expressions for the Γ matrices (eqn. (10)) and the mass operator eqn. (23) we can write eqn. (25) in the Hamiltonian form as

$$H\phi = \left(-i\boldsymbol{\omega}\cdot\boldsymbol{p}\,\tau_2 + m_1\tau_3 - m_2\tau_1\right)\phi = \boldsymbol{\tau}\cdot\boldsymbol{\Omega}\phi = \varepsilon\phi \tag{28}$$

where

$$\boldsymbol{\Omega} = -m_2\boldsymbol{i} + \left(\boldsymbol{\omega}\cdot\boldsymbol{p}\right)\boldsymbol{j} + m_1\boldsymbol{k},$$

$$\boldsymbol{\tau} = \tau_1\boldsymbol{i} - i\tau_2\boldsymbol{j} + \tau_3\boldsymbol{k} \tag{28a}$$

$\vdash\sqsubset$ is the generalized momentum in quaternion form spanned in the isospin space with the basis given by

$$\tau_1 = \begin{bmatrix} 0 & 1 \\ 1 & 0 \end{bmatrix} \quad , \quad \tau_2 = \begin{bmatrix} 0 & 1 \\ -1 & 0 \end{bmatrix} \quad , \quad \tau_3 = \begin{bmatrix} 1 & 0 \\ 0 & -1 \end{bmatrix} \tag{28b}$$

The term $\omega \cdot p$ is the momentum along the direction of the spin of the particle. Similarly $\vdash\sqsubset$ is the generalized momentum in the direction of isospin. Eqn. (28) treats the masses m_1 and m_2 on equal footing with the linear momentum. We call $\sqsubset$ as the *covariant momentum*. Its square gives

$$\varepsilon^2 = \sqsubset^2 = p^2 + \left(m_1^{\,2} + m_2^{\,2}\right) = p^2 + m^2 \tag{29}$$

Eqn. (29) gives $\varepsilon = \pm|\sqsubset|$. This is the generalized equation of neutrinos. The generalization includes the massive fermions. We call such fermions as *covariant neutrinos* which posses the Hamiltonian as given in eqn. (28).

We see that particles having the same mass lie on the circle given by eqn. (22) while particles having the same energy lie on the sphere given by eqn. (29).

There occur three types of particle masses:

1. Massless particles: For $m_1 = 0$ and $m_2 = 0$, the particles are massless. For such particles $H^\dagger H = E^\dagger E$ and $H^\dagger E + E^\dagger H = 0$ *i.e.* the subspinors H and E are of equal norm and they are mutually orthogonal. Such spin half massless particles are neutrinos.
2. Scalar point mass particles for which $m_2 = 0$ but $m_1 \neq 0$ (there is breaking of the symmetry between the norms of H and E but their orthogonality is maintained). Similarly, particles for which $m_1 = 0$ but $m_2 \neq 0$ (there is symmetry between the norms of H and the E but their orthogonality is broken) are pseudosclar point mass particles. Leptons are the known point mass particles.
3. Particles for which $m_1 \neq 0$ and also $m_2 \neq 0$ (norm symmetry and the orthogonality both are broken) are binary mass particles. Nucleons are the best examples of this [8].

Nucleons are known binary mass compounds constituted of bare nucleon and pions. For protons the binary mass formula gives $M_p{}^2 = m_1{}^2(\mathrm{p}) + m_{\pi^0}{}^2$ and for neutrons $M_n{}^2 = m_1{}^2(\mathrm{p}) + m_{\pi^-}{}^2$. Experiments give M_p = 938.45 MeV, M_n = 939.85 MeV, m_{π^0} = 135 MeV, m_{π^-} = 141.5 MeV. This data gives from the above equations respectively $m_1(\mathrm{p})$ = 928.7 MeV and $m_1(\mathrm{p})$ = 929.1 MeV. The two estimates of the bare proton mass $m_1(p)$ excellently agree with each other as expected. Their difference is only 0.4 MeV which is just 0.043%. Similarly the second alternative is $M_p{}^2 = m_1{}^2(\mathrm{n}) + m_{\pi^+}{}^2$ and $M_n{}^2 = m_1{}^2(\mathrm{n}) + m_{\pi^0}{}^2$. Using the above data one will find here also good agreement between the two estimates of bare neutron mass $m_1(n)$. This strongly supports the binary mass nature of the particles.

3.3 Binding energy of pions

Since pions are constituents of nucleons we estimate their binding energy. The binding energy B of pions can be defined *e.g.* as

$$B(\pi^+) = m_1(\mathrm{n}) + m_{\pi^+} - M_p$$

This can be written as

$$B(\pi^+) = \frac{2m_1(\mathrm{n})m_{\pi^+}}{m_1(\mathrm{n}) + m_{\pi^+} + M_p}$$

Since m_{π^+} is very much less than proton mass and $m_1(\mathrm{n}) \cong M_p$ the binding energy approximates to $B \cong m_{\pi^+}$. This suggests that pions experience buoyancy force inside the nuclear fluid field by which they float and become weightless.

3.4 Spin of the particle

As in Dirac's theory, here also the Hamiltonian given by eqn. (26) does not commute with the orbital angular momentum $\boldsymbol{r} \times \boldsymbol{p}$. However, the total angular momentum $\boldsymbol{r} \times \boldsymbol{p} + \frac{1}{4}\mathrm{i}\,\boldsymbol{\alpha} \times \boldsymbol{\alpha}$ commutes with it and so $\boldsymbol{w} = \frac{1}{4}\mathrm{i}\,\boldsymbol{\alpha} \times \boldsymbol{\alpha}$ is identified as the spin operator. Since $\boldsymbol{w}^2 = \frac{3}{4}I$ the particle has spin $s = \frac{1}{2}$.

This completes the conversion of the electromagnetic GDM equations into the Dirac form (eqn.(25)). Now this equation describes spin $s = \frac{1}{2}$ compound mass fermions. This involves a mass operator M involving scalar and pseudoscalar masses. The electromagnetic charge source J is replaced by its *mass-charge* equivalent as given in eqn. (19).

4 Plane Wave Solutions In Deep

For free particles, the Dirac eqn. (25) has the following plane wave solution for spinor:

$$\phi = \begin{bmatrix} H(p) \\ E(p) \end{bmatrix} \exp(-ipx) \tag{30}$$

where $px = \varepsilon x_0 - \boldsymbol{p} \cdot \boldsymbol{x}$.

On substituting this solution into eqn. (25) we get the following connection between the subspinors $E(p)$ and $H(p)$

$$E(p) = -\left(\frac{m_2 + \boldsymbol{M} \cdot \boldsymbol{p}}{\varepsilon + m_1} \right) H(p) \tag{31}$$

$$H(p) = -\left(\frac{m_2 - \boldsymbol{M} \cdot \boldsymbol{p}}{\varepsilon - m_1} \right) E(p) \tag{31a}$$

These equations show that out of the eight components of the spinor ϕ there are only four linearly independent components for a given energy. Out of these four components, two belong to two spin states up and down while the remaining two will belong to the two isospin states $I_3 = +\frac{1}{2}$ and $I_3 = -\frac{1}{2}$. The GDM eqn. (25), therefore, describes a particle of spin $s = \frac{1}{2}$ and isospin $I = \frac{1}{2}$.

The solutions can be further improved by noting that the Hamiltonian eqn. (26) commutes with the helicity operator

$$h(p) = \frac{\boldsymbol{\omega} \cdot \boldsymbol{p}}{|\boldsymbol{p}|} = \boldsymbol{\omega} \cdot \boldsymbol{n} \tag{32}$$

where $\boldsymbol{n} = \frac{\boldsymbol{p}}{|\boldsymbol{p}|}$ is the unit vector. The eigen spinors of the Hamiltonian, therefore, are the eigen spinors of $\boldsymbol{\omega} \cdot \boldsymbol{n}$. Since $(\boldsymbol{\omega} \cdot \boldsymbol{n})^2 = 1$, the eigen values of $\boldsymbol{\omega} \cdot \boldsymbol{n}$ are $\lambda = \pm 1$. The equation $\boldsymbol{\omega} \cdot \boldsymbol{n}\, H = \lambda H$ bears the following solutions

$$H = \begin{bmatrix} E_0 \\ \boldsymbol{H} \end{bmatrix} = \begin{bmatrix} -i\lambda \boldsymbol{n} \cdot \boldsymbol{H} \\ (\boldsymbol{n} \cdot \boldsymbol{H})\boldsymbol{n} - i\lambda(\boldsymbol{n} \times \boldsymbol{H}) \end{bmatrix} \tag{33}$$

This indicates that the subspinors are complex. Writing $H = H_1 + iH_2$ (where H_1 and H_2 are real element *internal* subspinors) we get from (33)

$$H_1 = \begin{bmatrix} E_{10} \\ \boldsymbol{H}_1 \end{bmatrix} = \begin{bmatrix} \lambda \boldsymbol{n} \cdot \boldsymbol{H}_2 \\ (\boldsymbol{n} \cdot \boldsymbol{H}_1)\boldsymbol{n} + \lambda(\boldsymbol{n} \times \boldsymbol{H}_2) \end{bmatrix} \tag{33a}$$

and

$$H_2 = \begin{bmatrix} E_{20} \\ \boldsymbol{H}_2 \end{bmatrix} = \begin{bmatrix} -\lambda \boldsymbol{n} \cdot \boldsymbol{H}_1 \\ (\boldsymbol{n} \cdot \boldsymbol{H}_2)\boldsymbol{n} - \lambda(\boldsymbol{n} \times \boldsymbol{H}_1) \end{bmatrix} \tag{33b}$$

The subspinors H_1 and H_2 satisfy the following *inter alia* relations

$$\boldsymbol{M} \cdot \boldsymbol{n}\, H_1 = \lambda H_2 \quad \text{and} \quad \boldsymbol{M} \cdot \boldsymbol{n}\, H_2 = -\lambda H_1 \tag{34}$$

These equations show that H_1 and H_2 do not have definite helicity and that they are orthogonal to each other and also have equal norms *i.e.*

$$H_1^T H_2 = 0 \quad \text{and} \quad H_1^T H_1 = H_2^T H_2 \tag{34a}$$

The orthogonality condition leads to

$$(\boldsymbol{n} \times \boldsymbol{H}_1) \cdot (\boldsymbol{n} \times \boldsymbol{H}_2) = 0 \tag{35}$$

Geometrically this means that the plane containing $\boldsymbol{n}$ and $\boldsymbol{H}_1$ is orthogonal to the plane containing $\boldsymbol{n}$ and $\boldsymbol{H}_2$. This is the preservation of the orthogonality property of the electromagnetic fields of photon dynamics. There exists similar structure for the subspinor E. However, eqns. (31) indicate that the subspinors $E(p)$ and $H(p)$ are not orthogonal to each other and also that their norms are not equal since

$$E^{\dagger}E = \frac{\varepsilon - m_1}{\varepsilon + m_1} H^{\dagger}H \tag{36}$$

Thus the subspinor H is major and E is minor. This *inequality* leads to form two separate energy levels associated with the fields as explained below.

Using the plane wave solution we obtain the fermion number density N per unit energy as

$$N = \frac{\phi^{\dagger}\phi}{2\varepsilon} = \frac{H^{\dagger}H}{\varepsilon + m_1} = \frac{E^{\dagger}E}{\varepsilon - m_1} \tag{37}$$

For $N = 1$ this gives two energy states formed due to the fields as

$$S(H) = \tfrac{1}{2} H^{\dagger}H = \tfrac{1}{2}(\varepsilon + m_1) \tag{38}$$

and

$$S(E) = \tfrac{1}{2} E^{\dagger}E = \tfrac{1}{2}(\varepsilon - m_1) \tag{39}$$

Eqns. (38) and (39) give a clue that energy equal to m_1 is required to be supplied to the particle in the lower state $S(E)$ to jump to the upper $S(H)$ zero particle state. Conversely if the particle in the upper $S(H)$ state jumps to the lower $S(E)$ no particle state a particle of mass m_1 will be released. This explains the creation and absorption of massive *bare* particles due to the transitions between the two energy levels. These transitions are self interaction (individual) transitions. In addition to these there are mutual interaction (collective) transitions due to the non-orthogonality of H and the E fields. This interaction being pseudoscalar it creates pseudoscalar particle

of mass m_2. The mass m_1 forms a bare fermion while m_2 dresses it thereby forming a compound mass stable fermion.

Now we define the *chirality* of the particle as

$$X = \frac{1}{2} i \frac{\phi^\dagger \Gamma^5 \phi}{|\boldsymbol{p}|} = \frac{1}{2} i \frac{\left(E^\dagger H - H^\dagger E\right)}{|\boldsymbol{p}|} = i \frac{H^\dagger \boldsymbol{M} \cdot \boldsymbol{p} H}{|\boldsymbol{p}| H^\dagger H} = \frac{2\boldsymbol{s} \cdot \boldsymbol{p}}{|\boldsymbol{p}|} = 2h(p) \quad (40)$$

where $h(p)$ is the helicity of the particle and $\boldsymbol{s}$ is its spin vector defined as

$$\boldsymbol{s} = \frac{1}{2} i \frac{H^\dagger \boldsymbol{M}\, H}{H^\dagger H} \quad (40a)$$

Eqn. (40) indicates that chirality of the particle is twice its helicity and also that for real fields, chirality vanishes since for real fields

$$H^\dagger \boldsymbol{M}\, H = H^{\mathrm{T}} \boldsymbol{M}\, H = 0$$

By using the plane wave solutions and the normalization of fermion number (eqn. (37)) we get the various kinematical quantities in terms of the spinor fields as:

The four momentum of the particle is given by

$$p^\mu = (\varepsilon, \boldsymbol{p}) = V^\mu = \frac{1}{2} \bar{\phi} \Gamma^\mu \phi \quad (41)$$

This gives the energy and momentum of the particle as

$$p^0 = \varepsilon = \frac{1}{2}\left(H_0{}^2 + E_0{}^2 + \boldsymbol{H}^2 + \boldsymbol{E}^2\right) \quad (42)$$

and

$$\boldsymbol{p} = \boldsymbol{V} = E^\dagger \boldsymbol{M}\, H - H^\dagger \boldsymbol{M}\, E = E_0 \boldsymbol{H} + H_0 \boldsymbol{E} + \boldsymbol{E} \times \boldsymbol{H} \quad (43)$$

Likewise the axial vector is given by

$$A^\mu = (A^0, \boldsymbol{A}) = \frac{1}{2} i \bar{\phi} \Gamma^\mu \Gamma^5 \phi = 2\xi^\mu \quad (44)$$

where $A^0 = |\boldsymbol{p}|X = 2\xi^0$ (eqn. (40)) and $\boldsymbol{A}$ is given by

$$\boldsymbol{A} = \frac{1}{2} i\bar{\phi}\Gamma\Gamma^5\phi = \frac{1}{2} i\left(H^\dagger \boldsymbol{M}\, H + E^\dagger \boldsymbol{M}\, E\right) = 2\boldsymbol{\omega} \tag{45}$$

where $\boldsymbol{\omega}$ is the spin polarization three vector given by

$$\boldsymbol{\omega} = \left[\left(m_1 + \frac{m_2{}^2}{(\varepsilon + m_1)}\right)\boldsymbol{s} + \frac{(\boldsymbol{s}\cdot\boldsymbol{p})\boldsymbol{p}}{(\varepsilon + m_1)} + \frac{m_2\, \boldsymbol{s}\times\boldsymbol{p}}{(\varepsilon + m_1)}\right] \tag{46}$$

This is the generalized expression for polarization vector and it reduces to the standard formula for point mass particles by taking $m_2 = 0$ and $m_1 = m$.

In obtaining the above equations we have used the following identities

$$(\boldsymbol{M}\cdot\boldsymbol{p})^2 = -\boldsymbol{p}^2 \tag{47a}$$

$$\boldsymbol{M}(\boldsymbol{M}\cdot\boldsymbol{p}) = -\boldsymbol{p} - \boldsymbol{M}\times\boldsymbol{p} \tag{47b}$$

$$(\boldsymbol{M}\cdot\boldsymbol{p})\boldsymbol{M} = -\boldsymbol{p} + \boldsymbol{M}\times\boldsymbol{p} \tag{47c}$$

$$(\boldsymbol{M}\cdot\boldsymbol{p})\boldsymbol{M}(\boldsymbol{M}\cdot\boldsymbol{p}) = \boldsymbol{M}\,\boldsymbol{p}^2 - 2(\boldsymbol{M}\cdot\boldsymbol{p})\boldsymbol{p} \tag{47d}$$

Now we find that ξ^μ is orthogonal to p^μ

$$\xi^\mu p_\mu = 0 \tag{48}$$

This is in agreement with that in Particle Physics. The generalized ξ^μ thus maintains its orthogonality with the four momentum of the particle. This is equivalent to $V^\mu A_\mu = 0$.

We further find that

$$V^\mu V_\mu = \left[\frac{1}{2}\bar{\phi}\phi\right]^2 + \left[\frac{1}{2}\bar{\phi}\Gamma^5\phi\right]^2 = \left(m_1{}^2 + m_2{}^2\right) \tag{49}$$

and

$$A^{\mu}A_{\mu} = -4\left(m_1^{\,2} + m_2^{\,2}\right)\boldsymbol{s}^2 \tag{50}$$

Now, Fiers theorem [23] gives

$$\frac{1}{2}\left[V^{\mu}V_{\mu} + A^{\mu}A_{\mu}\right] + \left[\frac{1}{2}\bar{\phi}\phi\right]^2 + \left[\frac{1}{2}\bar{\phi}\Gamma^5\phi\right]^2 = 0 \tag{51}$$

With the corresponding expressions, eqn. (51) yields $\boldsymbol{s}^2 = \frac{3}{4}$. The particle, therefore, has spin $\frac{1}{2}$.

5 Lorentz Invariance of the GDM equations

It is obvious that the Dirac form of the GDM equations is Lorentz invariant since corresponding to the Lorentz transformations of coordinates $x'^{\mu} = a^{\mu}{}_{\nu}x^{\nu}$ there exists a matrix Λ (which transforms ϕ as $\phi' = \Lambda\phi$)such that

$$\Lambda\Gamma^{\mu}\Lambda^{-1} = a_{\nu}{}^{\mu}\Gamma^{\nu} \tag{52}$$

$$\Lambda M\Lambda^{-1} = M \tag{53}$$

Eqn. (52) does not have unique solution for the transformation matrix but eqn. (53) fixes it as

$$\Lambda = \exp\left[\frac{1}{2}\Gamma^{\mu}\Gamma^{\nu}\theta_{\mu\nu}\right], \quad \theta_{\nu\mu} = -\theta_{\mu\nu} \tag{54}$$

Here $\mu = 0$ or θ_{0i} corresponds to Lorentz transformations while $\theta_{ij} = \varepsilon_{ijk}\theta_k$ corresponds to rotation of coordinates. This transformation group has $\left(0, \frac{1}{2}\right)$ irreducible representation and so ϕ represents a spinor corresponding to spin - $\frac{1}{2}$ fermion. The Dirac form of the GDM equations now describes binary mass fermions.

6 Dynamical theory

Now we examine the theory of fermions as developed above in the light of the dynamical model developed by Nambu [20], [21], [22] [23]. In this model the vacuum is taken as the space filled with coherent mixture of massless fermions of opposite charge and opposite momentum (helicities) but parallel

spins. There exist two types of interactions between these particles: self interactions (individual excitations) and mutual interactions (collective excitations). Particles get excited by these interactions and jump to the upper states outside the vacuum and thereby acquire mass. The individual excitations provide bare (scalar) mass while the collective excitation provides pseudoscalar mass which dresses the bare mass and this is how the stable massive particle is formed from massless fermions.

We shall first show with the GDM eqn. (25) that vacuum is filled with coherent mixture of particle –antiparticle pairs. Then consider only individual excitations of particles in these pairs. This will form point mass fermion such as electron. Similarly we consider the case of collective excitation only. This will provide point pseudoscalar mass particles. Finally we shall consider both the individual as well as collective excitations. This will form a stable massive particle of composite mass such as nucleons (neutrons and protons).

6.1 Massless particle-antiparticle pair in vacuum

The Dirac eqn. (25) for massless particles (vacuum) gives two Weyl type equations satisfied by the subspinors H and E as

$$E = -\frac{\boldsymbol{M}\cdot\boldsymbol{p}}{|\boldsymbol{p}|}H = ih(p)H \tag{55}$$

and

$$H = \frac{\boldsymbol{M}\cdot\boldsymbol{p}}{|\boldsymbol{p}|}E = -ih(p)E \tag{56}$$

These equations are identical to eqn. (34) and so the subspinors H and E have real components. They do not have definite helicity. However, subspinors of definite helicities can be obtained from them by suitable combinations of them as follows

$$u_L^{+} = \tfrac{1}{\sqrt{2}}(H + iE) \text{ and } v_R^{-} = \tfrac{1}{\sqrt{2}}(H - iE) = u^{+*}{}_L \tag{57}$$

$$h(p)u_L^{+} = -u_L^{+} \quad \text{and} \quad h(p)v_R^{-} = v_R^{-} \tag{57a}$$

Here u_L^+ has left handed helicity while the spinor v_R^- has right handed helicity *i.e.*, they have opposite momentum and parallel spins (for parity invariance). Also they have opposite charges and they are massless too. Thus these subspinors form the appropriate pair as required for dynamical model. We write the pair as

$$\psi = \begin{pmatrix} u_L^+ \\ v_R^- \end{pmatrix} \tag{58}$$

6.2 The composite mass particles: The Covariant Neutrinos

Consider eqns. (31) and (31a) and combine the subspinors H and E to form subspinors of definite helicities as in eqn. (57). We get

$$\varepsilon u_L^+ = -\boldsymbol{\omega}\cdot\boldsymbol{p}\, u_L^+ + (m_1 - im_2)v_R^- \tag{59}$$

$$\varepsilon v_R^- = \boldsymbol{\omega}\cdot\boldsymbol{p}\, v_R + (m_1 + im_2)u_L^+ \tag{59a}$$

Theses equations are the conversions of eqn. (25) in the form of the equations of BCS theory of superconductivity. The second terms on their right hand sides represent joint effects of individual as well as of collective excitations. In the absence of these excitations, the subspinors u_L^+ and v_R^- have definite helicities. Thus helicity breaking leads to creation of mass of the particles. Writing eqns. (59) and (59a) in the Hamiltonian form we get $H\psi = \varepsilon\psi$ or

$$\begin{pmatrix} -\boldsymbol{\omega}\cdot\boldsymbol{p} & (m_1 - im_2) \\ (m_1 + im_2) & \boldsymbol{\omega}\cdot\boldsymbol{p} \end{pmatrix}\psi = \left[-(\boldsymbol{\omega}\cdot\boldsymbol{p})\tau_3 + m_1\tau_1 - im_2\tau_2\right]\psi = \varepsilon\psi \tag{60}$$

This can be written as

$$H\psi = \boldsymbol{\Gamma}\cdot\boldsymbol{\Gamma}\,\psi = \varepsilon\psi \tag{61}$$

where $\boldsymbol{\Gamma}\cdot\boldsymbol{\Gamma}$ is the covariant momentum operator in the direction of isospin spanned as

$$\boldsymbol{\Gamma}\cdot\boldsymbol{\Gamma} = m_1\tau_1 - im_2\tau_2 - (\boldsymbol{\omega}\cdot\boldsymbol{p})\tau_3 \tag{62}$$

This is the same concept as expressed in eqn. (28). Eqn. (62) is the conversion of eqn. (28) due to the introduction of the pair spinor ψ. Eqn. (61) describes *covariant neutrinos* as explained earlier. Eqn. (61) gives

$$\varepsilon = \pm\left|\sqsubset\right| = \pm\sqrt{\boldsymbol{p}^2 + m_1^{\,2} + m_2^{\,2}} \tag{63}$$

This is the generalization of the neutrino equation $\varepsilon^2 = \boldsymbol{p}^2$ or $\varepsilon = \pm|\boldsymbol{p}|$ (in electrodynamics this equation basically is for photons). The massive fermions with momentum $\sqsubset$ (eqn. (62)) are then equivalent to massless neutrinos. For this reason we call the massive fermions as *covariant neutrinos*. True neutrinos lie in vacuum while covariant neutrinos are their excitations. This justifies the generalization of the electrodynamics from photons to neutrinos and then for *covariant neutrinos.*(Likewise we can have *covariant boson.*

7 Summary

That we have formulated electrodynamics for massive fermions itself is new and therefore each result of it is either new or provides new links to understand the old experimental observations. Let us list them in brief.

1. Maxwell's electrodynamics describes massless photons and Generalized Electrodynamics describes massless neutrinos and massive spin-1 [8] bosons and spin-$\frac{1}{2}$ fermions. This brings fermions and bosons on equal footing under the single theory of Generalized Electrodynamics.
2. Masses of fermions as well as of bosons [8] originate from fields. This result is a consequence of the equation of continuity in the electrodynamical theories. However, that masses arise from fields has been investigated by Nambu [20], [21], [22], [23]. on the basis of BCS theory of superconductivity. Our results, however, are direct consequences of conservation of fermion number and chirality.
3. The theory considers isospin-$\frac{1}{2}$ along with the spin-$\frac{1}{2}$ fermions. However, the mass difference between the isospin masses did not occur since contribution from isospin is not included in the theory. The situation of integral isospin fermions is also not considered which may require the use of Clifford algebra and Dirac vector [24], [25], [26].
4. The theory is Lorentz invariant and also chirality and fermion number invariant.

5. The fermion theory explains the composite structure of particle masses, the case of nucleons fits well.
6. The theory leads to the concept of combining masses with linear momentum in isospin space which we refer to as covariant momentum. Such particles are covariant particles (equivalently massless).
7. The theory explains also how masses arise in the dynamical model of Nambu [20], [21], [22], [23].

9 Acknowledgements

One of us (SVV) expresses her thanks to Professor S.C. Mehrotra and also to the President, S.B. Education Society and the Principal, S.B. College of Science for the encouragements she is receiving from them.

References

[1] L. Lorenz , *Philos. Mag.* 34 (1867) 287.

[2] H. C. Potter, *Lorenz on light: A precocious photon paradigm* arXiv:0811.2123v1 [physics.gen-ph], 13 Nov 2008.

[3] H. C. Potter, *Lorenz fields convey energy as nadelstrahlung,* arXiv:0903.4083v2 [physics.gen-ph] 11 May 2009.

[4] J. D. Jackson, *Comment om 'Maxwell equations and the redundant gauge degree of freedom,* Eu. J. Phys. 31 (2010) 79-84.

[5] M. T. Teli, *Four component electromagnetic fields and Electrodynamics,* Pramana, 24 (1985) 485-497.

[6] M. T. Teli, *Supersymmetric Electrodynamics,* Ind. J. of Pure & App. Phys., 38 (2000) 407-410.

[7] M. T. Teli and G. H. Jadhav, *Classical theory of weak interactions and vector bosons through four comoponent electro-gravitodynamics*, Ind. J. of Pure & App. Phys, 39 (2001) 191-197.

[8] S. V. Vaidya and M. T. Teli, *Generalized electrodynamics: The origin of mass from vacuum,* Had. J. 34, no. 4 (2011) 411- 424 .

[9] S. V. Vaidya, *Study of electrodynamics of electron*, Ph. D. Thesis, Dr. Babasaheb Ambedkar Marathwada University, Aurangabad, 2002.

[10] B. Lehnert, *An extended Electromagnetic theory,* Physica Scripta, 59 (1999) 89.

[11] P. K. Anastasovski, T. E. Bearden, C. Ciubotaru et al. *Classical Electrodynamics without the Lorenz condition: Extracting energy from the vacuum,* Physica Scripta, 61 (2000) 513-517.

[12] B. Lehnert, Physica. Scripta. 66 (2002) 105.

[13] B. Lehnert, *Boundary conditions and spin of a dense light beam,* Physica Scripta, 74 (2004) 139.

[14] B. Lehnert Physica.Scipta. 72 (2005) 359.

[15] K. J. van Vladeren and A. Waser, *Generalization of classical electrodynamics to admit a scalar field and longitudinal waves,* Hadronic J. 24 (2001) 609-628.

[16] K. J. van Vladeren, *Generalization of classical electrodynamics for the prediction of scalar field effects,* arXiv:physics /0305098v1 [physics.class-phy 21 may 2003.

[17] B. S. Rajput, A. S. Kumar and O. P. S. Negi. Letter Nuovo Cimento, 34 (1982) 1180.

[18] B. S. Rajput, A. S. Kumar and O. P. S. Negi. Letter Nuovo Cimento, 36 (1983) 75.

[19] B. J. Smith and M. G. Raymer , New J. Phys., 9 (2007) 414.

[20] Y. Nambu and G. Jona-Lasinio, *A dynamical model of Elementary particles based on an analogy with Superconductivity I,* Phys Rev., 122 **(1961)** 345.

[21] Y. Nambu and G. Jona-Lasinio, *A dynamical model of Elementary particles based on an analogy with Superconductivity II,* Phys Rev., 124 (1961) 246.

[22] Y. Nambu and D. Lurie, *Chirality conservation and soft pion* production, Phys Rev,. 128 (1962) 1429.

[23] Y. Nambu and E. Shrauner, *Soft pion emission induced by electromagnetic and weak interactions,* Phys Rev., 128 (1962) 862.

[24] W. A. Rodrigues Jr., E. Recami , A. Maia Jr. and M. A. F. Rosa, *The classical problem of the charge and pole motion. A satisfactory formalism by Clifford algebra,* Physics Letters, 220 (1989), 195.

[25] M. A. F. Rosa, E. Recami and W. A. Rodrigues Jr., *A satisfactory formalism for magnetic monopoles by Clifford algebras,* Physics Letters 173 (1986), 233-236.

[26] A. Maia, Jr., E. Recami, W. A. Rodrigues, Jr. and M. A. F. Rosa, *Magnetic monopoles without string in the Kahler-Clifford algebra bundle: A geometric interpretation*, J. Math. Phys., 31 (1990), 502.